A COMPARATIVE MINERALOGICAL AND GEOCHEMICAL STUDY OF SULPHIDE MINE-TAILINGS AT TWO SITES IN NEW MEXICO, USA

By

Michelle Paulette Boulet

A Thesis
Submitted to the Faculty of Graduate Studies
in Partial Fulfilment of the Requirements
for the Degree of

MASTER OF SCIENCE

Department of Geological Sciences
University of Manitoba
Winnipeg, Manitoba, Canada

THE UNIVERSITY OF MANITOBA

FACULTY OF GRADUATE STUDIES

*****

COPYRIGHT PERMISSION PAGE

A COMPARATIVE MINERALOGICAL AND GEOCHEMICAL STUDY OF SULPHIDE MINE-TAILINGS AT TWO SITES IN NEW MEXICO, USA

by

MICHELLE PAULETTE BOULET

A Thesis/Practicum submitted to the Faculty of Graduate Studies of The University of Manitoba in partial fulfillment of the requirements of the degree

MASTER of SCIENCE

ABSTRACT

A comparative study of sulphide mine-tailings from two sites near Silver City in southwest New Mexico has shown the need for environmental monitoring in a geological context. The Cyprus-Piños Altos and Cleveland deposits consist of Cu and Zn skarn mineralization in the Piños Altos Mountains of New Mexico. Primary ore minerals in both deposits include chalcopyrite, sphalerite and galena. The Cyprus-Piños Altos Mine ceased operation in 1995 and the Cleveland Mill closed in 1950. The deposits have similar mineralogical characteristics; however, the tailings are different in terms of age, degree of oxidation and method of disposal.

The Cyprus-Piños Altos tailings (CPAT) are stored in a lined, bermed impoundment. They are dominantly water-saturated and there are no secondary phases. The grains are not cemented and show no evidence of primary-mineral dissolution. The geochemical data show a predominantly primary signature. The tailings-pond water is neutral to slightly alkaline (pH from 7 to 8.3), partly as a result of processing methods.

The Cleveland mill tailings (CMT) were deposited in a valley at the headwaters of an ephemeral stream. They are highly oxidized and differentially cemented. They have undergone numerous wet/dry cycles, resulting in extensive oxidation. Secondary minerals predominate, and consist mainly of jarosite, goethite, hematite, and Fe oxyhydroxides and oxyhydrosulphates. The pH of the stream draining the CMT is as low as 2.15. Maximum metal contents in the stream immediately downstream from the tailings are 5305 ppm Zn, 454 ppm Cu, 1.16 ppm Pb, 17.5 ppm Cd, 1.4 ppm As, and 0.01 ppm Hg.

The Cyprus-Piños Altos and the Cleveland deposits had similar primary mineralogical assemblages and geochemical signatures. Because of differences in style of deposition and time since deposition of the tailings, present metal-residence sites differ substantially. The advanced age and well-drained nature of the CMT have promoted extensive oxidation and dissolution of primary phases. In contrast, the saturated condition of the CPAT and the short time since their deposition have resulted in limited alteration of primary minerals. Thus, the CPAT may be viewed as an analogue for the CMT early in its weathering history.

Average Pb concentrations in tailings are 12 times higher than average Cd

concentrations, but average dissolved Pb concentrations in the stream are up to 12 times lower than dissolved Cd concentrations. This relationship indicates that while Pb is relatively immobile, Cd is easily mobilized out of the tailings in dissolved forms. Low mobility of Pb within the tailings and low concentrations of Pb in acidic drainage indicate that this element may be less of a threat to the environment than other, more mobile, toxic elements (e.g., Cd) that are present in lower concentrations in tailings. Zn is highly mobile, due to relatively high solubility of Zn sulphate. Results of mechanical transport of sediment downstream is an important mechanism in mobilizing As from the tailings, while chemical transport appears minimal. Thus, an understanding of mineralogy of tailings and the solubilities of secondary minerals is necessary to accurately predict the toxicity of sulphide mine-wastes.

ACKNOWLEDGMENTS

I would like to give special thanks to my graduate advisor Dr. Adrienne C.L. Larocque for her guidance, criticism and encouragement. Our intense brain-storm sessions provided me with the inspiration for research and the knowledge for scientific interpretation. Throughout the last two years, she's always found time for me and has given me support beyond her call of duty. She has provided me with endless opportunities that I will carry with me throughout my career and my life. G.Y.S.V.G.

I would also like to thank Don Lillie, Candy Ross and Dean Davis from the Mining Remedial Recovery Group for logistical assistance; Cyprus-Piños Altos Corporation for access to the Deming tailings impoundment; Albert Arrey, formerly of Cyprus-Piños Altos Corporation, and Jim Stimac currently of Unocal Geothermal Corporation for assistance with sampling.

I am grateful to Sergio Mejia for his assistance with SEM analysis, Ron Chapman for his patience and assistance with the EMP, Neil Ball and Mark Cooper for their help with XRD analysis, and Wayne Blonski for his help on the ICP. I would also like to thank Ann Brown and Janice Liwanag for their help in the microbiology lab. This thesis would not be possible without the support and encouragement of the faculty, staff and graduate students in the Department of Geological Sciences; thank you to all.

A manuscript arising from this thesis work benefitted tremendously from thorough and constructive reviews by Virgil Lueth and Virginia McLemore of the New Mexico Bureau of Mine. The thesis itself was improved by comments from Dr. Frank Hawthorne and Dr. Hélène Perreault. This research was supported by grants from the University of Manitoba and the Natural Sciences and Engineering Research Council of Canada awarded to Dr. Larocque.

I'd like to give special thanks to Léo Nicolas for his patience, encouragement and support during the last 5 years, as well as his help with the microbiology details; you've been more than wonderful. Finally, I'd like to thank my parents and my brothers for their support and inspiration; you've made me who I am today. Mom and Dad, there are no words to tell you how much you mean to me and how much I appreciate you being there for me; I couldn't have done this without you. Thank you.

Dedicated to my parents,

Robert and Paulette,

my brothers,

Joel, Serge and Daniel,

and

in loving memory

of my grandparents,

Rosario and Yvonne Marion.

TABLE OF CONTENTS

LIST OF FIGURES

LIST OF TABLES

CHAPTER 1

INTRODUCTORY REMARKS

1.1 Introduction

Growing public concern about metal contamination at and around mine-tailings sites has indicated the importance of understanding natural processes that control the mobility of these metals. Aqueous transport of metals is governed by fundamental chemical processes; understanding these processes is necessary to predict and modify how metals move through the environment. In addition to their potential environmental impact, mine-tailings may provide future sources of additional revenue through reprocessing. A comparative mineralogical and geochemical study of sulphide mine-tailings from the Cyprus-Piños Altos mine-tailings (CPAT) and Cleveland mill tailings (CMT) in southwest New Mexico (Fig. 1.1) has shown that a geological perspective on this environmental problem is necessary. Mine-tailings mineralogy is complex, multi-phase and controls the mobility of metals in and out of the tailings environment. Mineralogy and geochemistry of tailings is a function of the type of deposit, grade of ore, proportion of sulphides, and buffering capacity of the tailings, as well as local and regional climate (temperature and precipitation).

Mineralogical studies of mine-tailings are important for developing environmental remediation plans because most ore minerals are very sensitive to changes in environmental conditions, especially temperature, humidity, pH and Eh. Elements released by oxidation and dissolution of primary ore minerals may be incorporated into secondary minerals by precipitation, sorption, or ion exchange, or they may be removed from the tailings in solution,

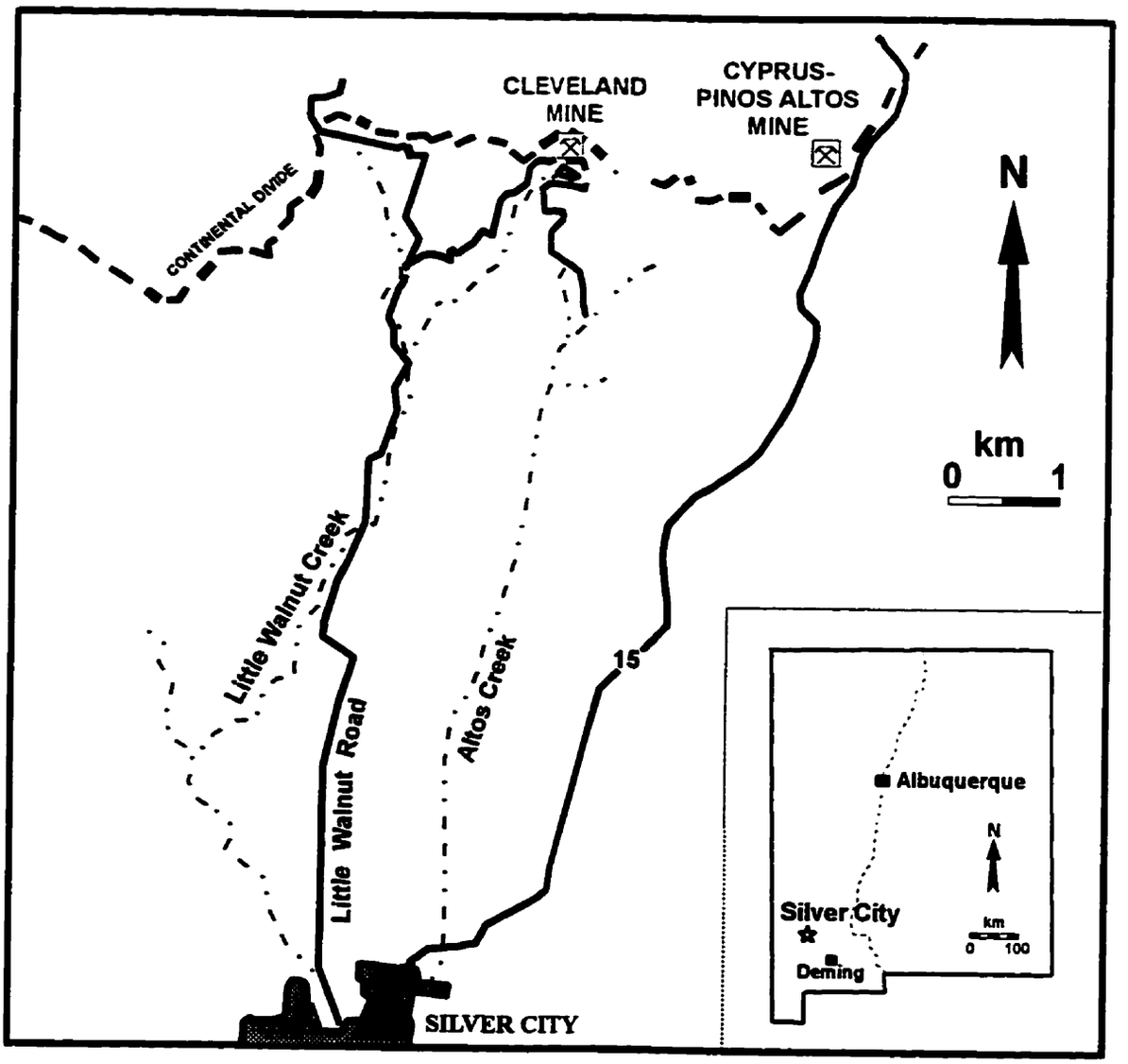

Figure 1.1: Location map of the Cleveland and Cyprus-Piños Altos mines and the Deming mill.

thereby contaminating surface and groundwater. With a thorough understanding of the chemical reactions and mineral transformations that occur in tailings, along with knowledge of the mineralogy and mineral chemistry of the primary assemblage, it is possible to predict the toxicity of mine-tailings and their effluents. This is the first step in preventing mobilization of metals in our environment and in effectively remediating existing sites.

1.2 The Study Sites

The Cyprus-Piños Altos and Cleveland deposits have similar gross mineralogical characteristics; however, the tailings are different in terms of age, degree of oxidation and style of disposal. Over half a million tonnes of tailings from the Cyprus-Piños Altos mine have been deposited at the Deming mill since 1990. The tailings were deposited in a polyethylene-lined, bermed impoundment, beginning in 1992 (Fig. 1.2); prior to 1992, the tailings were deposited in an unlined pond. The principal elements extracted were Cu, Fe and Zn, with Au and Ag as by-products. Table 1.1 shows the average head grades and tailings grades. The Piños Altos mine and mill ceased operation in 1995.

Table 1.1 Head and tailings grades for the Cyprus-Piños Altos mine in 1995.

Element	Ore Grade[1]	Tailings Grade
Cu	5 %	0.15 %
Fe	15 %	11 %
Pb	0.074 %	0.6 %
Zn	0.21 %	0.065 %
Ag	44.3 g/tonne	10.2 g/tonne
Au	0.62 g/tonne	0.093 g/tonne

[1] Albert Arrey, formerly of Cyprus Piños Altos Corporation, personal communication, 1995

The CMT were deposited in a valley at the headwaters of an ephemeral stream at the mill site (Fig. 1.3). The Cleveland mine was actively mined from 1915 to 1945 and periodically mined from 1945 to 1950, at which time the mine was closed (Soulé, 1948; Anderson,

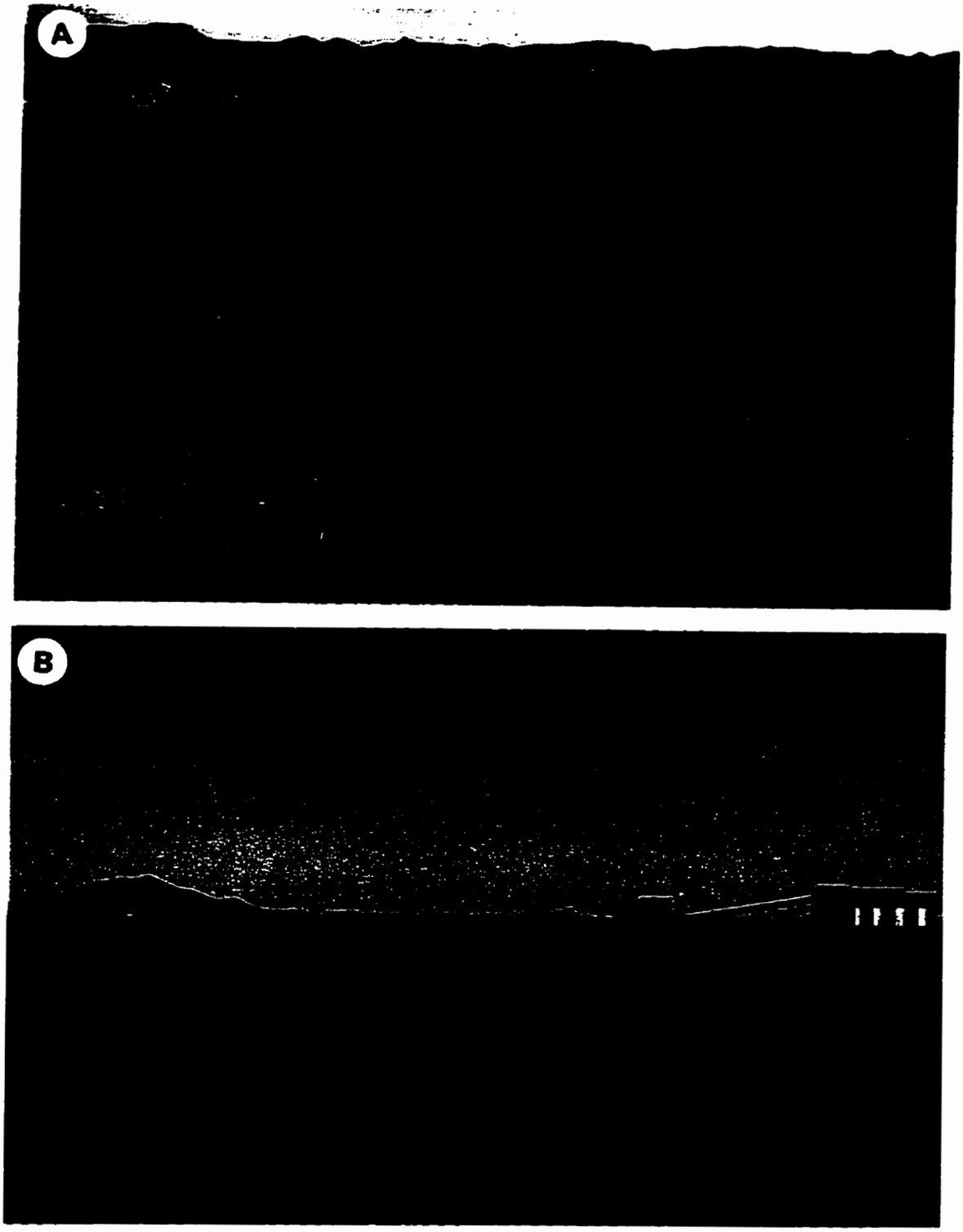

Figure 1.2: Cyprus-Piños Altos tailings impoundment in 1995: (A) polyethylene-lined bermed tailings impoundment with dry and water-saturated tailings; (B) water-filled impoundment with broad tailings cone developed at the spout; the mill is in the background.

1957); the site has since been abandoned. The mine is located approximately 500 m northeast of the mill site. The main tailings pile has a total volume of 22,900 m^3 (U.S. EPA, 1993) and is subdivided into the east pile (CMTE) and west pile (CMTW). At the Cleveland mine, the principal elements extracted were Zn, Cu, and Pb, with Au and Ag as by-products. Table 1.2 shows the range of head grades from 1915-1945, and the average tailings grades as of 1995. The U.S. Environmental Protection Agency has declared the Cleveland mill tailings a Superfund site in 1989 due to the occurrence of high concentrations of As in the tailings, and its generation of acidic metal-rich drainage.

Table 1.2 Range of head grades from 1915-1945 and average tailings grades from 1995 for the Cleveland mine.

Element	Ore Grade[1]	Tailings Grade[2]
Cu	0.2 - 0.563 %	0.061 %
Fe	not available	17.21 %
Pb	0.517 - 2.2 %	0.0058 %
Zn	8.9 - 14.9 %	0.12 %
Ag	46 - 131 g/tonne	53.7 g/tonne
Au	0.062 - 0.31 g/tonne	0.056 g/tonne

[1] Soulé (1948)
[2] Samples collected in 1995

1.3 Tailings: Mineralogical Classification

According to the classification of Jambor and Owens (1993), tailings minerals are divided into four categories: primary, secondary, tertiary, and quaternary. Primary minerals are those that have been finely crushed, mill-processed and deposited in the tailings pile, but

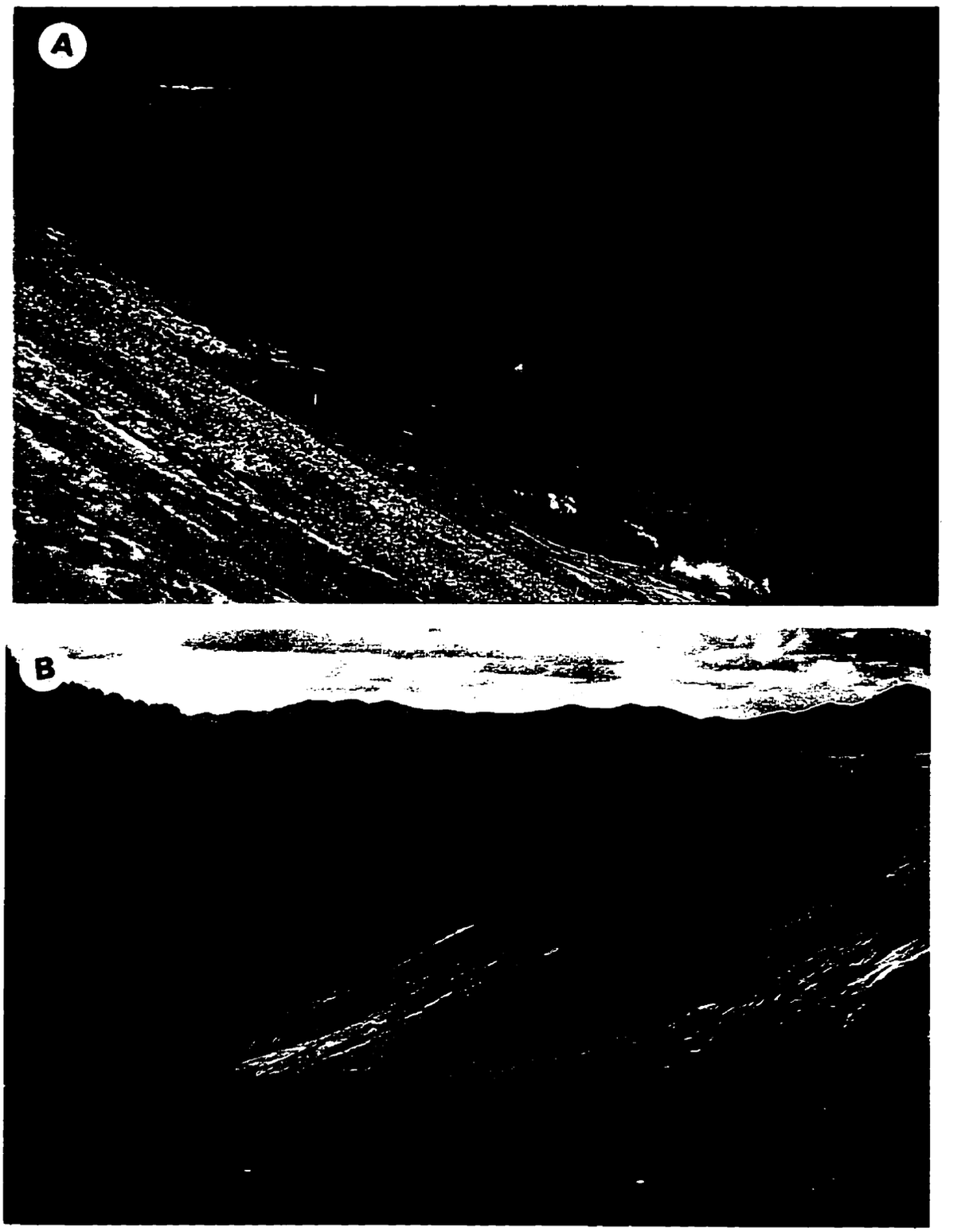

Figure 1.3: Cleveland mill-tailings in 1995 with the (A) east pile and (B) west pile following the wet season; basal wet mark in (A) is the ephemeral stream draining the tailings (mill-valley tributary.

remain unaltered. Secondary minerals are formed within the impoundment by chemical weathering reactions. Tertiary minerals form during the drying of tailings samples once they have been removed from the impoundment, typically by precipitation from pore water. Quaternary minerals form as result of surface oxidation of the tailings samples during storage after removal from the impoundment, once the samples have dried.

1.4 Mechanisms of Oxidation

Sulphide-bearing mine-tailings constitute an environmental problem due to their susceptibility to oxidation. The mechanisms of oxidation are dominated by the presence of: (1) oxygen and water, or (2) S-oxidizing bacteria. The oxidation of pyrite can follow a number of pathways, depending on the pH and Eh of the environment (Ptacek and Blowes, 1994; McIntosh et al., 1997), as in this two-step reaction sequence where S is oxidized (reaction 1), followed by Fe^{2+} (reaction 2):

$$\underset{pyrite}{FeS_2\,(s)} + 7\,O_2 + 2\,H_2O \rightarrow 2\,Fe^{2+}\,SO_4 + 2\,H_2SO_4 \qquad (1)$$

$$Fe^{2+} + \tfrac{1}{4}\,O_2 + H^+ \rightarrow Fe^{3+} + \tfrac{1}{2}\,H_2O \qquad (2)$$

At pH > 4, Fe^{3+} will precipitate as Fe hydroxides (reaction 3), oxyhydroxides and oxyhydrosulphates (Ptacek and Blowes, 1994; McIntosh et al., 1997):

$$\underset{Fe\ oxyhydroxide}{Fe_2(SO_4)_3} + 4H_2O \rightarrow 2FeO{\cdot}OH + 3H_2SO_4 \qquad (3)$$

However, at pH < 4, Fe^{3+} remains in solution and enhances the oxidation of pyrite:

$$14\,\underset{AMD}{Fe^{3+}} + \underset{pyrite}{FeS_2\,(s)} + 8\,H_2O \rightarrow 15\,Fe^{2+} + 2SO_4^{2-} + 16\,H^+ \qquad (4)$$

Thus reaction 4 produces much more acid then reactions 1 and 2. Acid mine-drainage (AMD) is characterized by low pH, high sulphate concentrations, and the presence of dissolved metals, particularly Fe (Gould et al., 1994). Therefore, to minimize pyrite oxidation and AMD generation, the pH must be maintained above 4 for better AMD control.

The presence of S-oxidizing bacteria such as *Thiobacillus thiooxidans* and *Thiobacillus ferrooxidans* (Suzuki et al., 1994; Gould et al., 1994), contribute to the production of AMD. The CMT acidic drainage may be due to these bacteria, whereas the neutral pond waters of the CPAT do not seem to contain these bacteria; both these hypotheses are verified in this study by laboratory experiments. Reaction 5 shows the general oxidizing reactions promoted by these bacteria (Gould et al., 1994; McIntosh et al., 1997)):

$$\underset{\textit{pyrite}}{2\,FeS_2} + 15/2\,O_2 + H_2O \rightarrow 2\,Fe(SO_4)_3 + H_2SO_4 \qquad (5)$$

These oxidation reactions are written in terms of pyrite oxidation, as it is the most common sulphide mineral in mine-tailings. Other sulphides present in the mine-tailings, such as pyrrhotite , sphalerite, chalcopyrite, and galena, may also be oxidized by *Thiobacillus thiooxidans* and *Thiobacillus ferrooxidans* (Greenway, 1996; Boulet, 1995; Spence, 1994). The most acid-producing reaction is that involving pyrrhotite oxidation.

The acid-neutralizing capacity of tailings is governed by a series of buffer reactions described by Ptacek and Blowes (1994). The first buffering reaction is the dissolution of calcite, which maintains the tailings pore water at a pH between 6 and 7. Once the calcite reserve in the tailings is consumed, the pH of pore water drops to approximately 5.5; at this pH, the dominant buffering reaction is the dissolution of siderite ($FeCO_3$). Once the siderite reserves are consumed, the pH of the pore water drops again to between 4 and 4.5, where

aluminum hydroxides (e.g., $Al(OH)_3$) are consumed as the dominant buffering reaction. At this stage, remaining silicates are dissolved completely with the exception of quartz. As the aluminum hydroxides are consumed, the pH drops below 3.0 where the dissolution of iron hydroxides ($Fe(OH)_3$) is the dominant buffering reaction.

1.5 Previous Work

Early tailings studies were related to mine waste dumped into local rivers, lakes and coastal inlets; this method of tailings disposal was thought to be the "ideal tailings pond" (Thompson, 1975). In fact, these tailings ponds caused many problems for local aquatic life. Thompson (1975) studied the effects of Cu-tailings disposal in a coastal inlet on Vancouver Island, British Columbia on benthic organisms and Cu release. The results of that study showed that there had been a decrease in benthic organism population, and Cu release from the tailings by organism perturbation was low. Thompson (1975) concluded that the effects of tailings disposal in natural water systems were primarily physical in nature, where the blanket of tailings overtop the natural sediment reduced benthic food supply dramatically. Release of Cu into the water was low, although some benthic and burrowing organisms had a tendency to ingest Cu.

Lesaca (1975) monitored transition-metal concentrations (Fe, Ni, Cu, Hg) in natural waters that were used as tailings disposal sites in the Philippines. This study found that the siltation effect of tailings affected the ecology of the aquatic environment, and that water quality degradation has negatively impacted agricultural areas and the fishing industry.

Such pioneering studies as those by Thompson (1975) and Lesaca (1975) set many studies

in motion to determine the effects of mine-tailings on rivers, lakes, wetlands and coastal regions. As a result of these sorts of studies, many laws and guidelines are now in place to regulate and, in many cases, prevent such activities.

Much of the current literature on mine-tailings mineralogy and geochemistry has been published in the last decade. The implementation of the MEND (Mine Environment Neutral Drainage) program in Canada shows that the Canadian mining community is aware of and willing to work on the environmental problems plaguing the mining industry. This resulted in many studies and research projects on mine-tailings dynamics.

From 1986 to 1994, a series of reports from the Canadian Centre for Mineral and Energy Technology (CANMET) written done on mine-tailings impoundments, including the Waite Amulet mine-tailings in Québec (Petruk and Pinard, 1986; Jambor, 1986, 1987). These reports documented mineralogical variations in alteration products with depth in the tailings, and the character and depth of oxidation in the tailings. The results of these studies helped to identify the "typical" oxidized-tailings minerals such as goethite, lepidocrocite, ferrihydrite, jarosite and gypsum (Jambor, 1986); Jambor (1987) observed a distinct separation between oxidized/unsaturated zones above the water table and unoxidized/saturated zones below the water table.

Another CANMET study was done on the Heath Steele old tailings impoundment in New Brunswick, focusing on tailings characterization in terms of mineralogical variations (Jambor and Blowes, 1989) and mineral dissolution (Jambor et al., 1992). Observations by Jambor and Blowes (1989) are similar to those of Jambor (1987) in his study on Waite Amulet; they documented abundant Fe oxides/oxyhydroxides in the oxidized zone, and minimal

alteration/dissolution in the unoxidized zone. Jambor et al. (1992) documented strong evidence for silicate- and carbonate-mineral dissolution in the low-pH zone (vadose zone) of the impoundment.

Other than mineralogical studies, studies on different aspects of mine-tailings include: acid-mine drainage (Taylor and Wheeler, 1994; Scharer et al., 1994; Orava and Swider, 1996; Alpers et al., 1994; Blowes and Ptacek, 1994; Bell and Bullock, 1996), pore-water chemistry (Kalin et al., 1992; McGregor, 1994; Al et al., 1994) , tailings physical hydrology (Robertson, 1994), tailings impoundment modelling and remedial engineering (Frind and Molson, 1994; Barbour et al., 1996), and tailings microbiology (Gould et al., 1994; Suzuki et al., 1994).

The southwest part of New Mexico has been an important mining district; many mines have been abandoned while others are still in operation. This mining district has been active for over a century, during a time when mine wastes were disposed of carelessly (i.e., without any attempt to protect the environment). The Hanover tailings and Bullfrog tailings sites, located in the same county as the Cleveland site, have received attention due to their oxidized nature and potential for acid generation (Baker, 1993; Walder et al., 1994). The Bullfrog site has since been remediated by consolidation of all tailings piles into a single pile, grading of slopes, and topsoil coverage and seeding (Baker, 1993).

Walder et al. (1994) did an element mobility study on the Bullfrog, Hanover and Cleveland tailings. In contrast to the results of this study for the Cleveland site, their results concluded that pre-mining alteration was the primary cause of alteration of sulphides, notably pyrite, and the acid-neutralizing potential of the tailings was positive (i.e., AMD would not

occur). Walder (1993a, 1993b) suggested that the chemical variations with depth at Bullfrog and Hanover were the result of variations in ore recovery rather than oxidation and leaching of metals. Baker (1993) studied the Hanover and Bullfrog sites with regard to metal mobility in soils and tailings. The results of her study showed that element mobility by dissolved aqueous transport is low for these sites, and that windblown particulates are the dominant form of metal distribution into the local environment.

Studies on the Cleveland site started in 1989 with the declaration of the site as a U.S. EPA Superfund site. A remedial investigation (RI) report was done to assess the health and safety of the site and degree of groundwater contamination caused by AMD, and to propose remediation methods. The RI concluded that (1) the site would have some long-term effects on human health, but these effects are strongly dependent on the exposure time of the individual to the tailings; (2) groundwater contamination is low to non-existent, and does not affect nearby wells; (3) remedial measures should be taken, the most acceptable and cost effective being off-site reprocessing/recycling of metals, followed by off-site stabilization/solidification of the tailings and off-site disposal and capping (U.S. EPA, 1993).

Bench-scale treatability studies were done to see if reprocessing/recycling of metals is effective (Ecology and Environment, 1993a), and to identify the best method of stabilization/solidification (Ecology and Environment, 1993b). Reprocessing was found to be ineffective due to the abundance of Fe oxide/oxyhydroxides (U.S. EPA, 1994). No method of stabilization/solidification was proposed, but the use of a cement-based agent was recommended due to its acid-neutralization potential (Ecology and Environment, 1993b; U.S. EPA, 1994).

Despite the feasibility studies on the Cleveland site, no decision has been reached as to what the future of the site will be, and to this day, the tailings remain untreated. However, some attempts have been made to neutralize the AMD by the construction of a limestone dam downstream, and the emplacement of sediment traps to minimize mechanical transport of tailings downstream. The CPA tailings have not been studied previously.

1.6 Purpose of Study

The objectives of this study are as follows: (1) to identify residence sites of transition metals in minerals and in the tailings impoundment, and relate mineral transformations that occur during weathering to the generation and composition of acidic drainage; (2) to compare the two sites in terms of mineral reactions and geochemical signatures; (3) to investigate the processes which control metal mobility in mine-tailings and nearby drainage waters.

1.7 Contributions of this Study

The approach taken in this study is, in some aspects unique, and has not been previously attempted for mine-tailings studies. For example, the mobility of metals from their primary host to secondary host is predicted using variation diagrams, a form of geochemical representation often used in igneous and metamorphic petrology. The reasons for this approach is two-fold: (1) the tailings were too dry to use the conventional approach of pore-water chemistry examination; (2) no literature discusses element mobility in a *semi-arid* environment; therefore, a different approach had to be taken to study this problem.

CHAPTER 2

GEOGRAPHICAL AND GEOLOGICAL SETTING

2.1 Mining History

The Piños Altos mining district, Grant County, New Mexico, contains many mines, most of which were active in the mid-1800's to mid-1900's. This historic mining district is centered on the Piños Altos Mountains, approximately 12 km north of Silver City. Both the Cleveland and Cyprus-Piños Altos deposits occur in the Piños Altos mining district. In 1860, the first mining camp, Birchville, thrived; it was named after it's discoverer/founder, Mr. Birch (Wootton, 1940), and was later renamed Piños Altos, as it remains today. Piños Altos was a prominent Au-mining town due to the occurrence of rich placer deposits. Two years following the first discovery, Au was discovered and mined (Lindgren et al., 1910). Although Au was the primary metal mined, Ag, Cu and Pb were mined by at least 1903 (Lindgren et al., 1910). With the discovery of limestone-replacement ore bodies, Zn started to be mined and recovered after 1910, at which time the mining products of Pb and Zn became as popular as Au in this district (Lasky and Wootton, 1933). The Cleveland deposit had been discovered by 1910, but active mining at this site only started in 1915 for Pb, Zn, Cu, Au and Ag (Paige, 1910; Soulé, 1948). The Cleveland deposit was mined intermittently from 1915 to 1950, at which time the site was abandoned. A mill for the Cleveland ore was built 500 m from the mine, and the tailings were deposited at the mill site. In 1915, the Piños Altos mine reported having ore-recovery difficulties (Bush, 1915), and was closed shortly after.

In 1971, the Exxon Company, USA, prospected undiscovered deposits in the old Piños

Altos mining district (McKnight and Fellows, 1978). Drilling at Piños Altos encountered Pb-Zn mineralization. The mine opened, but closed a few years later. In 1990, this mine was re-opened, and the resultant tailings (which are the tailings sampled for this study) were stored in the new CPA tailings impoundment in Deming.

2.2 General Geology

The mineral deposits of the Piños Altos mining district are located in a contact metamorphic/metasomatic aureole surrounding the Piños Altos granodiorite stock (Fig. 2.1; McKnight and Fellows, 1978). The Piños Altos stock makes up the majority of the Piños Altos mountain peaks. The Piños Altos Mountains are underlain by a faulted, east-dipping Pennsylvanian-age sequence of quartzite and limestone (Ecology and Environment , 1993c). During the Laramide orogeny in the Late Cretaceous, compressional tectonics resulted in the emplacement of the Piños Altos granodiorite stock and many diorite porphyry dikes and sills in contact with Pennsylvanian sediments (Paige, 1910; McKnight and Fellows, 1978; North and McLemore, 1986). This intrusion resulted in the formation of two types of deposits: (1) fissure filling in intrusive rocks; (2) mineral replacement in limestone (Paige, 1910), occurring mostly in the Oswaldo Limestone Formation of the Magdalena Group. The Cyprus-Piños Altos deposit is located in the higher-temperature Cu-rich zone of alteration (Fig. 2.1; McKnight and Fellows, 1978) which contains both types of mineralization, and is classified as a Cu skarn. The Cleveland deposit is located in the lower-temperature Zn-Pb-Ag zone of alteration (Fig. 2.1); it consists of only mineral-replacement bodies in impure, shaley limestone, and is classified as a Zn skarn (Bush, 1915; North and McLemore, 1986). In both

deposits, the most common ore minerals are chalcopyrite, sphalerite, galena, pyrite and minor smithsonite (a supergene alteration product of hydrothermal sulphide mineralization). Au and Ag occurred mainly as fissure fillings in the Cyprus-Piños Altos deposit, and as by-products in the Cleveland deposit. Common gangue minerals in both deposits include quartz, calcite, garnet, magnetite, hematite, epidote, hedenbergite, wollastonite and diopside (North and McLemore, 1986; Walder et al., 1994).

2.3 Tailings-Site Geology

The limestone formations underlying the Cleveland mill and mill-valley tributary are Pennsylvanian-age Oswaldo and Colorado Formations. A northeast trending west-dipping fault can be traced through the centre of the main tailings pile, parallel to the walls of the valley. The west pile overlies the Beartooth Quartzite and the east tailings overly the Oswaldo Limestone Formation. Downstream from the mill, Little Walnut Creek stream bed is underlain by the Colorado Limestone Formation, the groundwater aquifer for local domestic wells downstream (Ecology and Environment, 1993c).

The Cyprus-Piños Altos mine is located near the town of Piños Altos on the eastern slope of the Piños Altos Mountains. The Cyprus-Piños Altos ore was transported to the town of Deming, New Mexico, for mill processing (Fig. 1.1). These tailings were deposited in a polyethylene-lined bermed impoundment. The Piños Altos tailings impoundment is located on flat-lying unconsolidated Quaternary alluvium.

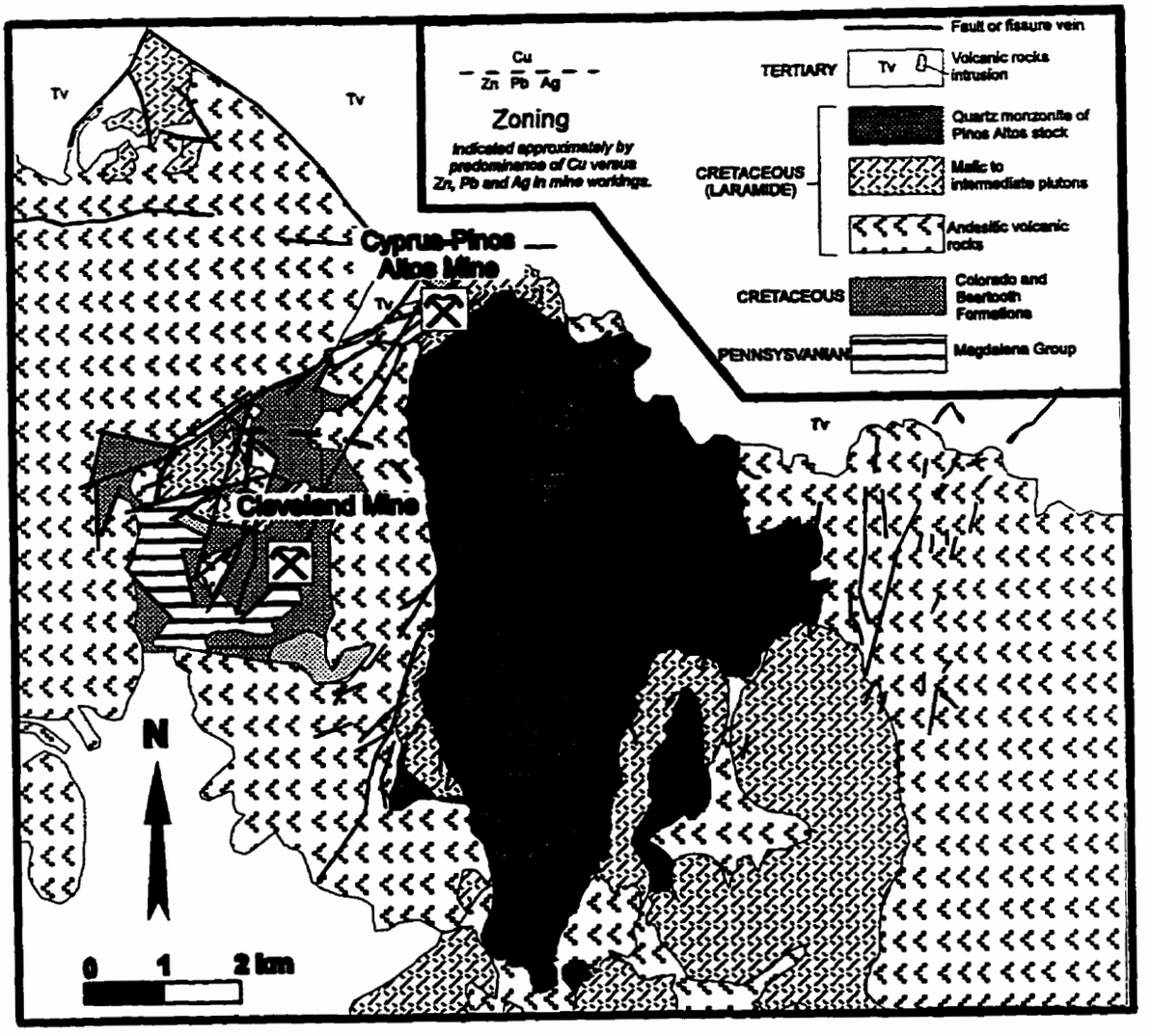

Figure 2.1: Geological map of northeastern part of the Grant County mining district, New Mexico (modified from McKnight and Fellows, 1978).

2.4 Geographical Setting

The climate of southwestern New Mexico around Grant County is variable, but is classified as semi-arid because evaporation exceeds precipitation in most areas (Trauger, 1972). In the desert lowlands where Deming is located, the climate is closer to arid; there is a strong southwest-prevailing wind direction. Precipitation occurs mostly during the summer

months as evening thundershowers; annual precipitation averages 40 cm (Baker, 1993). The CPAT impoundment is located in the flat, arid, Chihuahuan desert lowland. The Cleveland mine and mill site (Fig. 2.2) is located 3 km west of Piños Altos, in the semi-arid, mountain woodland on the western flank of the Piños Altos Mountains.

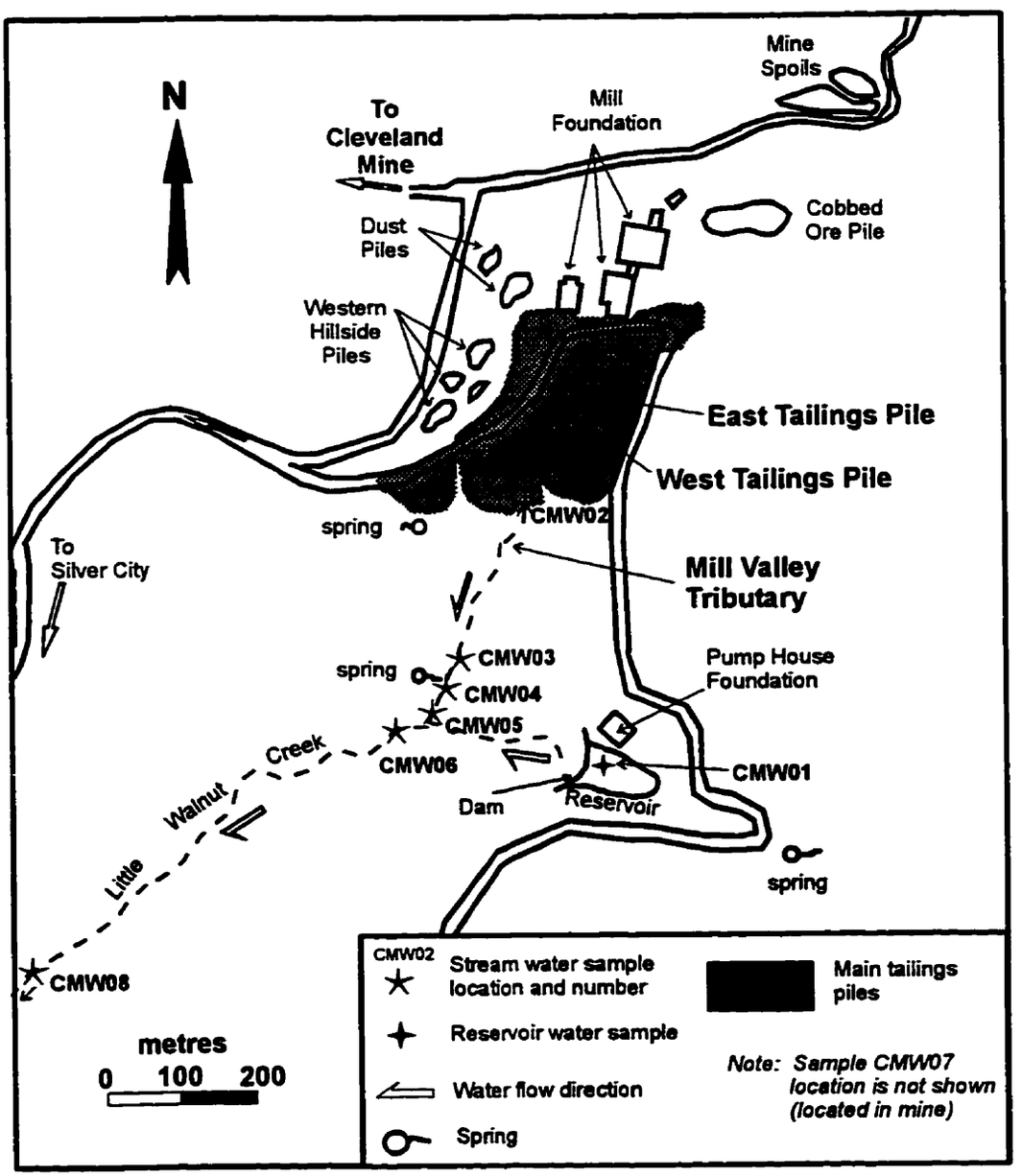

Figure 2.2: Cleveland mill-tailings site with stream-water sample locations (modified from Ecology and Environment, 1993c).

CHAPTER 3

METHODOLOGY

3.1 Sample Collection

Two trips were taken to the study sites. In February 1995, Adrienne Larocque and Jim Stimac collected tailings and water samples, took photographs and made observations at both sites. These samples are the subject of this thesis. During a return trip in November 1996, Adrienne Larocque and I collected tailings and waters samples at the CMT site for further study at a later date. Photographs were taken and observations were made, some of which are presented in this thesis.

In February 1995, one third of the CPAT impoundment had tailings exposed above the pond water level; the mill closed in August 1995 as additional tailings were deposited. At the time of the visit in November 1996, the mill was closed and the impoundment was two thirds to three quarters full. A sprinkler system was set up to help evaporation of the remaining pond water (Fig. 3.1). A strong southwesterly wind blew over the tailings impoundment; this caused the dry tailings to be blown out of the impoundment and deposited downwind, preferentially around vegetation (Fig. 3.1). During the first visit, the polyethylene lining was in good condition; during the second visit, the lining was extensively torn in several places along the edges (Fig. 3.2).

Samples of the tailings and the surrounding waters were collected at both sites in February 1995. Tailings samples were chosen according to differences in grain size, water saturation, colour and cementation. At the Cyprus-Piños Altos tailings impoundment, a

Figure 3.1: Cyprus-Piños Altos tailings impoundment in 1996 with sprinkler system to accelerate evaporation of pond water (whitish area as along the far wall); and windblown tailings collecting around vegetation outside of the impoundment (foreground).

Figure 3.2: Torn polyethylene lining of the Cyprus-Piños Altos tailings impoundment in 1996.

vertical sequence of six tailings samples (PAT003 to PAT008) was collected at 15 cm vertical intervals (Table 3.1) using a hand-held auger. Surface tailings also were collected, as was tailings pond water. Due to the physically unstable nature of much of the subaerial tailings material, sampling was restricted to a small region of the impoundment for safety reasons. At the Cleveland mill-tailings impoundment (Fig. 2.2), a sequence of four tailings samples (CMT001 to CMT004; Table 3.1) was taken from an erosional trench which exposed the tailings stratigraphy. Surface samples also were collected from both the east (CMT001 to CMT007) and west (CMT008 to CMT011, CMT013) piles. One stream-sediment sample was collected (CMT012). Water samples were collected at various locations along the mill-valley tributary which drains the tailings piles and empties into Little Walnut Creek. Upstream from this confluence, Little Walnut Creek has been dammed to form a reservoir (Fig. 2.2).

Table 3.1 Vertical sequence depth to samples.

CPAT Sample #	Depth in vertical sequence (cm)	CMT Sample #	Depth in vertical sequence (cm)
PAT003	4	CMT001	0
PAT004	25	CMT002	11
PAT005	40	CMT003	14
PAT006	55	CMT004	46
PAT007	70		
PAT008	85		

Dry and slightly moist tailings samples were collected in resealable plastic bags. Moist and water-saturated tailings and stream-sediment samples were collected in 1 L Nalgene bottles.

Water samples were filtered through 0.45 μm-pore filter paper in a magnetic holder and collected in a side-arm flask. The flask was rinsed with the first volume of filtrate in order to "precontaminate" the flask. The second volume of filtrate was stored in 125 mL Nalgene bottles. At the time of collection, the temperature and pH of the waters were measured using a pH/temperature meter. After filtering, the waters were acidified to a pH between 1.5 to 2 with concentrated nitric acid to prevent any dissolved metals from precipitating.

3.2 Sample Preparation

Tailings samples were dried in covered watch glasses. Once dry, a 60-mL volume of each bulk tailings sample was crushed to a fine powder using a tungsten-carbide crucible and ring grinder. Selected dry uncrushed CPAT samples (PAT001 to PAT008) were sieved using stainless steel sieves numbers 5 (> 4 mm), 10 (4-2 mm), 18 (2-1 mm), 35 (1-0.5 mm), 60 (0.5-0.25), 120 (0.25-0.125 mm), and 230 (0.125-0.062 mm) for grain size analysis. CMT was not sieved due to the variable degree of cementation of the grains. Bulk powdered samples were mounted on glass slides by the acetone-slurry method for X-ray diffraction analysis (XRD). Water samples were filtered again immediately before ICP analysis.

Bulk samples were mounted on stubs for scanning-electron microscope (SEM) analysis. Samples of bulk tailings also were impregnated with epoxy and made into polished thin-sections. Highly-cemented samples were cut perpendicular to the layering within the sample. Caution was taken during the slide preparation to prevent water contact with delicate and soluble secondary- and tertiary- mineral assemblages; oil-based products were used as cooling agents during cutting.

3.3 Analysis of Tailings and Water Samples

3.3.1 Water-sample Analysis

At the University of Manitoba, samples of acidic drainage, reservoir water and tailings pond water (CMW 01 to CMW 02 for CMT stream water; PATW 01 and PATW 02 for CPAT pond water) were analyzed with a Liberty 2000 inductively- coupled plasma (ICP) emission spectrometer for dissolved metals (Ag, As, Cd, Cu, Fe, Hg, Pb, total S, Se and Zn). Detection limits for each element are listed in Appendix A.

3.3.2 Bulk Tailings Sample Analysis

Crushed bulk samples (minimum of 2 g) were sent to Activation Laboratories in Ancaster, Ontario, for geochemical analysis. A total of 46 elements was analyzed in each sample using a combination of instrumental neutron-activation analysis (INAA) and ICP methods (Actlabs package 1H). Detection limits are listed in Appendix B. Sulphide (S), sulphate (SO_4) and carbonate (as evolved CO_2) were determined by Leco combustion, using an infrared detector (Actlabs package 4F). Structurally-bound water and residual moisture (H_2O^+ and H_2O^-, respectively; Rollinson, 1993) was determined by gravimetry. The geochemical results aided in the identification of mineral phases by limiting the XRD peak search to minerals and inorganic phases containing particular elements.

3.3.3 Mineral Identification

Two methods of X-ray diffraction were used to help identify the minerals in each sample. Using a Philips X-ray generator with a fully-automated PW 1710 X-ray powder system,

continuous scans from 3° to 70° were done on all the CPAT samples and selected CMT samples (excludes CMT013). The resulting diffractograms (Appendix C) were entered into a computer and a mineralogical search was done using PEAKSEARCH Micro Powder-diffraction Search Match software (μPDSM) to identify the major crystalline phases present in the samples. The CMT samples gave poor search results due to the nature of the minerals and the limitations imposed by the continuous-scan method. Selected CMT samples were re-analyzed using a step-scan on the same XRD instrument. The step-scan conditions used were: starting angle of 10°, finishing angle of 70°, step increments of 0.1°, and counting-time interval of three seconds. The step-scan method provides better peak resolution, and therefore identified phases which were not found in the results of the continuous-scan analysis. The criteria for a positive mineral identification was a high similarity index (> 60), a maximum of 3 to 9 lines missing in the pattern (depending on the intensity of the lines and total number of lines for a given pattern), and a compatible relative intensity.

In an attempt to identify individual minerals in the CMT, the Gandolfi XRD method was used. A pin-head size portion of a single phase was isolated from a sample and mounted on a glass fibre. The mount was then installed and centered in a 114 mm Gandolfi camera and exposed to X-rays for 4 hours. Once the X-ray sensitive film was developed, the diffraction lines were measured and their relative intensity determined. This information was entered into the computer and analyzed by the PEAKSEARCH software. The Galdolfi camera was used only on one separated phase due to the amount of time needed to do each sample.

3.3.4 Mineral Analysis

Mineral analysis was done both quantitatively using a Cameca SX50 electron-microprobe(EMP) and qualitatively using a Cambridge Instrument Stereoscan 120 SEM . Selected grain-mounts and thin-sections were observed by SEM, and EDX spectra were used to identify the major elements present, and subsequently to help determine the minerals present. Selected grains in thin-sections were quantitatively analyzed using an electron microprobe (Appendix D). Primary sulphides were quantitatively analyzed from ore and tailings samples; secondary phases were unstable under the electron beam, and were therefore not analyzed quantitatively. The standards used for EMP analysis were pyrite ($2FeS_2$) for Fe and S; sphalerite (2ZnS) for Zn and S; chalcopyrite ($2CuFeS_2$) for Fe, Cu and S; cobaltite (4Cobalt) for Co, Cd and As; and chromite (4Chromite) for Cr. The analyses were all done with an accelerating voltage of 20 kV and beam current of 20 nA.

3.4 Bacterial-Growth Procedure

All ecosystems consist of an integral assortment of bacterial species that live together and are dependent on each other for survival; this interdependence makes the isolation of a single bacterial species very difficult. To isolate certain bacterial species, a medium is designed to optimize the growth conditions of a certain bacterium (e.g. pH, temperature, nutrients). This allows preferential growth of a certain species of bacteria.

Bacteria have been known to thrive in tailings environments, and are commonly the cause of AMD (Gould et al., 1994). To verify if there are any active bacteria in the CPAT and CMT, two different growth media, one for each site, had to be used, due to the different pH

of the two sites. The growth medium used to inoculate CMT012 is designed to optimize the growth conditions of *T. ferrooxidans* and *T. thiooxidans* (Suzuki et al., 1990). Therefore, if evidence of bacterial growth is seen in the flasks inoculated with this growth medium, this indicates that *Thiobacillus ferrooxidans* and *Thiobacillus thiooxidans* are present. In contrast, the growth medium used to inoculate PAT001 has a higher pH, and would optimize the growth of mesophiles (i.e., bacteria with a pH range of 6.0-8.0; Gould et al., 1994). Some of these mesophiles may include *Thiobacillus thioparus*, *Thiobacillus denitrificans*, and *Thiobacillus novellus* (Kuenen et al., 1992; Gould et al., 1994).

One water-saturated sample from each site was used to check for the presence of bacteria. The CPAT sample PAT001 included tailings and water (mostly effluent water); the CMT sample chosen was CMT012. Sample CMT012 is a saturated stream-sediment sample; due to the low water-content of the CMT, the stream-sediment sample was the only water-saturated sample from this site.

A portion of CMT012 was inoculated to see if there were any bacteria present. A growth medium described by Suzuki et al. (1990) was used, and consists of 0.2 g $(NH_4)_2SO_4$, 0.1 g K_2HPO_4 and 0.4 g $MgSO_4 \cdot 7H_2O$, diluted with deionized water to a total volume of 1L; concentrated HCl was added to adjust the pH to 2.3. 90 mL of growth medium was added to three erlynmeyer flasks and capped with a foam stopper.

The erlynmeyer flasks and medium were put in an autoclave in order to sterilize the bottles and liquid medium. In order to minimize airborne bacterial contamination, aseptic techniques were used; each time the foam stopper was removed, the flask was flamed, both before and after the addition or removal of a substance, and the flask was held at an angle.

A bulk Fe solution was made by dissolving 10 g $FeSO_4 \cdot H_2O$ in a 250-mL beaker of deionized water; the pH was then adjusted to 2.3 by adding 10 mL of 95% H_2SO_4. The Fe solution was filter sterilized (Suzuki et al., 1990) to remove any bacteria present in the components making up the Fe solution, and then stored in a sterilized Nalgene bottle. In each erlynmeyer flask, 10 mL of the Fe solution was added to the medium, giving a final volume of 100 mL. Using a metal spatula, a small amount (~ 1-2 g) of CMT012 sediment and water was added to each erlynmeyer, and then let sit at room temperature for six weeks.

To inoculate PAT001, a different medium was used due to the neutral pH of the sample water. The medium used for the CPAT sample is commonly used for the growth of bacteria on magnetite (Brown et al., 1997). The growth medium consists of 5 g ammonium citrate, 0.5 g K_2HPO_4, 0.5 g $MgSO_4 \cdot 7H_2O$, and 0.2 g $CaCl_2 \cdot 2H_2O$ dissolved in 1L of water; the pH was adjusted to 6.8. The Fe solution consisted of 1 g $FeCl_2$ dissolved in 250 mL of deionized water. Three erlynmeyer flasks were prepared with 90 mL of medium and 10 mL of Fe solution, and sterilized in the autoclave. A small sample (~ 1-2 g) of tailings and water from PAT001 was added to the sterilized medium, and left to sit at room temperature for six weeks. The same precautions for airborne contamination were taken.

During the six weeks of incubation, all flasks were occasionally agitated and observations were made. At the end of six weeks, all PAT001 flasks showed evidence of bacterial growth, whereas the CMT012 did not. To verify if the bacteria in PAT001 were acidophile (i.e., bacteria that thrive at pH < 4), and include *Thiobacillus ferrooxidans* and *Thiobacillus thiooxidans*, approximately 2 mL of the liquid in a inoculated PAT001 flask was transferred into two of the inactive CMT012 inoculate flasks; the third CMT012 flask was not re-

inoculated and was kept as a control. The re-inoculated CMT012 flasks were left at room temperature for two weeks; periodical shaking and observations were made.

Prior to inoculation and periodically during inoculation, a drop of each sample was observed under the microscope in oil immersion at a magnification of 1000 to look for the presence of any bacteria.

CHAPTER 4

CYPRUS-PIÑOS ALTOS MINE-TAILINGS RESULTS

4.1 Mineralogy

The Cyprus-Piños Altos tailings (CPAT) have a buff-grey colour and are dominantly water-saturated, except near the effluent spouts where dry to slightly moist tailings form a broad cone. During processing, ore from the Cyprus-Piños Altos mine was crushed to a very fine sand size where 65 percent of the grains were ≤ 125 μm in diameter and 100 percent of the grains were ≤1 mm in diameter. The primary sulphide-tailings mineralogy (Table 4.1) consists of pyrite, chalcopyrite, sphalerite, and galena; McKnight and Fellows (1978) also identified bornite, arsenopyrite and tetrahedrite. Gangue minerals include calcite, quartz, magnetite, grossular, diopside, and andradite; North and McLemore (1986) also identified wollastonite and hedenbergite. Of the primary-mineral assemblage, calcite, quartz

Table 4.1 Cyprus-Piños Altos tailings primary mineralogy.

Major Sulphide Ore Minerals	Minor Ore Minerals	Major Non-sulphide Gangue	Minor Non-sulphide Gangue
pyrite chalcopyrite sphalerite galena	bornite arsenopyrite tetrahedrite tennantite covellite	calcite quartz magnetite grossular andradite diopside	wollastonite hedenbergite hematite

and pyrite are dominant, also making up the majority of the coarser grain-size fraction. Petrographic analysis of the tailings shows that these tailings are little altered, lacking any

evidence of significant dissolution of primary minerals. A lime slurry was added to the tailings during processing to maintain a neutral to slightly alkaline pH. The alkaline nature of the tailings pond water is above the pH needed for the dissolution of calcite (Ptacek and Blowes, 1994). The absence of calcite-buffering reactions is supported by the presence of pristine calcite grains with angular grain boundaries (Fig. 4.1).

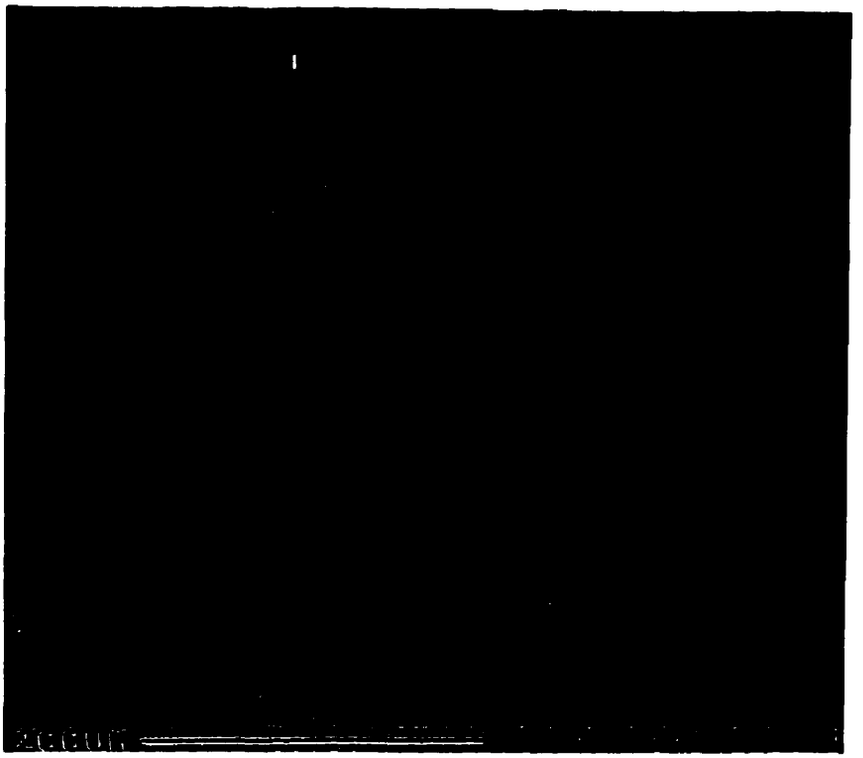

Figure 4.1: False-colour backscattered-electron (BSE) scanning-electron-microscope (SEM) image of calcite in CPAT. The calcite has smooth cleavage edges, indicating that calcite dissolution is not occurring.

Secondary minerals are absent in these tailings. Tertiary minerals occur throughout the dried tailings samples, mostly as precipitates coating primary-mineral surfaces. The only tertiary mineral identified is gypsum, which occurs mainly as microscopic rosettes in fractures

and at corners of the grains, or as radiating clusters of crystals along grain edges (Fig. 4.2). Gypsum occasionally coats entire grains. Quaternary minerals have not been identified.

Figure 4.2: Secondary-electron (SE) image of tertiary gypsum rosettes on the surface of diopside from CPAT.

4.2 Geochemistry

Table 4.2 summarizes compositional data for tailings and ore concentrate from the Cyprus-Piños Altos deposit. Sulphide S contents in the CPAT range from 1.10 to 2.44 wt. %. Sulphate contents range from below detection (< 0.01 wt. %) to 0.95 wt. %. Structurally-bound water content (H_2O^+) ranges from 0.75 wt. % to 1.84 wt. %. Carbonate values range from 4.9 to 11.1 wt. %. Solid-phase tailings metal concentrations range from 715 to 9702 ppm (parts per million) for Cu, 197.5 to 1060.5 ppm for Zn, 111 to 948

Table 4.2 Geochemical data for CPA tailings and concentrate.

Elements	Al	Ag	Au	As	Ca	Cd	Cu	Fe	K	Na	Pb	Sb	Zn	S	SO_4	CO_2	H_2O^+
Units	wt.%	ppm	ppb	ppm	wt.%	ppm	ppm	wt.%	wt.%	wt.%	ppm	ppm	ppm	wt.%	wt.%	wt.%	wt.%
Errors	±0.01	±0.05	±1	±1	±0.005	±0.1	±1	±0.01	±0.01	±0.01	±1	±0.1	±0.5	±0.01	±0.001	±0.001	±0.01
PAT001	2.29	8.30	215	110	16.800	4.1	2228	12.10	0.33	0.09	314	50.0	560.5	1.35	0.030	7.25	0.91
PAT002	2.34	15.40	430	83	16.985	7.9	9702	12.80	0.25	0.05	615	38.0	1050.0	2.44	0	6.26	0.76
PAT003	2.25	15.8	398	91	17.420	7.6	6931	15.10	0.16	0.04	948	36.0	1060.5	2.49	0	5.31	0.86
PAT004	2.61	9.90	430	60	17.105	4.0	4245	12.50	0.24	0.09	278	19.0	560.0	1.60	0.897	4.90	0.77
PAT005	2.49	6.10	252	51	19.265	2.5	2363	12.70	0.27	0.08	167	10.0	437.0	1.07	0.428	5.89	0.83
PAT006	2.36	8.40	388	42	18.550	3.5	2871	12.40	0.29	0.08	137	9.0	547.5	1.10	0	6.66	0.77
PAT007	2.55	9.35	330	47	18.710	3.4	2683	10.90	0.32	0.10	124	9.9	534.0	1.29	0.0329	7.98	0.88
PAT008	2.62	9.80	828	43	18.815	2.9	2056	11.10	0.32	0.09	111	5.7	500.0	1.20	0.508	8.45	0.75
PAT009	2.42	6.75	149	96	16.650	2.2	1113	10.30	0.49	0.11	231	41.0	437.5	1.14	0.945	11.10	1.84
PAT010	2.29	1.25	90	70	18.510	1.9	715	10.40	0.34	0.08	265	30.0	197.5	0.921	1.560	8.64	1.30
PAT011	2.57	6.30	287	57	17.840	3.9	2651	11.80	0.30	0.11	167	24.0	590.0	1.26	0.179	5.75	1.13
PAT012[+]	0.34	161.05	2280	290	2.190	78.7	99999	24.00	0.03	0.01	1444	220.0	8712.0	24.40	0	0.06	2.56

[+] mill concentrate

Detection limits are listed in Appendix B.

ppm for Pb, 6.1 to 15.8 ppm for Ag, and 90 to 823 ppb (parts per billion) for Au.

A vertical sequence of six tailings samples (PAT003 to PAT008) was collected at 15 cm intervals. The tailings in the section range in grain-size from coarse to medium sand; they are grey-brown to brown in colour, and are progressively more water-saturated with increasing depth in the section. Geochemical depth-profiles are shown in Figure 4.3. Similar trends can be observed for sulphide S, Ag, Cd, Cu, As, Pb, Sb, Fe and Zn, where the upper-most interval is enriched in these elements and concentrations decrease in abundance with depth. In contrast, the CO_2, SO_4 and Al depth-profile shows the reverse trend, increasing with depth. The amounts of structurally-bound water (H_2O^+) approach detection limits throughout the section.

Geochemical variation diagrams for metals in the CPAT are shown in Figures 4.4 and 4.5; for the metal species plotted, positive linear correlations exist. Best-fit lines were derived using a linear regression. The variation diagrams in Figures 4.6 and 4.7 all show negative correlations with the exception of Figures 4.6E and 4.7E, which have a positive correlation. In Figure 4.5F, all the samples, with the exception of one, plot below the oxidation line in the unoxidized field. Figures 4.5, 4.6 and 4.7 have mixing lines plotted for common minerals. For example, in Figure 4.5A, the mixing line shows the relationship between a pyrite-rich and pyrite-poor assemblage; this will be hereafter referred to as the pyrite line. In Figure 4.5, the CPAT assemblage falls above the pyrite line, and below the sphalerite, covellite, chalcopyrite, galena, arsenopyrite, and tennantite lines. In Figure 4.6, the CPAT assemblage has a low sulphate content overall, and falls above the jarosite, rozenite, and gypsum lines, but below the goslarite, chalcanthite and galena lines. In Figure

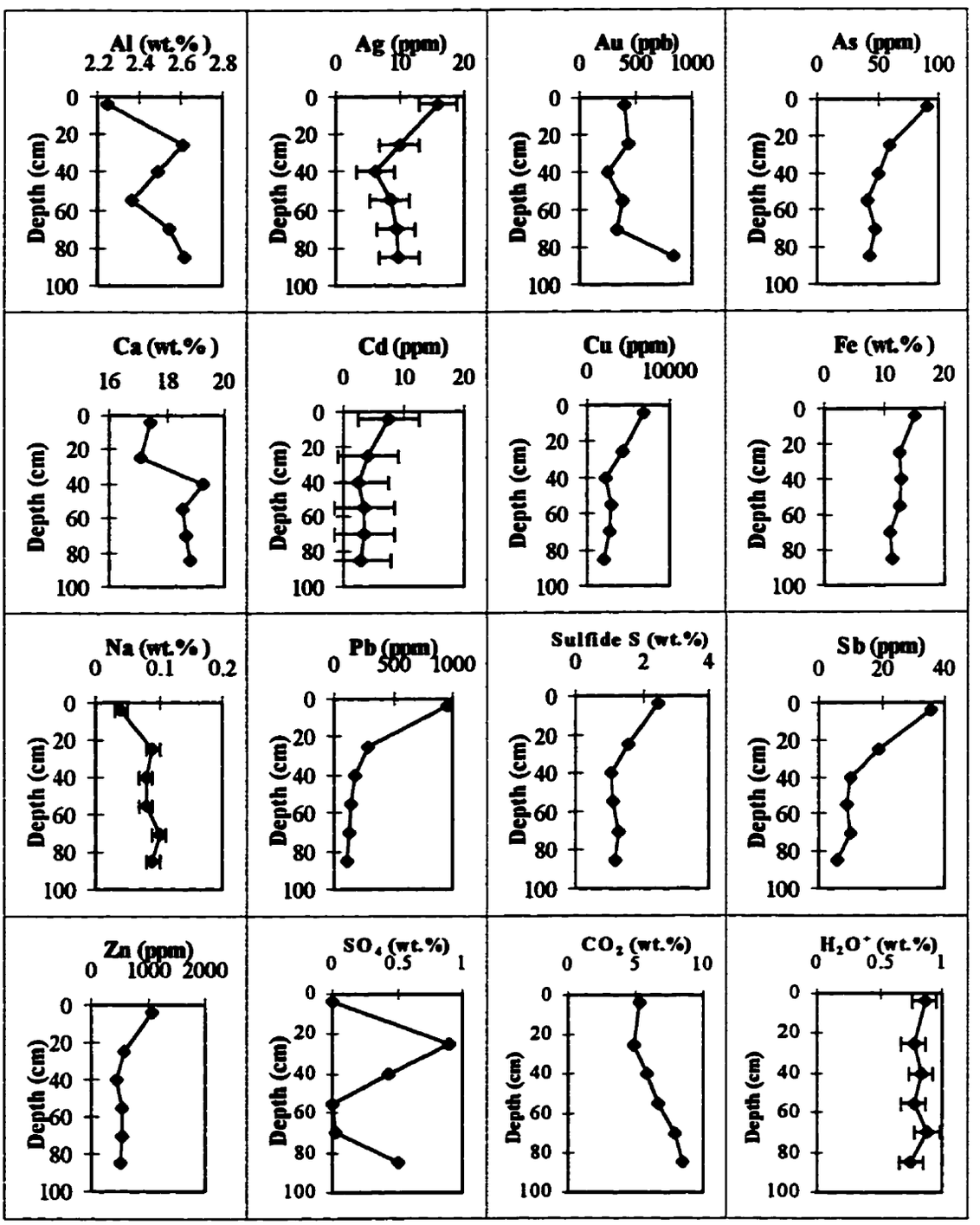

Figure 4.3: Solid-phase geochemical depth-profiles of a vertical section through the upper metre of the Cyprus-Piños Altos tailings; error bars are plotted for errors which exceed the size of the data point marker.

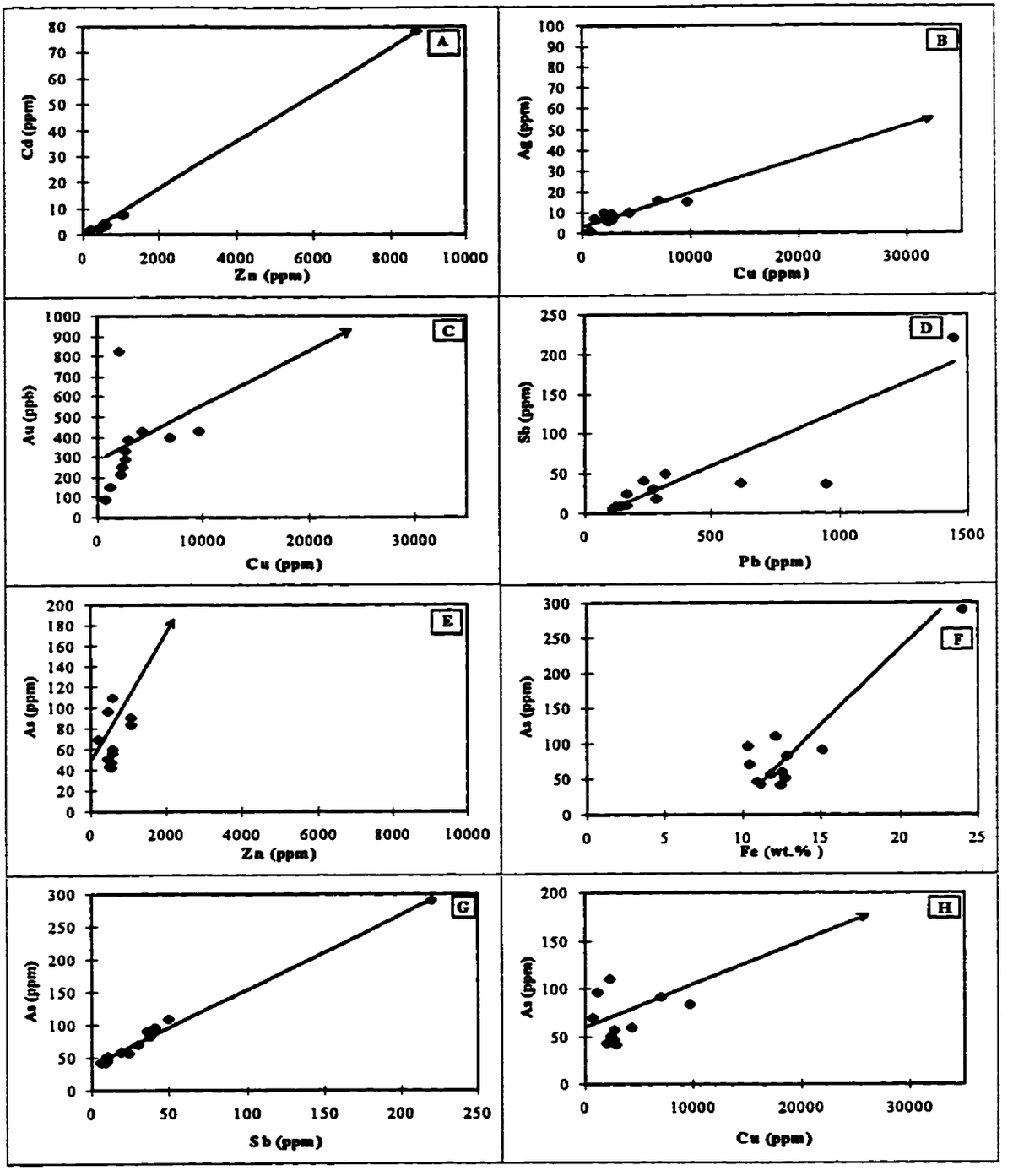

Figure 4.4: Variation diagrams for CPAT geochemical results. Arrows point to the value for ore concentrate from the Cyprus-Piños Altos mine. Error bars are smaller than the data point markers (therefore not visible). Correlation coefficients (r) for these plots are as follows: (A) 1.000 (P); (B) 0.999; (C) 0.927; (D) 0.860; (E) 0.950; (F) 0.904; (G) 0.994; and (H) 0.947.

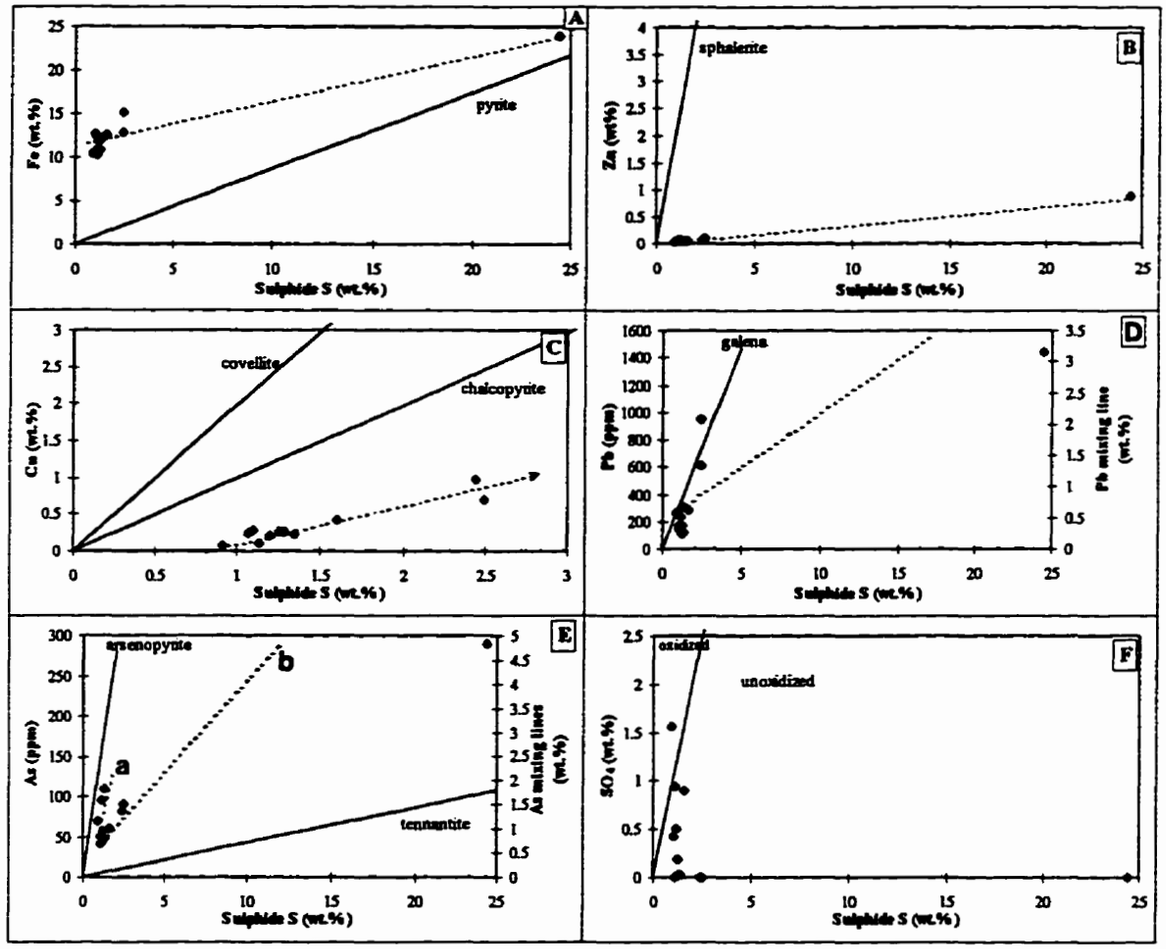

Figure 4.5: Metal concentrations in CPAT plotted as a function of sulphide S. Solid lines are mixing lines and dashed lines are the best-fit lines for the assemblage; arrows point to the value for the ore concentrate from the CPA mill. The mixing lines in D and E are plotted on the secondary y-axis. Error bars are smaller than the data point markers (therefore not visible). Correlation coefficients (*r*) for the best-fit lines are: (A) 0.953; (B) 0.999; (C) 1.000; (D) 0.842; (E) (a) 0.462 and (b) 0.993; and (F) no best-fit line drawn.

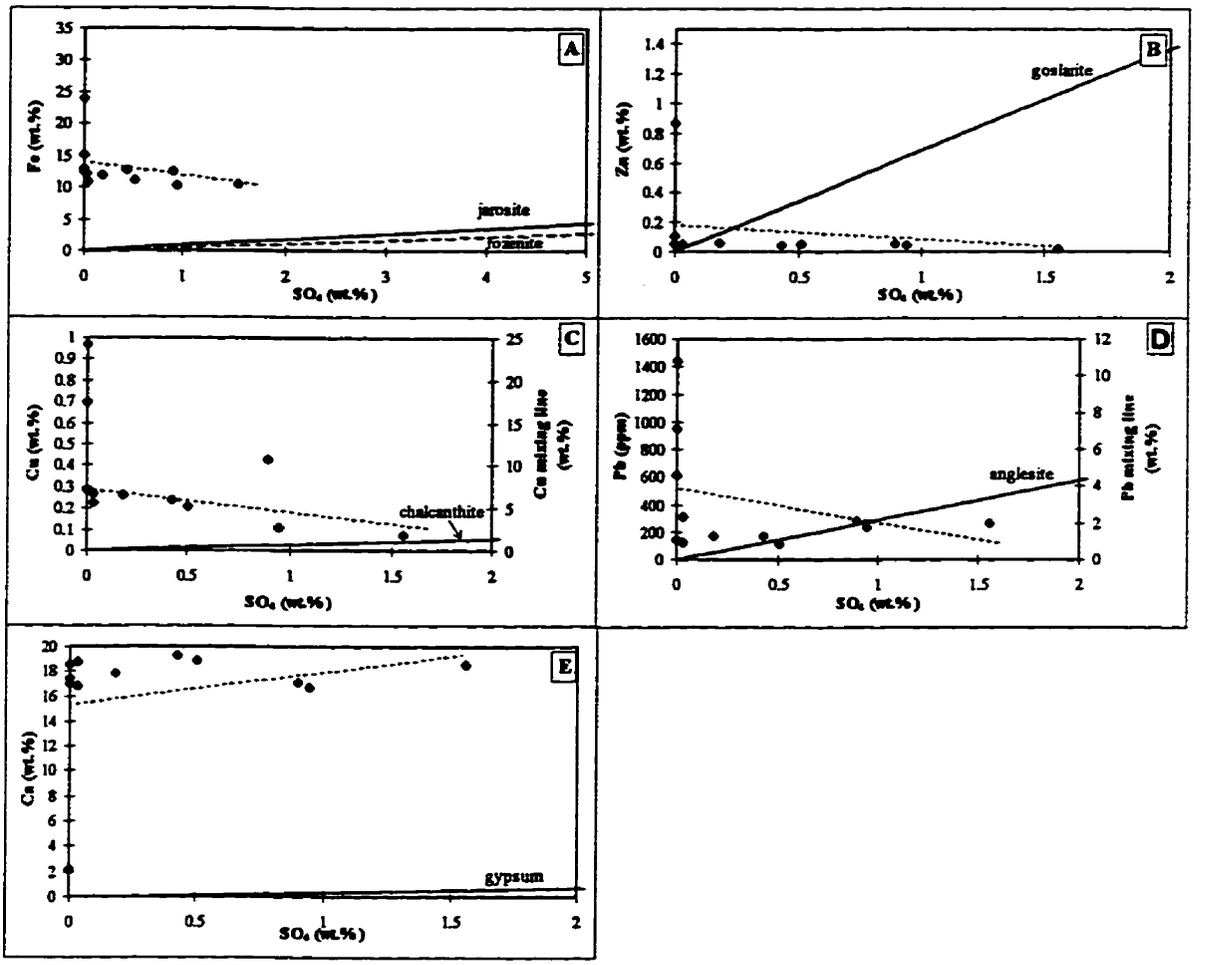

Figure 4.6: Element concentrations in CPAT plotted as a function of SO_4. Solid lines are mixing lines and dashed lines are the best-fit lines for the assemblage; arrows point to the value for the ore concentrate from the CPA mill. The mixing lines in C and D are plotted on the secondary y-axis. Error bars are smaller than the data point markers (therefore not visible). Correlation coefficients (r) for the best-fit lines are: (A) -0.41; (B) -0.302; (C) -0.279; (D) -0.339; and (E) 0.238.

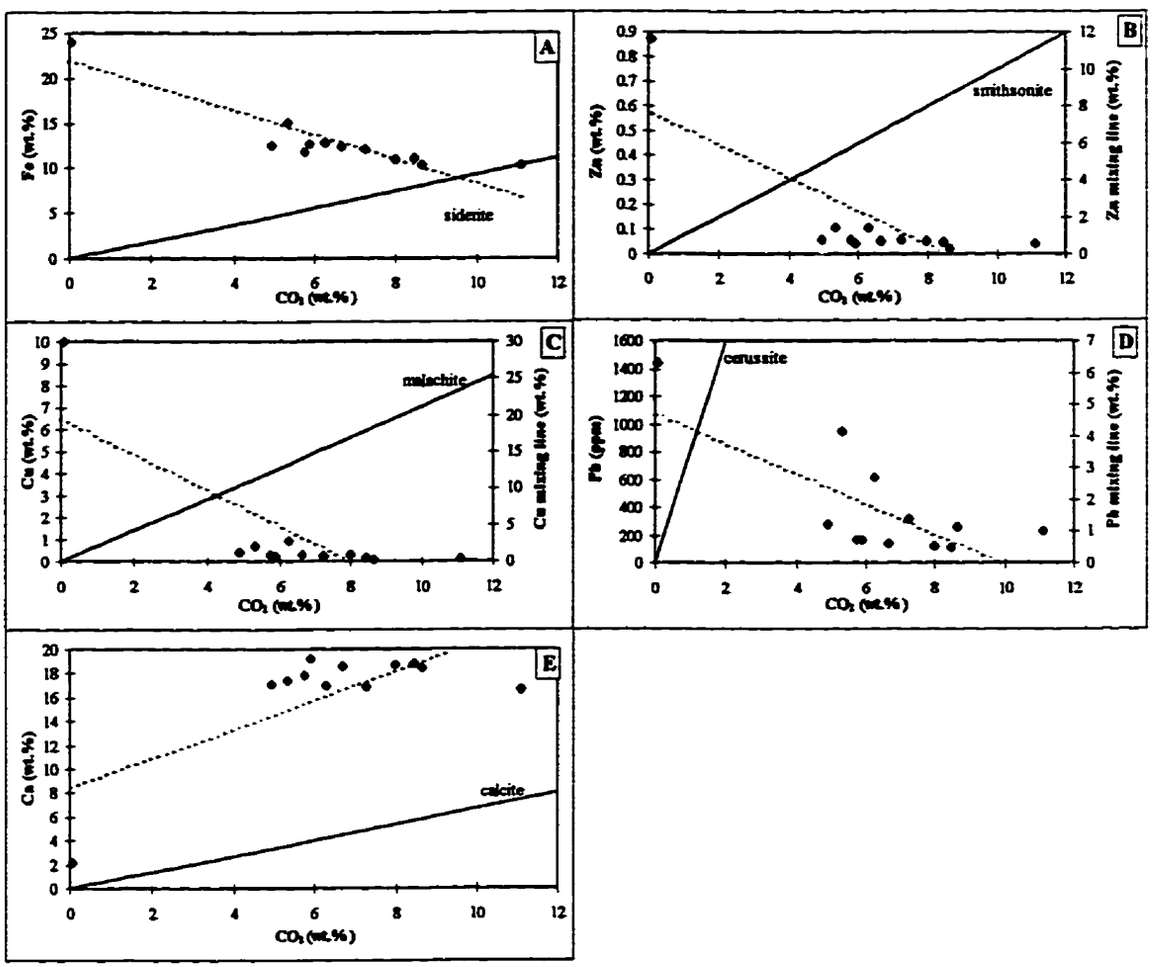

Figure 4.7: Element concentrations in CPAT plotted as a function of CO_2 (carbonate). Solid lines are mineral mixing lines and dashed lines are the best-fit lines for the assemblage. The mixing lines in B, C and D are plotted on the secondary axis. Error bars are smaller than the data point markers (therefore not visible). Correlation coefficients (r) for the best-fit lines are: (A) -0.891; (B) -0.79; (C) -0.79; (D) -0.752; and (E) 0.741.

4.7, the assemblage falls above the siderite and calcite line, and below the smithsonite, malachite and cerussite lines.

4.3 Pond-Water Chemistry

At the time of sampling, water in the CPAT tailings pond was neutral to slightly alkaline (pH of 7.00 to 8.27). Water in the impoundment consisted mainly of mill-derived effluents, rather than rain water. Dissolved-metal concentrations were as follows: 0.03 ppm As, 0.01 ppm Fe, 0.04 ppm Pb, 51 ppm S, 0.01 ppm Se and 0.07 ppm Zn; Ag, Cd, Cu and Hg concentrations were all below detection (Appendix A).

4.4 Bacterial-Growth Observations

The inoculation of the PAT001 sample gave positive results. Within two weeks, the medium became slightly cloudy, indicative of bacterial growth. After the third week, an orange precipitate had formed around part of the rim of the flask and the medium was much more cloudy. There were some whitish filaments floating in the media which were probably dead bacterial cells. The pH increased to 8.63, from 6.8. By the fifth week, the water was very cloudy and brownish in colour, and the tailings had changed from their original buff-grey colour to a rusty brown colour; more orange precipitate coated the walls of the flask (Fig. 4.8). Observing the liquid medium under a microscope in oil immersion at a magnification of 1000, an abundance of bacteria were seen swimming around. Different shapes of bacteria were visible, including bacilli, cocci and spirillium.

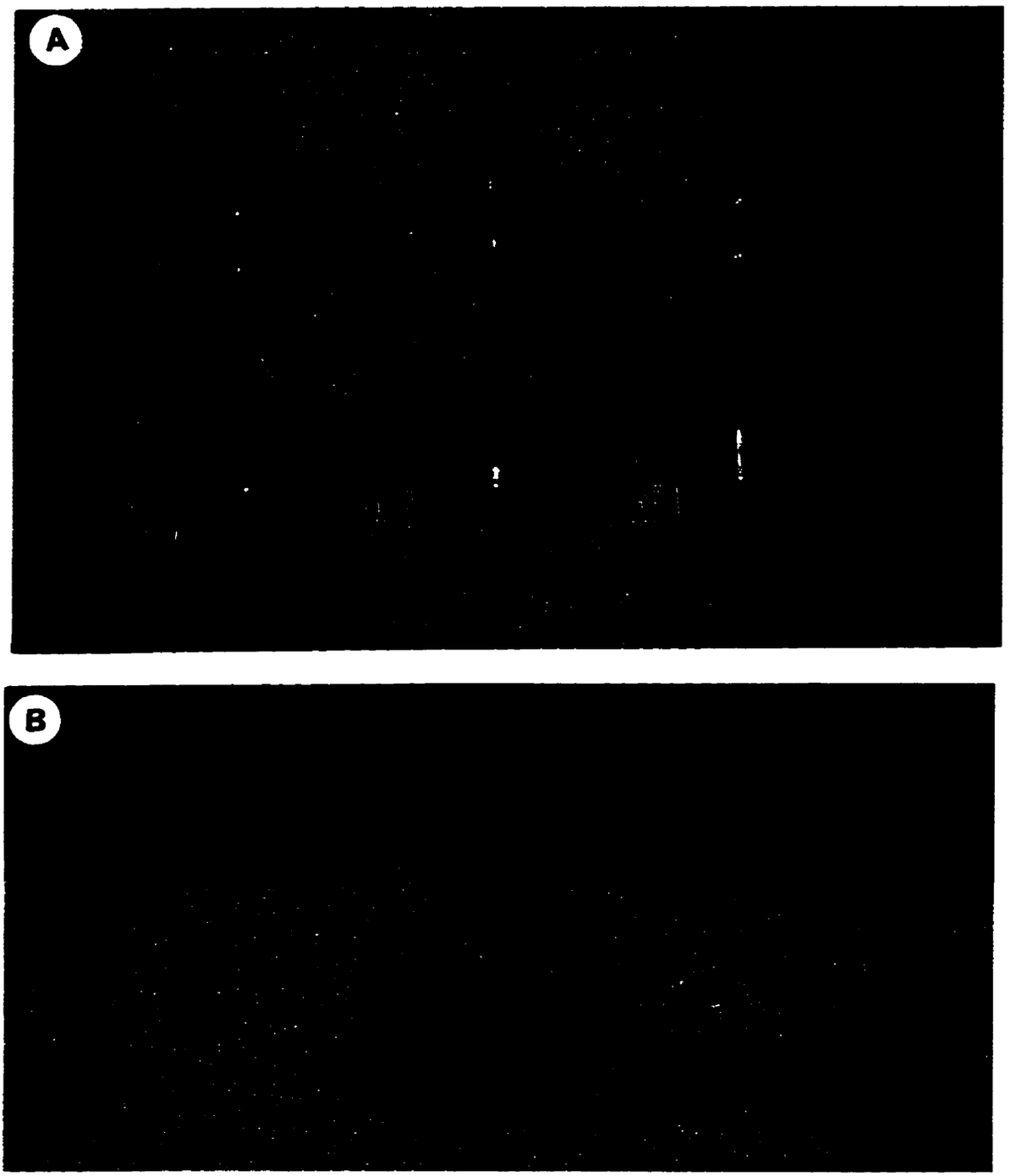

Figure 4.8: (A) CPAT bacterial growth flask experiment; (B) the cloudy liquid, brown colour of the tailings, and orange precipitate on the walls of the flask all indicative of bacterial growth.

4.5 Sieve Analysis

The CPAT sieve analyses are plotted in a histogram (Fig. 4.9) and as depth profiles (Fig. 4.10; Appendix F). The histograms for surficial samples PAT001 and PAT002 show distributions compatible with ripple crest/trough grain-size sorting; PAT001 is a sample of a ripple crest, and PAT002 is a sample of a ripple trough. The PAT001 dominant grain-size is 125 to 62 μm, and PAT002 dominant grain-size is 500 to 250 μm. The vertical section (PAT003-PAT008) histograms showed the same grain-size distribution through the section; the dominant grain-size is 250 to 125 μm. In general, the tailings consist 65% of grains ≤ 125 μm in diameter, and 100% of grains ≤ 1 mm in diameter. Depth profiles of different grain sizes show no correlation with chemistry (Fig. 4.3).

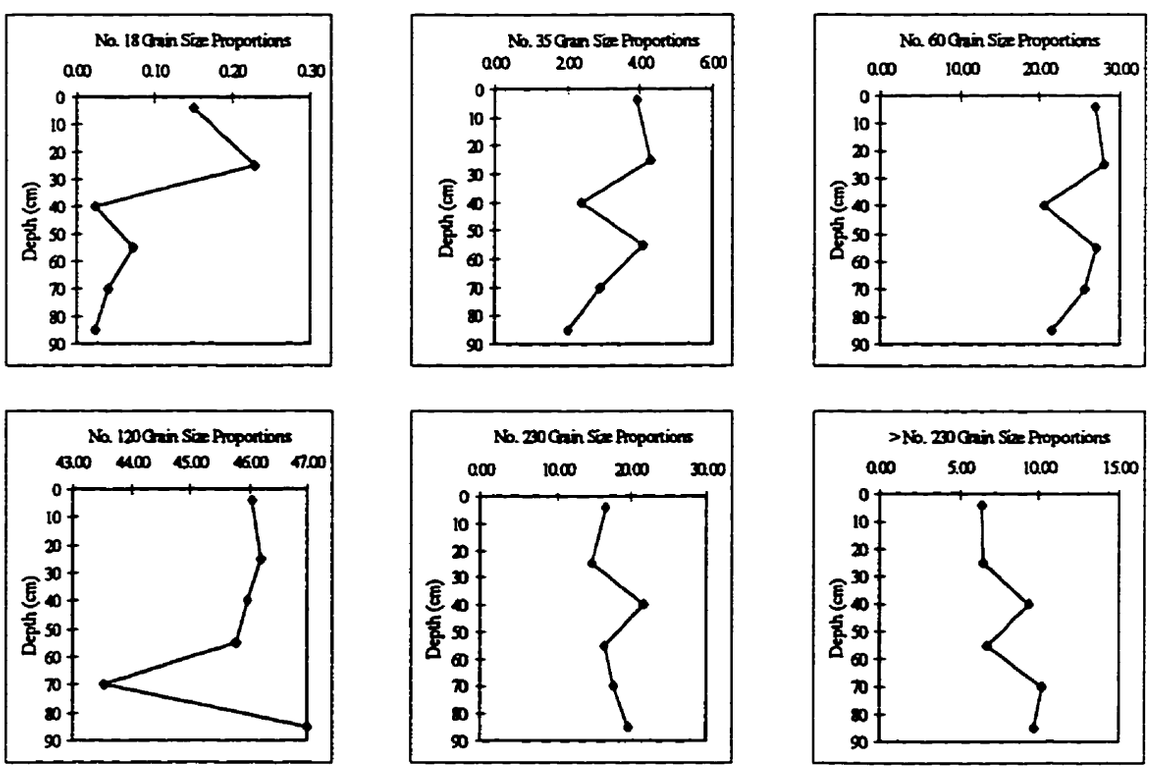

Figure 4.9: CPAT sieve result histograms showing grain size distribution.

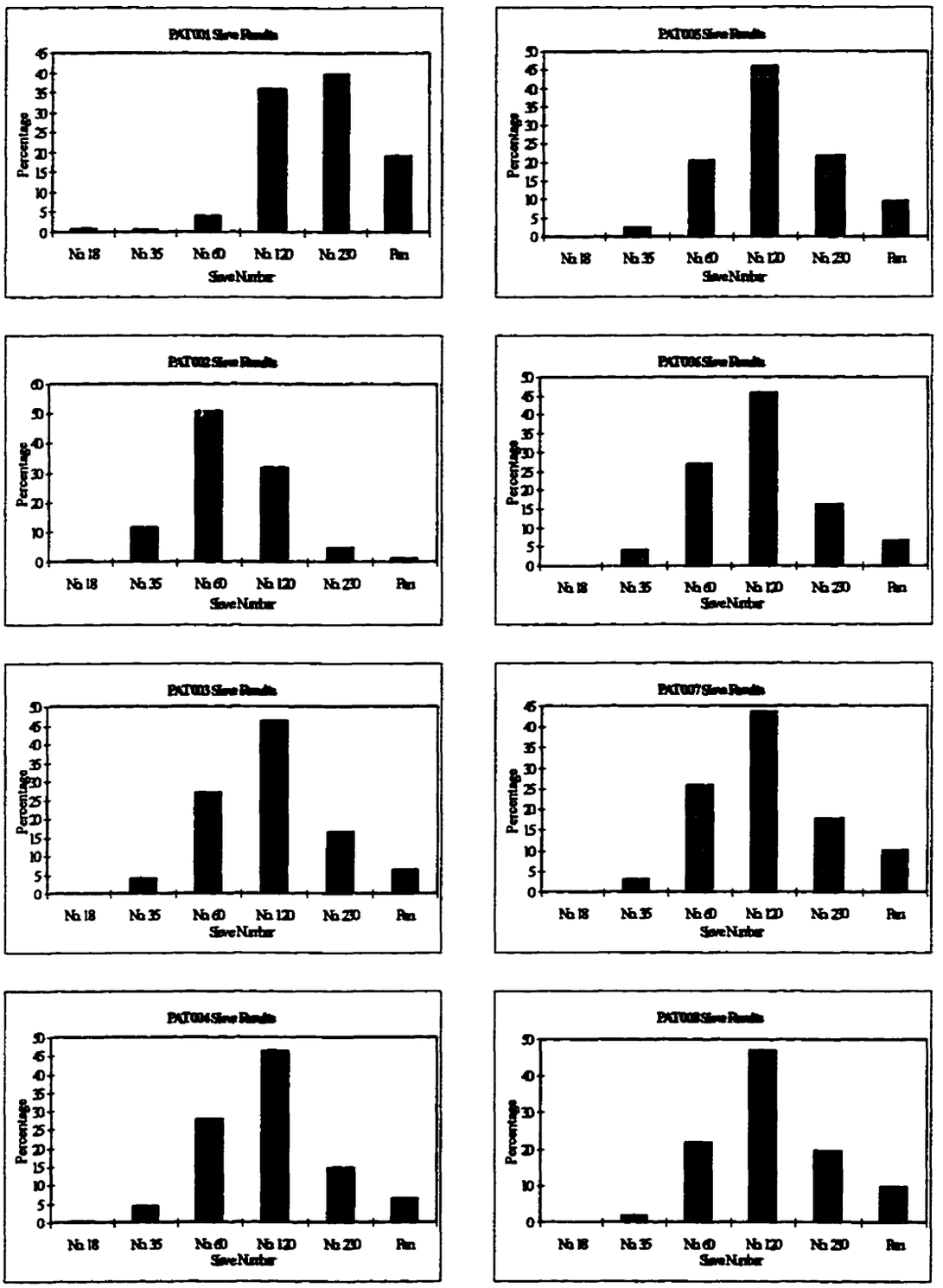

Figure 4.10: CPAT normalized sieve results plotted as depth profiles for samples PAT003 to PAT008.

CHAPTER 5

CLEVELAND MILL-TAILINGS RESULTS

5.1 Mineralogy

The east pile of the CMT is dark brown, whereas the west pile is dominantly rusty orange-yellow. The mineralogy of each side reflects the orebody zone that was being mined at the time. No tailings from other mine sites were deposited at this site (U.S. EPA, 1993). The appearance of the tailings are dependent on the time of year: during the wet winter-spring months, the tailings are well flushed and generally more moist (Fig. 1.3); during the drier summer-fall months, the tailings are drier and have many surficial blooms (Fig. 5.1 and 5.2). The results of wet-dry cycles are visible at a small scale with the formation of dessication cracks on the surface of grains (Fig. 5.3). During the November 1996 visit, the CMTE pile in particular had a darker brown colour with many white blooms, giving the tailings an irridescent appearance (Fig. 5.1A). In November 1996, the CMTW pile had much more spotty colour variations (Fig. 5.1B), whereas in February 1995, the colour was more uniform.

The primary-mineral assemblage of these tailings has been almost completely dissolved or oxidized only; a small fraction of primary minerals still remain. The primary sulphide minerals include pyrite, sphalerite, chalcopyrite, and minor galena and arsenopyrite; gangue minerals include quartz, calcite, grossular, andradite, magnetite, hematite, and diopside (Paige, 1910; Walder et al., 1994). Although it has not been observed in these samples, McKnight and Fellows (1978) have reported tennantite in the Cyprus-Piños Altos deposit. This mineral also may

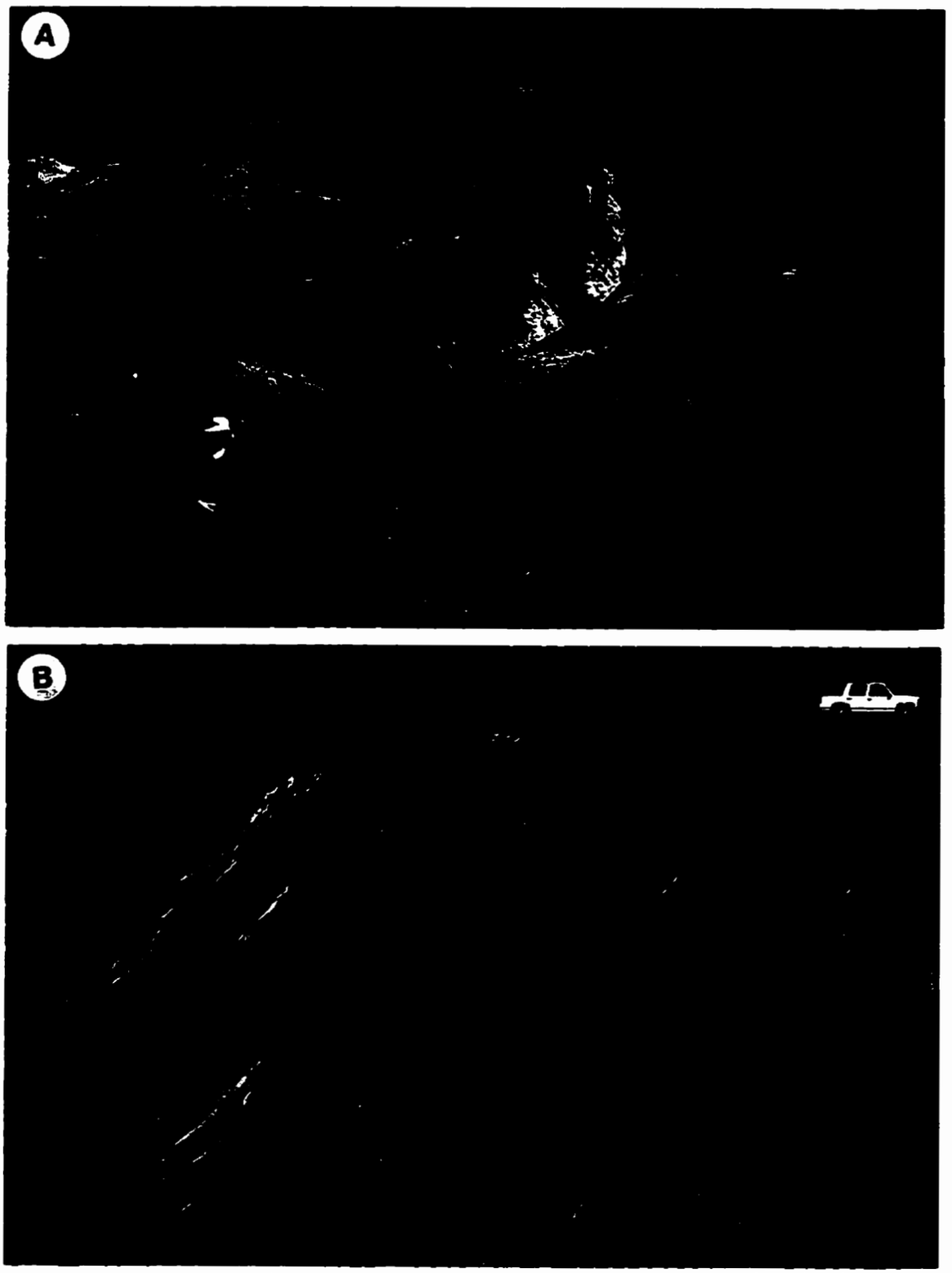

Figure 5.1: Cleveland mill (A) east and (B) west tailings piles in 1996 during the dry season.

Figure 5.2: Whitish surficial blooms on the west CMT surface.

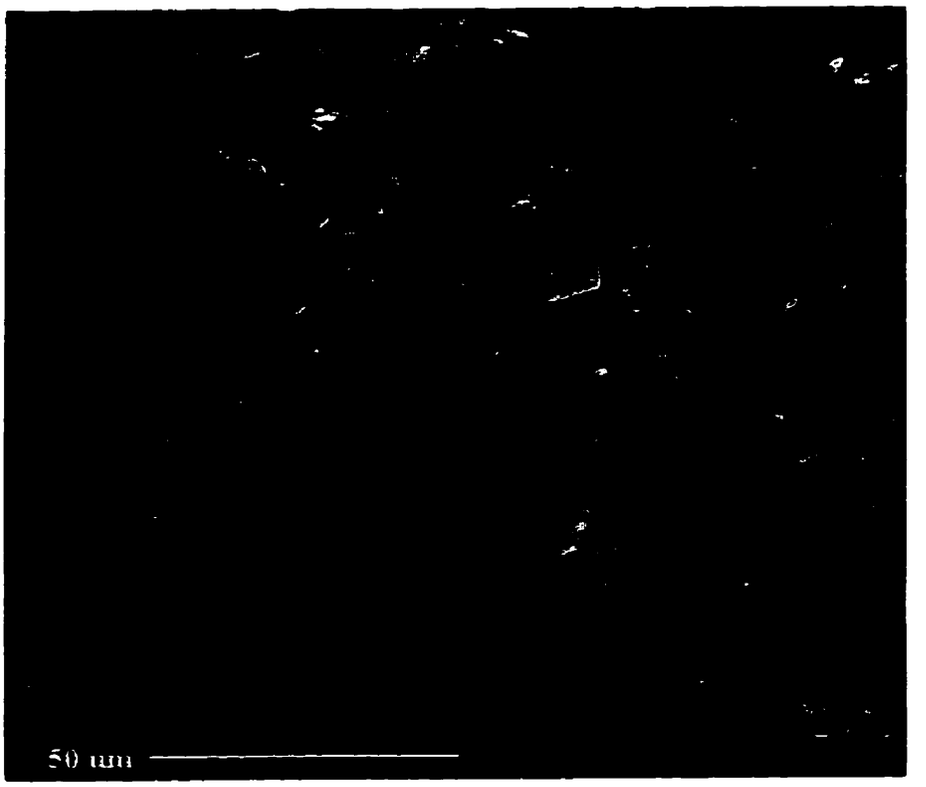

Figure 5.3: SEM of dessication cracks of a secondary precipitate on the surface of a primary mineral.

be present in the CMT, and is of environmental concern because it contains As. Table 5.1 summarizes the Cleveland mine ore (CMO) and tailings mineralogy.

Table 5.1 Cleveland Mill-Tailings Mineralogy.

Mineralogical Classification	Minerals
Primary	pyrite, chalcopyrite, sphalerite, galena, arsenopyrite, tetrahedrite-tennantite, calcite, quartz, grossular, andradite, magnetite, hematite, diopside, hedenbergite, wollastonite, siderite, smithsonite, covellite, bassanite, goslarite
Secondary	gypsum, goethite, jarosite, natrojarosite, plumbojarosite, argentojarosite, hydronium jarosite, hematite, maghemite, native sulfur, anglesite, rosasite, silver sulphate, hydrated lead carbonate, chalcocite, malachite, lepidocrocite, ferrihydrite, shwertmannite, epsomite, chalcanthite, boyleite
Tertiary	gypsum, melanterite
Quaternary	rozenite, (szomolnokite)*, (bianchite)

* minerals in parentheses are uncertain as to their classification;
Chemical formulae of secondary, tertiary and quaternary minerals are given in Appendix E.

The most abundant primary minerals which still occur in the tailings are pyrite and quartz; sphalerite and chalcopyrite also are present, but in very small quantities. Most calcite has been dissolved as a result of buffering reactions; however, some is still present at the extreme base of the CMTE tailings in the unoxidized zones (Fig. 5.4). Most primary minerals, particularly sulphide minerals, have been either completely or partially dissolved or replaced, resulting in skeletal or zoned grains. Pyrite and sphalerite grains show well-developed complex alteration patterns. Highly-fractured sulphide grains have a skeletal appearance where there is abundant

Figure 5.4: (A) Photograph showing the contact relationship between the oxidized and unoxidized tailings, and (B) their respective zones (modified from McGregor, 1994).

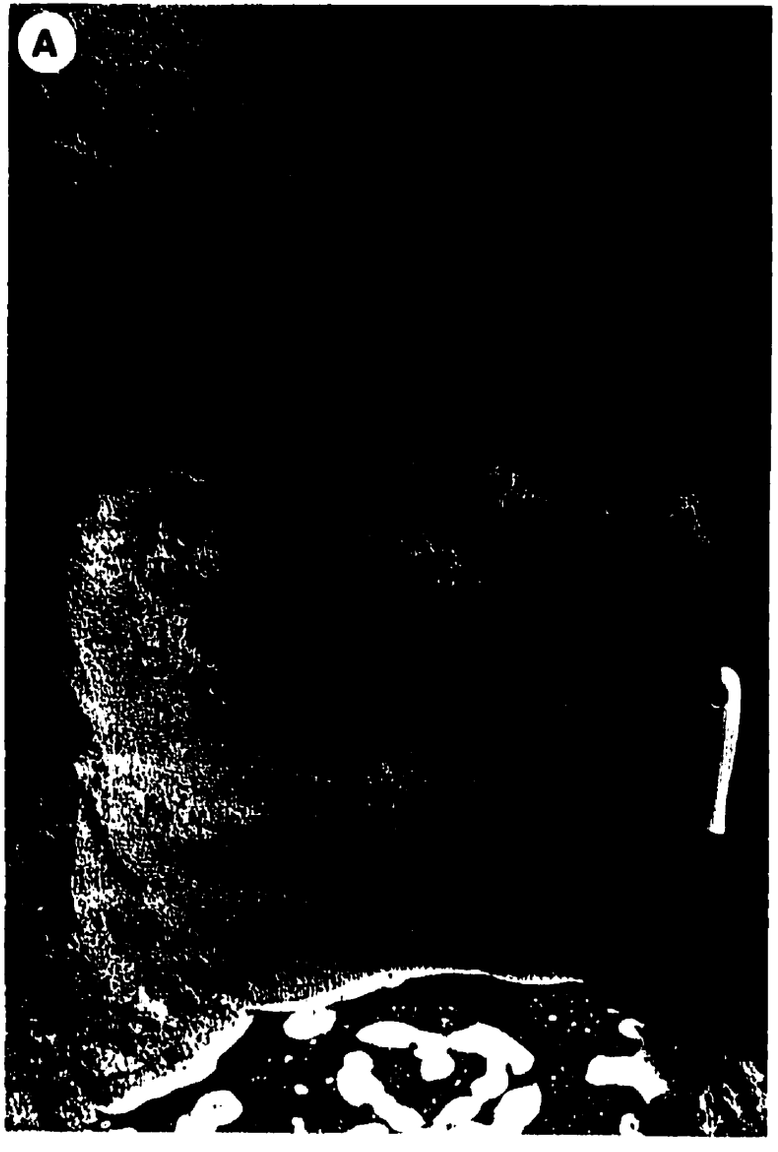

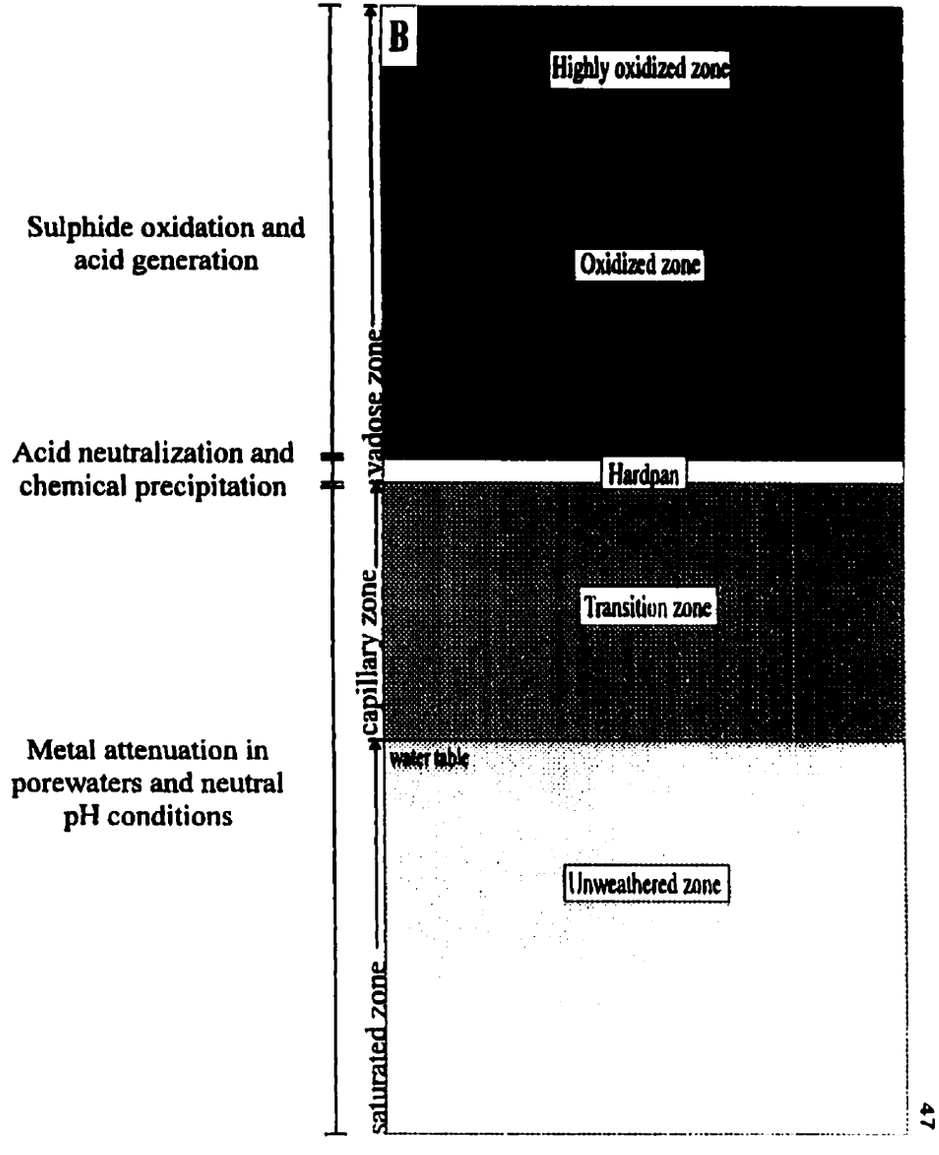

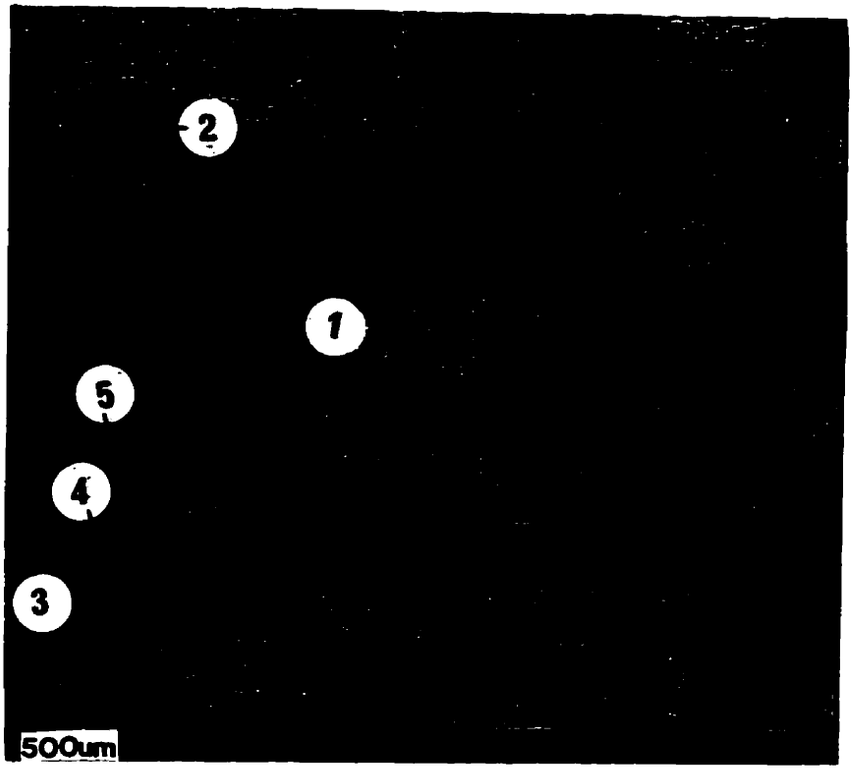

Figure 5.5: False-colour BSE image of an extensively altered pyrite: (1) Fe-depleted grain with a well-developed (2) three-layer rim of hematite, Zn-bearing Fe oxyhydrosulphate and a thin rim of tertiary gypsum. The brighter regions within the grain represent remnant pyrite; the dark centre is a cavity caused by grain plucking during slide preparation. (3) Quartz grain with a complex coating of precipitates; (4) mainly Fe-rich gypsum; (5) Zn-bearing Fe-oxyhydrosulphate.

alteration product making up the grain. Less-fractured sulphide grains have a zoned appearance, with a core of primary sulphide and a series of alteration rims. The innermost zone of altered pyrite commonly consists of specular hematite and Fe oxyhydrosulphates (Fig. 5.5). The middle zone commonly consists of Zn-bearing Fe-oxyhydrosulphates/sulphates. The outermost zone consists of gypsum and jarosite. The oxidation of sphalerite also results in a layered rind of secondary minerals (Fig. 5.6). The innermost zone consists of native S,

Figure 5.6: Photomicrograph of altered sphalerite with an (1) unaltered core, (2) an inner alteration rim of native S and (3) an outer rim of a hydrous Fe-sulphate; field of view is 1.7 mm; plane-polarized light.

and the outermost rim consists of a multi-layer rim of hydrous Fe-sulphates. The oxidation products of chalcopyrite are similar to those of pyrite, except that there are Cu and Zn impurities in the Fe-sulphates.

Primary quartz is coated commonly with layers of Zn-bearing hydrous or non-hydrous Fe-sulphates, secondary and tertiary gypsum, and jarosite (Fig. 5.5). Secondary gypsum commonly has Fe and/or Zn impurities. The grain is often cemented to surrounding particles by secondary and tertiary gypsum. Secondary minerals are abundant in the tailings, giving them their distinct rusty colour. Microscopic examination of the secondary minerals revealed distinct colours of material. This feature along with EDX spectra and XRD, has been used

to develop a "colour index" which identifies the dominant mineral in each sample. Five colour categories have been defined: metallic grey, yellowish-brown (Munsell hue 5YR 4/6), bright orange (approximately Munsell hue 5YR 6/8), reddish-brown (Munsell hue 7.5YR 3/6),

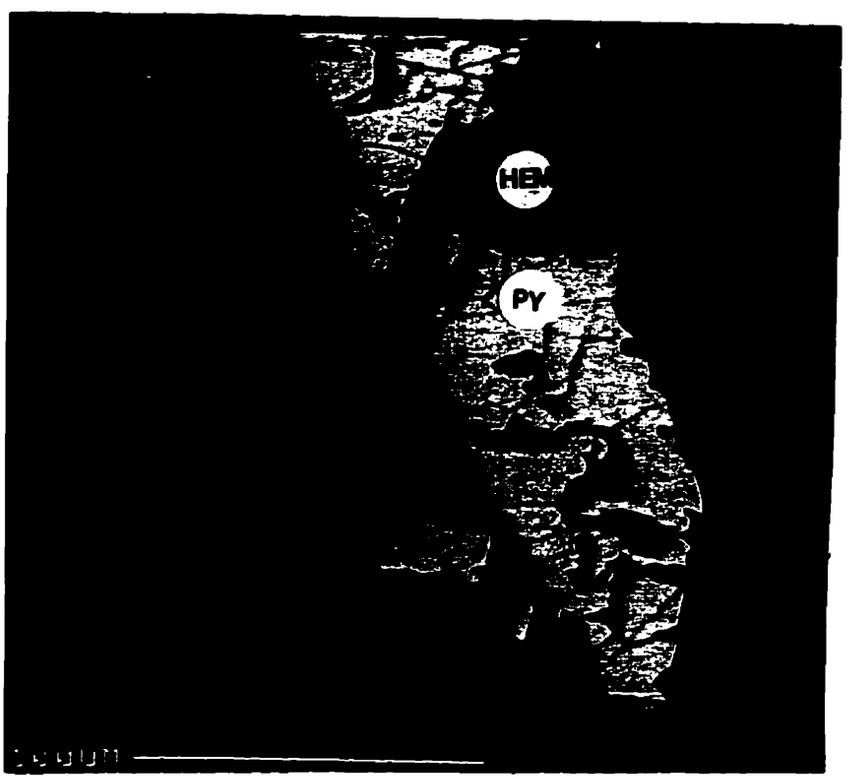

Figure 5.7: False-colour BSE image of altered pyrite with an alteration rim of hematite.

bright yellow (Munsell hue 2.5YR 8/8) and straw yellow (Munsell hue 10YR 8/6; Jambor, 1994). The dominant phases making up the samples corresponding to this index are specular hematite (Fe_2O_3), goethite (α-FeOOH), lepidocrocite (γ-FeOOH), ferrihydrite ($5Fe_2O_3 \cdot 9H_2O$), schwertmannite ($Fe_8O_8(OH)_6SO_4$), and jarosite ($KFe_3(OH)_6(SO_4)_2$), respectively. The presence of an iron oxide with the formula Fe_2O_3, in direct contact with altered pyrite, was confirmed by EMP analysis (Fig. 5.7); however, the exact phase (hematite

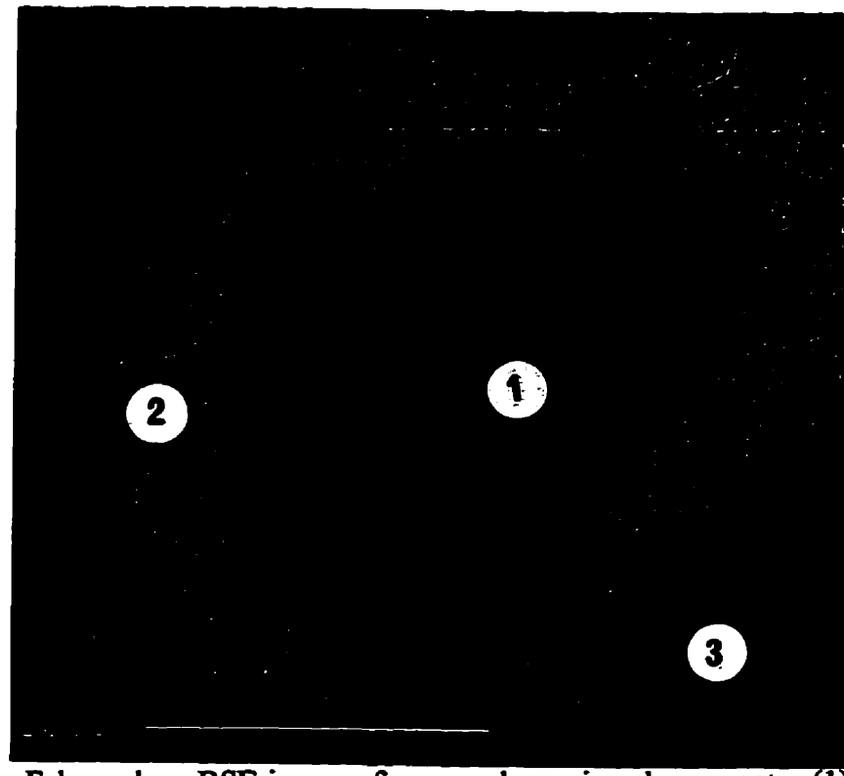

Figure 5.8: False-colour BSE image of a secondary mineral aggregate; (1) Zn-bearing secondary gypsum aggregates cemented by Zn-bearing natrojarosite (lighter regions), (2) secondary precipitate of Zn- and Cu-bearing natrojarosite, and (3) tertiary gypsum.

versus maghemite) is uncertain. It likely is hematite, as this has been found to be a product of pyrite oxidation in coal wastes; maghemite is a product of magnetite alteration (Jambor, 1994). Gypsum and various Fe-oxyhydroxides and sulphates also make up a minor portion of the secondary phases. These phases result from the oxidation of sulphides. They coat the remaining primary minerals and differentially cement them. At various intervals throughout the tailings, these secondary minerals have cemented the tailings to form hardpan and encrusted layers (Fig. 5.8). Secondary gypsum occurs throughout as a cementing mineral, and as massive irregular clumps coated with a thin layer of Fe-oxyhydroxides. Secondary gypsum commonly has traces of Fe and Zn, likely as inclusions. Jarosite occurs as small clusters of acicular crystals (~ 5μm long), or as continuous coatings on grains as bands of

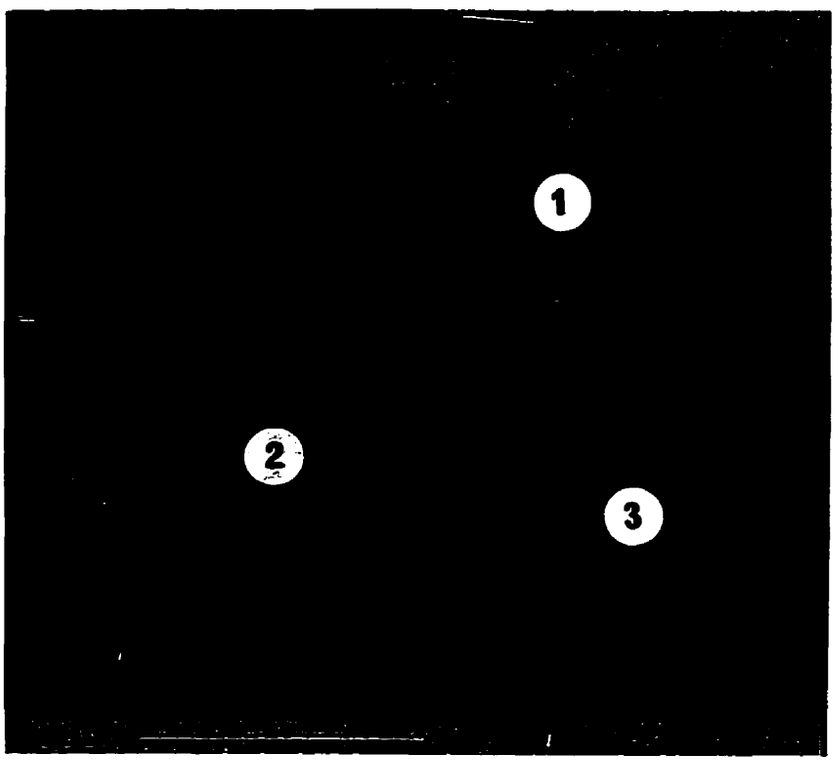

Figure 5.9: False-coloured BSE image of (1) feathery secondary jarosite and (2) Zn-bearing Fe hydrous sulphate coating (3) quartz.

fine, feathery radiating crystals (Fig. 5.9). Secondary minerals identified by the PEAKSEARCH program are listed in Table 5.1.

Secondary minerals exhibit many different textures. Most of these minerals occur as extremely fine-grained particles (Fig. 5.10A), or as continuous precipitated layers (Fig. 5.10B). Occasionally, they occur in more delicate forms such as acicular needles (Fig. 5.10C), fine surficial lacy networks (Figure 5.10D), or as small delicate boxworks (Figure 5.10E). Figure 5.10F shows the texture of an altered pyrite, where the alteration rim has a distinct needle-like appearance; the rim consists of hematite.

Most of the samples were dry when collected; however, precipitation of minerals from

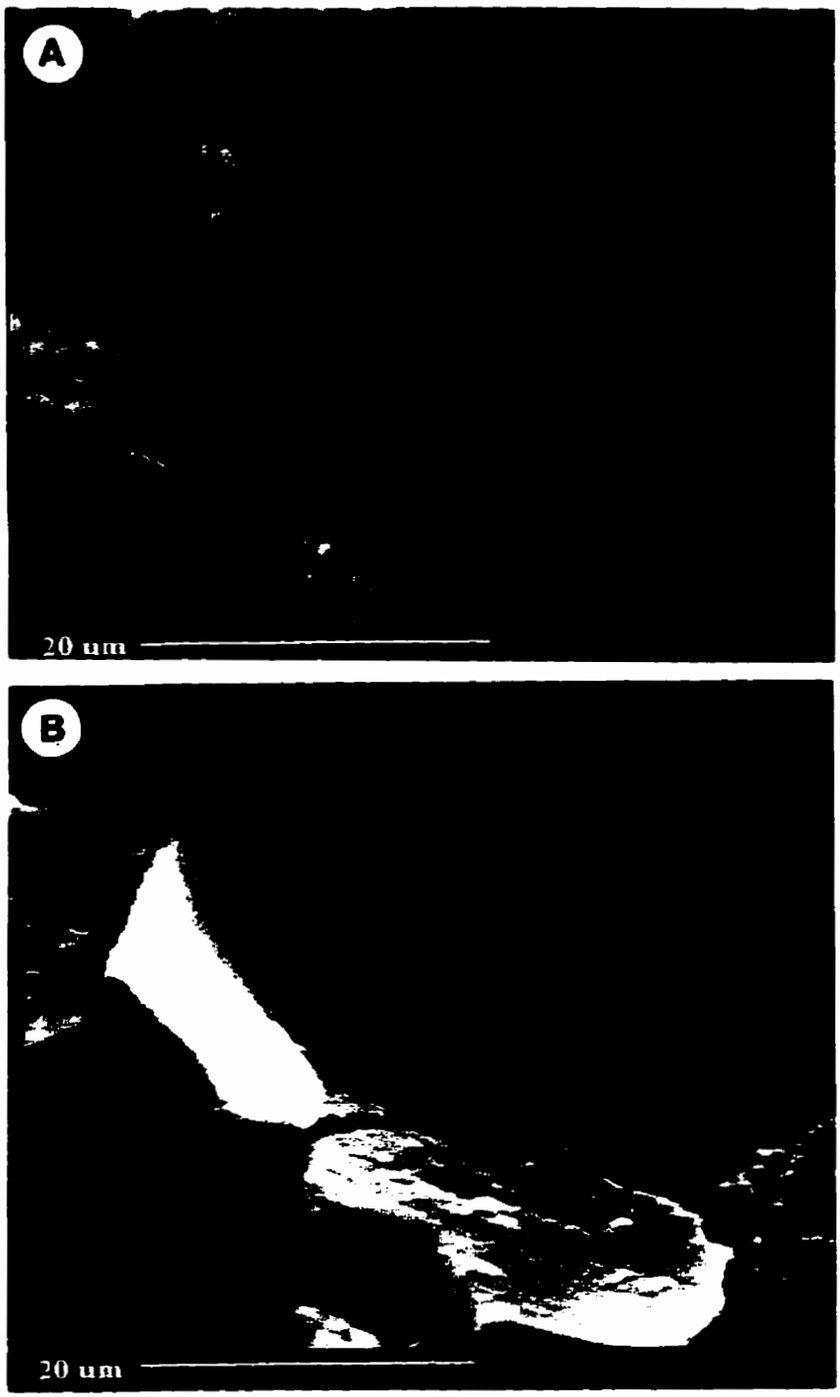

Figure 5.10: SEM of secondary mineral textures in the CMT. (A) Very fine-grained goethite. (B) Thick Fe-oxyhydroxide precipitate on altered pyrite. (C) Acicular crystals of secondary hydrated Fe-sulphate. (D) SEM of delicate lacy precipitate of native S. (E) Boxwork of secondary mineral, possibly goethite or lepidocrocite. (F) Surficial texture of altered pyrite, needle-like texture is a cross between hematite and an extremely S-depleted pyrite. (continued on following pages)

Figure 5.10 continued

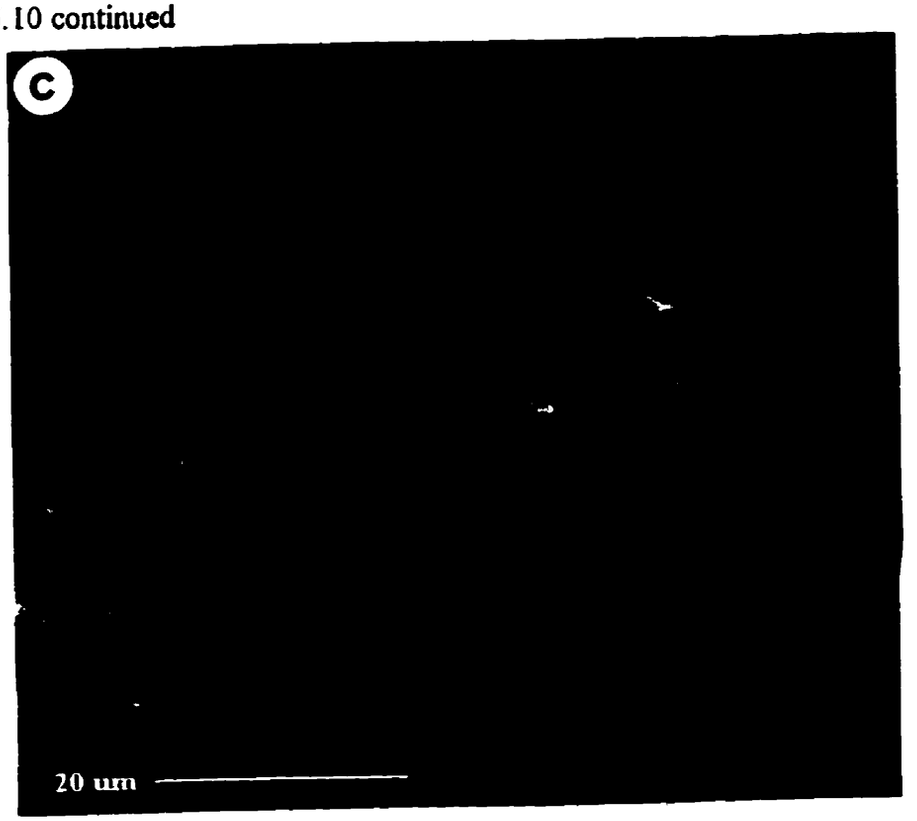

Figure 5.10 continued

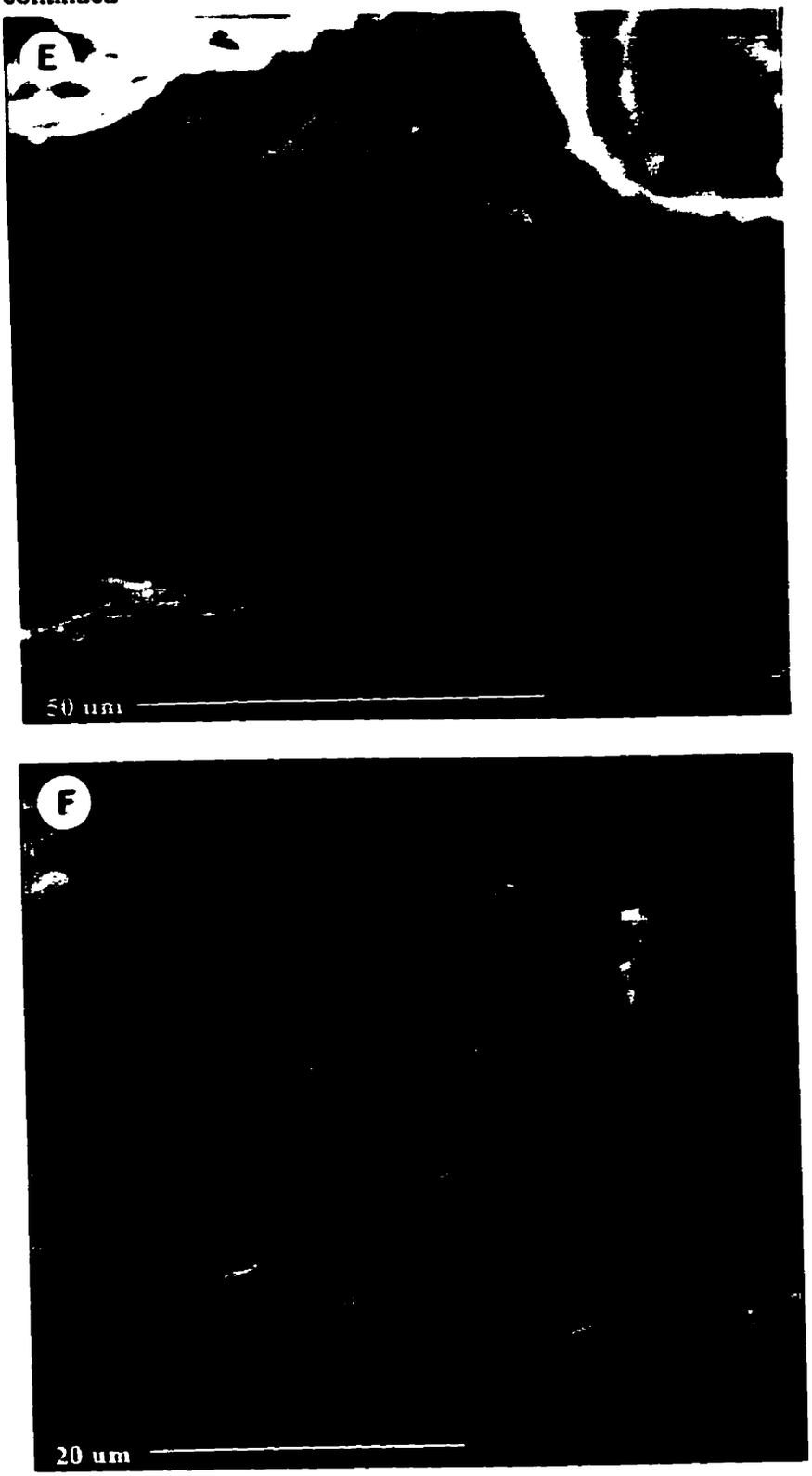

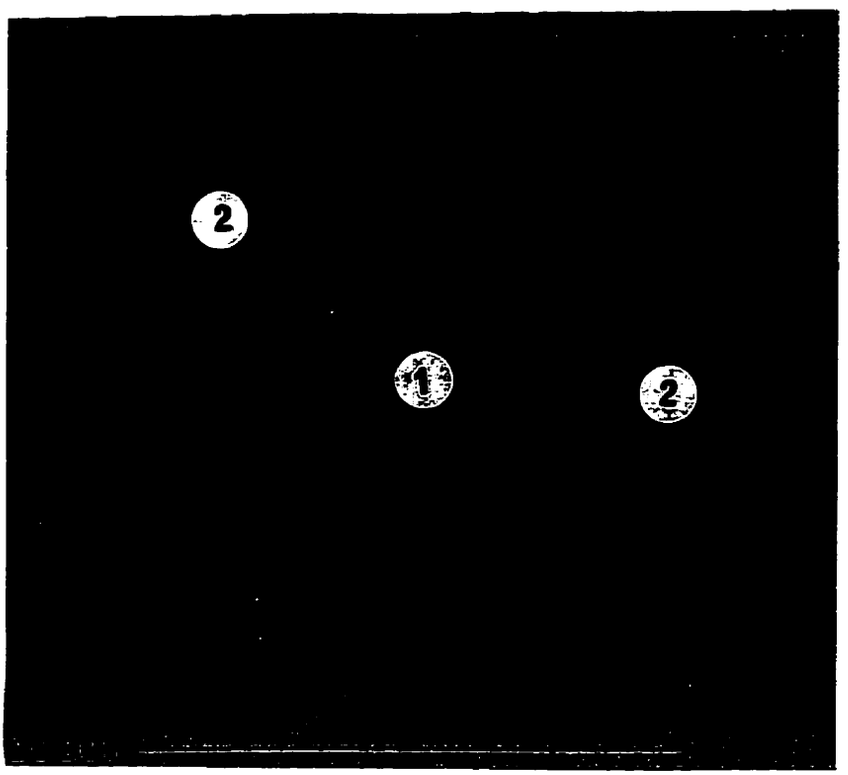

Figure 5.11: False-colour BSE image of (1) stubby tertiary gypsum crystals surrounding (2) quartz.

residual pore waters formed tertiary hydrous sulphates in some samples (Table 5.1). The most abundant tertiary mineral is gypsum. Tertiary gypsum is clean and occurs as small white blooms in cracks and corners; it forms either radiating clusters of acicular crystals (similar to Fig. 4.2), or clumps of small stubby crystals (Fig. 5.11). Melanterite ($FeSO_4 \cdot 7H_2O$) was identified in the CMTE; it occurs as clear pale-blue filiform crystals, 0.1 to 1 cm long. A quaternary mineral identified is rozenite ($FeSO_4 \cdot 4H_2O$); rozenite has been previously identified as a tailings quaternary mineral (Jambor, 1994). Other possible quaternary minerals include szomolnokite ($FeSO_4 \cdot H_2O$) and bianchite ($(Zn,Fe)SO_4 \cdot 6H_2O$).

Table 5.2 Geochemical data for CM tailings and ore.

Elements	Al	Ag	Au	As	Ca	Cd	Cu	Fe	K	Na	Pb	Sb	Zn	S	SO_4	CO_2	H_2O^+
Units	wt.%	ppm	ppb	ppm	wt.%	ppm	ppm	wt.%	wt.%	wt.%	ppm	ppm	ppm	wt.%	wt.%	wt.%	wt.%
Errors	±0.01	±0.05	±1	±1	±0.005	±0.1	±1	±0.01	±0.01	±0.01	±1	±0.1	±0.5	±0.01	±0.001	±0.001	±0.01
CMT001	0.49	34.05	18	93	10.120	2.2	701	7.08	0.24	0.01	488	14.0	451.0	10.10	29.600	0.011	9.56
CMT002	0.52	32.30	8	85	7.710	3.8	979	9.95	0.22	0.01	408	14.0	821.0	13.90	30.000	0.015	9.55
CMT003	0.50	41.90	170	72	8.430	4.9	1259	9.25	0.22	0.02	535	17.0	1505.5	13.40	31.800	0.051	10.47
CMT004	0.51	33.70	12	66	6.400	195.5	5442	13.00	0.17	0.01	412	14.0	41212	16.80	30.300	2.290	8.24
CMT005	0.59	139.7	22	3.7	9.720	1.4	2308	2.06	0.33	0.02	1533	41.0	201.5	10.70	29.500	0	10.43
CMT006	0.59	51.60	0	120	6.210	76.9	16173	14.70	0.14	0	427	19.0	22356.5	15.20	0	0.359	5.69
CMT007	0.68	45.80	7	86	9.155	36.4	31738	12.60	0.08	0	378	16.0	7777.0	17.10	32.400	0.417	10.02
CMT008	0.33	61.60	327	31	0.750	11.7	4231	32.50	0.04	0	601	19.0	15600.0	15.10	25.900	0	10.46
CMT009	0.37	80.75	15	42	1.405	11.2	1374	31.30	0.07	0.01	888	24.0	14475.5	14.00	4.780	0.018	5.82
CMT010	0.22	7.10	0	36	0.155	38.0	2315	20.10	0.01	0	133	2.90	16473.0	NA	NA	NA	NA
CMT011	0.36	61.40	40	44	1.600	3.5	933	36.80	0.04	0	531	15.0	12428.0	12.80	23.700	0.007	9.13
CMT012'	0.84	25.45	9	190	5.340	11.0	741	10.10	0.32	0.08	406	17.0	4068.5	5.81	15.500	0.011	8.56
CMT013	0.41	56.70	187	46	3.200	1.9	1202	36.20	0.10	0.01	718	18.0	10720.0	4.51	11.100	0.015	5.95
CMO-1*	0.12	58.20	0	98	0.140	823.5	12666	21.20	0.02	0	360	13.0	141000.0	24.00	13.500	1.35.000	0.40

NA = not available; * ore sample; ' stream sediment; west tailings samples: CMT001 to CMT007; east tailings samples: CMT008 to CMT011, CMT013;
Detection limits are listed in Appendix B.

5.2 Geochemistry

Solid-phase metal and complex-ion concentrations vary greatly in these tailings: 0.0 (below detection) to 32.4 wt. % sulphide S, 4.51 to 17.10 wt. % SO_4, 0.00 to 2.96 wt. % CO_2, 701 to 31738 ppm Cu, 451 to 31738 ppm Cu, 451 to 41212 ppm Zn, 133 to 1533 ppm Pb, 7.1 to 139.7 Ag, and 0 to 347 ppb Au. Ore sample (CMO-1) metal concentrations fall below the highest concentration in the tailings, with the exception of Zn and sulphide S. Table 5.2 summarizes all the solid-phase CM tailings and ore geochemical results in this study. Lower concentrations of As were measured in this study (3.7-190 ppm) than reported by previous workers (e.g., 276 ppm reported by Ecology and Environment (1993a), 366 ppm reported by Ecology and Environment (1993b)). The highest levels observed in this study come from a stream-sediment sample downstream from the CMT in the mill-valley tributary. Arsenic concentrations in the stream water were below detection limits (< 0.003 ppm).

Table 5.3 CMT sample descriptions for depth-profiles.

Sample #	Color (Munsell hue)	Texture	Depth (cm)
CMT001	rusty orange (10YR 5/8)	mostly loose grains, slightly cemented	0 - 10
CMT002	yellow-green with dark rusty orange base (10YR 6/6)	loose with small cemented grains	10 - 13
CMT003	rusty brown-orange (approx. 7.5 YR 5/6)	loose with small cemented grains	13 - 46
CMT004	dark grey-brown with unoxidized pyrite and silicates (7.5 YR 3/2 to 5/6)	highly cemented with secondary minerals (hardpan)	46 - 50

Samples were collected on the surface of the tailings and from a vertical section through the upper 50 cm of the west tailings (Table 5.3). The distribution of elements through the vertical profile is shown in Figure 5.12. Several different geochemical trends are apparent in the depth-profiles. The most common trend shows a gradual increase in concentration with depth and a pronounced increase in concentration in the hardpan (CMT004). Elements showing this trend include Cd, Cu, Zn and Fe. Elements that show an increase above the hardpan (CMT003), include Ag, Au, Na, Sb and Pb. Arsenic has a unique profile; the concentration decreases with depth and is lowest in the hardpan. Sulphide S concentrations increase gradually with depth. The sulphate profile varies little with depth with the exception of a slight increase above the hardpan; a similar trend is observed for structurally-bound water. The carbonate depth-profile is identical to that shown by Cd, Cu, Zn and Fe.

Geochemical variation diagrams for CMT show a variety of element relationships (Fig. 5.13). Positive correlations exist between Cd and Zn, Sb and Pb, and As and Cu. Negative, poorly defined correlations exist between Ag and Cu, Au and Cu, As and Zn, As and Fe, and As and Sb. The CMT data points in Figures 5.14, 5.15 and 5.16 are scattered throughout most of the diagrams; the same mineral-mixing lines are plotted in Figures 5.14, 5.15 and 5.16, as in Figures 4.5, 4.6 and 4.7. Best-fit lines for the CMTE and CMTW sample are superimposed to compare trends. Correlation coefficients for best-fit lines are indicated in the figure captions. Overall, the east tailings have better correlation factors (r) than the west tailings. The east tailings have negative trends, except for in Figure 5.14B and C, and Figure 5.15A, B and C. No best-fit lines for the east tailings are shown in Figure 5.16 due to the low carbonate content in those samples. In Figure 5.14F, most of the samples plot above the

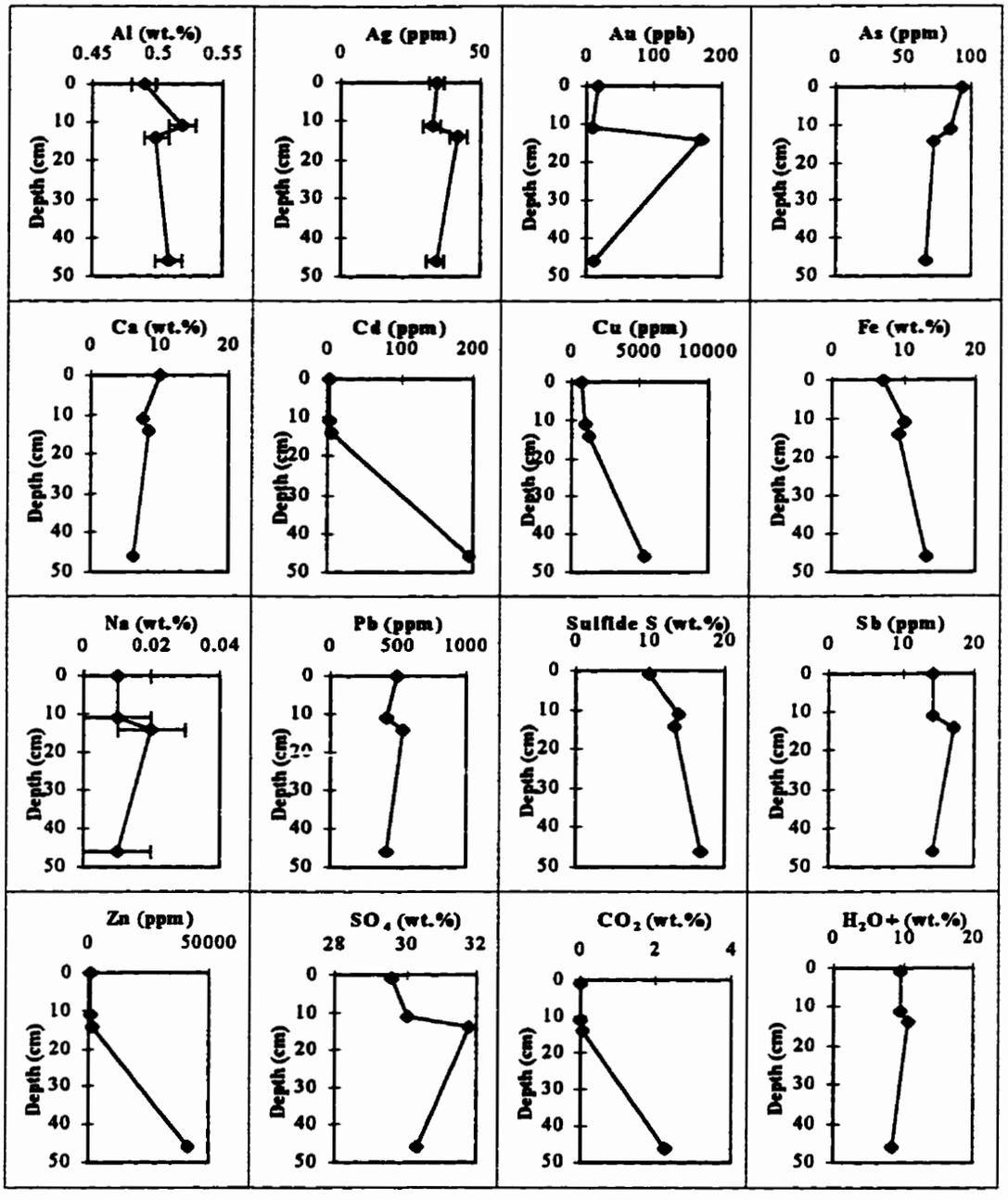

Figure 5.12: Solid-phase geochemical depth-profiles of a section through the upper 50 cm of the CMT; the top of hardpan is at 46 cm; error bars are plotted for errors which exceed the size of the data point marker.

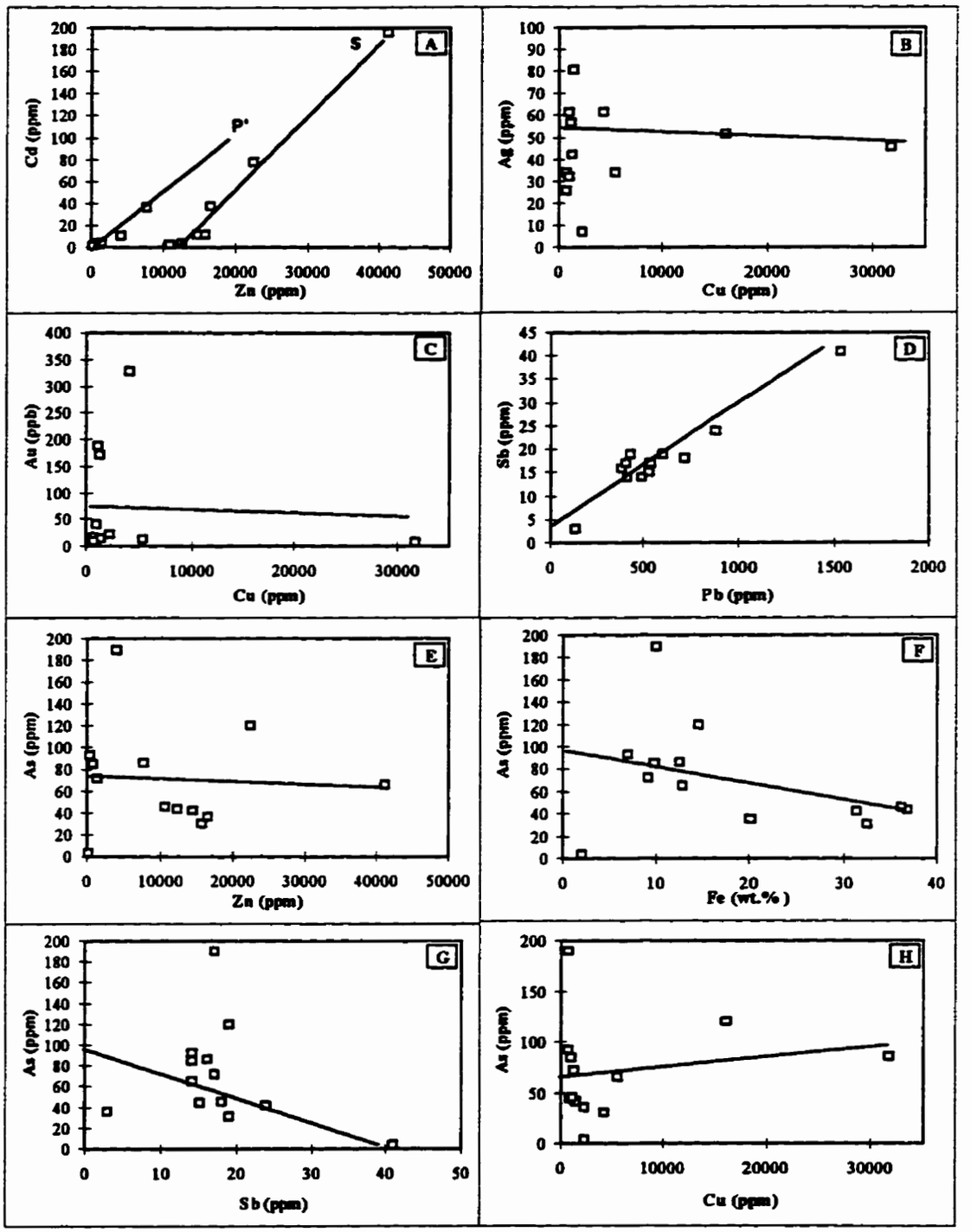

Figure 5.13: Variation diagrams of CMT geochemical results. Error bars are smaller than the data-point markers (therefore not visible). Correlation coefficients (*r*) for the best-fit lines are as follows: (A) 0.971 (P'), 0.993 (S); (B) -0.044; (C) -0.194; (D) 0.953; (E) -0.096; (F) -0359; (G) -0.287; and (H)0.177.

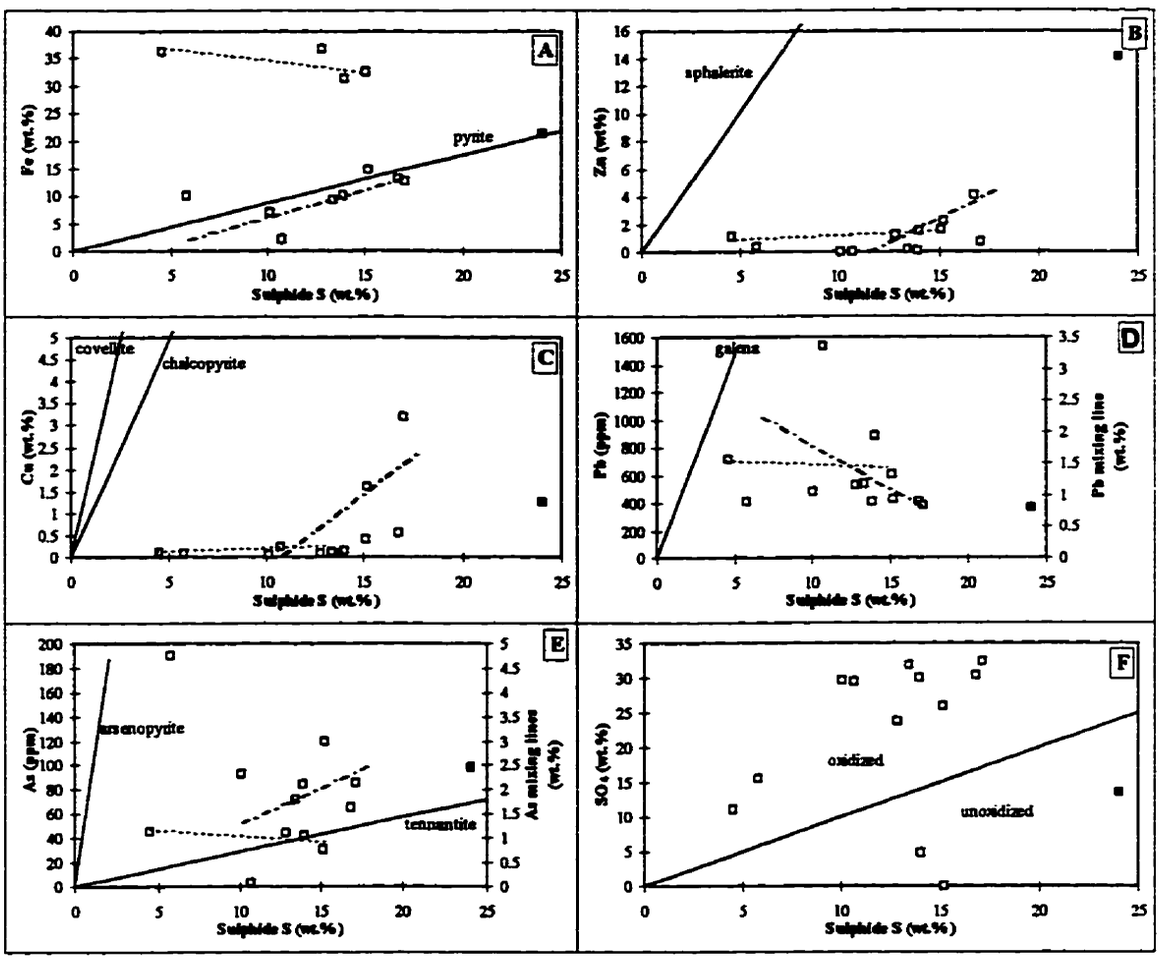

Figure 5.14: Element concentrations in CMT plotted as a function of sulphide S. Solid lines are mixing lines, dashed lines are the best-fit lines for the CMTE assemblage, and dash-dot lines are the best-fit lines for the CMTW pile assemblage; ■ represents CM ore. The mixing lines in D and E are plotted on the secondary y-axis. Error bars are smaller than the data-point markers (therefore not visible). Correlation coefficients (*r*) for the best-fit lines of the east and west piles, respectively, are: (A) -0.611, 0.851; (B) 0.897, 0.664; (C) 0.373, 0.669; (D) -0.1, -0.585; (E) -0.665, 0.387; and (F) no best-fit line calculated.

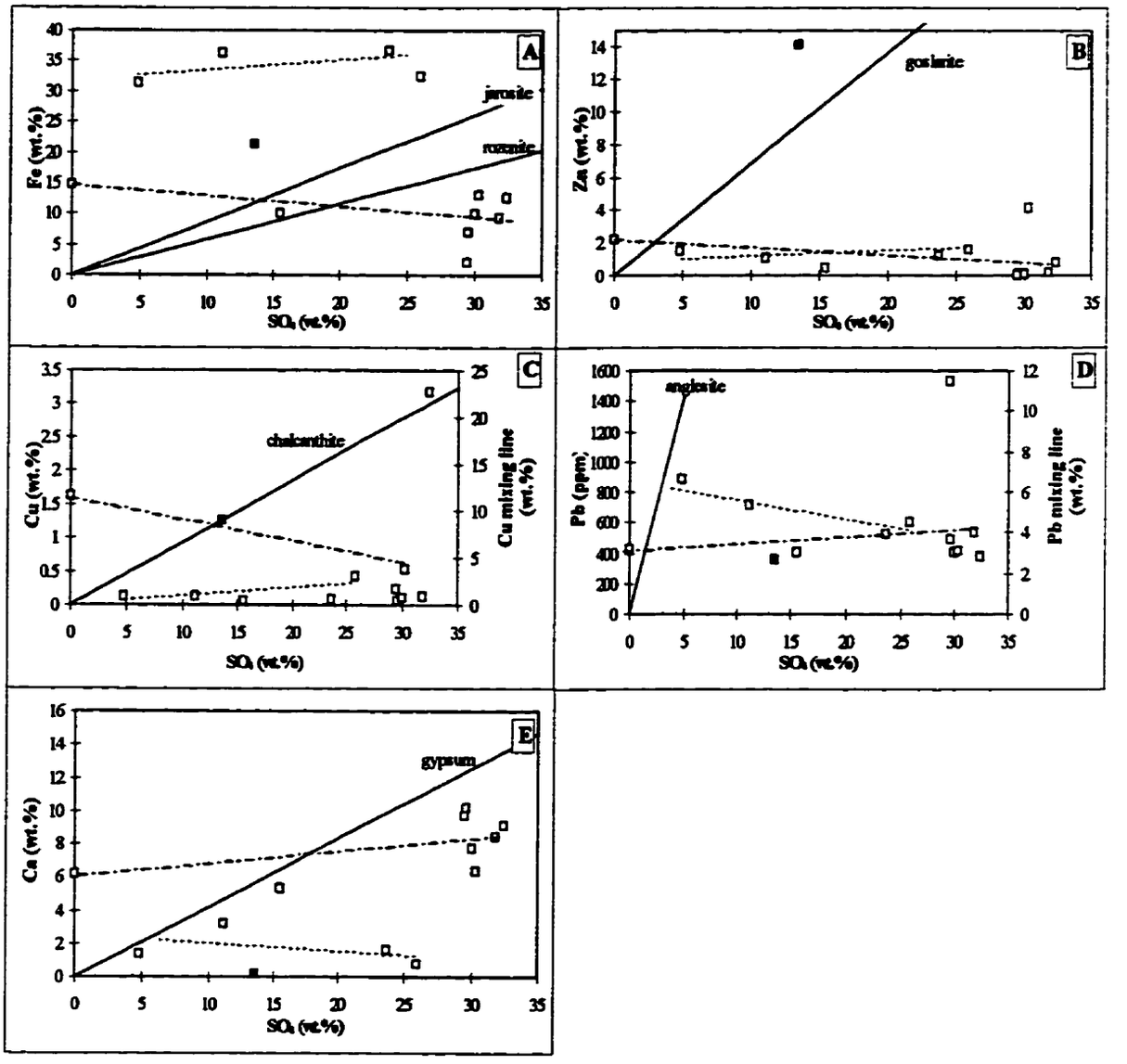

Figure 5.15: Element concentrations in CMT plotted as a function of SO_4. Solid lines are mixing lines, dashed lines are the best-fit lines for the east pile assemblage, and dash-dot lines are the best-fit lines for the west pile assemblage; ■ represents CM ore. The mixing lines in C and D are plotted on the secondary y-axis. Error bars are smaller than the data-point markers (therefore not visible). Correlation coefficients (r) for the best-fit lines of the east and west piles, respectively, are: (A) 0.315, -0.454; (B) 0.236, -0.327; (C) 0.339, -0.228; (D) -0.941, 0.138; and (E)-0.453, 0.571.

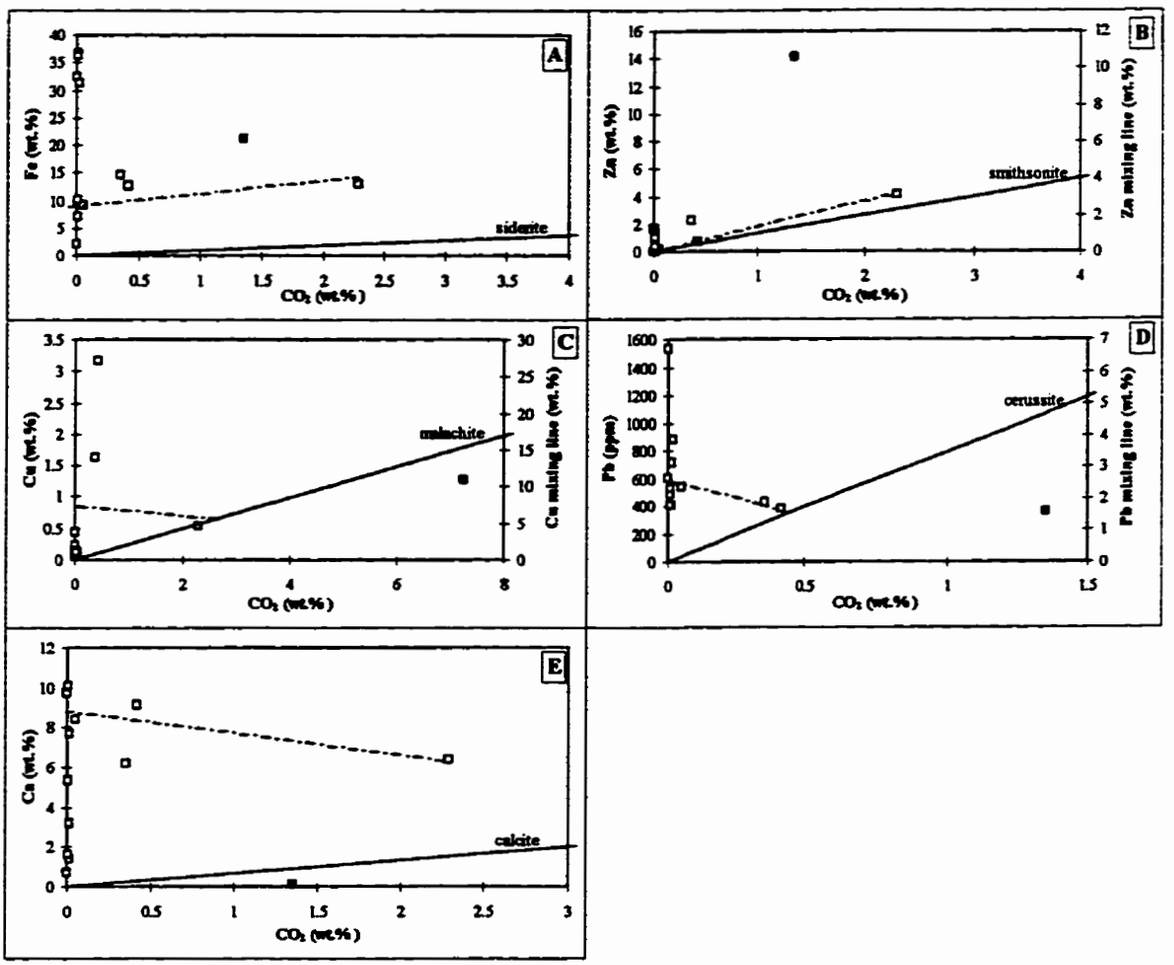

Figure 5.16: Element concentrations in CMT plotted as a function of CO_2 (carbonate). Solid lines are mineral mixing lines, dashed lines are the best-fit lines for the east pile assemblage, and dash-dot lines are the best-fit lines for the west pile assemblage; ■ represents CM ore. The mixing lines in B, C and D are plotted on the secondary y-axis. Error bars are smaller than the data-point markers (therefore not visible). Correlation coefficient (*r*) for the best-fit lines for the east (line not drawn) and west piles, respectively, are: (A)-0.061, 0.478; (B) -0.452, 0.927; (C) -0.585, 0.091; (D) 0.813, -0.282; and (F) 0.590, -0.592.

oxidation line in the oxidized zone; the oxidation line represents the conversion of one mole of sulphide S to sulphate S (i.e., oxidized S), thus has a slope of 1. Tailings data all plot below the mixing lines for sphalerite, chalcopyrite, galena, and arsenopyrite (Fig. 5.14B, C, D and E, respectively). The CMTW pile data (Figure 5.14A) fall roughly along the pyrite line; in contrast, the west pile data plot distinctly above the pyrite line. The trend of the CMTW pile in Figure 5.14B has a more positive slope than the CMTE pile, and follows the sphalerite line more closely. This same trend is observed in the case of Cu (Figure 5.14C) with the chalcopyrite line. The Pb and As data (Figure 5.14D and E) are very scattered, showing no distinct relationships between the east and west piles and the corresponding mixing lines. The ore sample plots directly on the pyrite line, but below all the other mixing lines in Figure 5.14.

The variation diagrams in Figure 5.15 show the scattered nature of the data points. The east and west data points show no distinct differences between the two piles, with the exception of the Fe versus SO_4 and Ca versus SO_4 (Fig. 5.15A and E, respectively), whereas the east tailings contain higher Fe and lower Ca than the west pile. In most of the variation diagrams in Figure 5.15, the data points fall below the mixing line with the exception of one sample. In contrast, the ore sample plots above the mixing lines in the Fe and Zn diagrams (Fig. 5.15A and B, respectively).

In Figure 5.16, the variation diagrams distinctly show the low carbonate content of the tailings. The west tailings only have positive trends in Figure 5.16A and B, but have low correlation factors. All the tailings samples plot above the mixing lines, whereas the ore sample plots below the mixing lines in the Cu, Pb and Ca diagrams (Fig. 5.16C, D and E,

respectively).

5.3 Stream-Water Chemistry

Figure 5.17 shows dissolved-metal concentrations of water samples collected at varying distances downstream from the Cleveland mill-tailings in 1995 (samples CMW02 to CMW06, and CMW08 in Fig. 2.2; Appendix A). Immediately below the tailings, the pH of the stream water was 2.3 and metal concentrations were high (Fig. 5.17). The stream-water colour was dark brown, indicative of high concentrations of dissolved metals (Fig. 5.18), and its acidic nature dissolved the carbonate bedrock along the stream bed. At a distance of 300 m

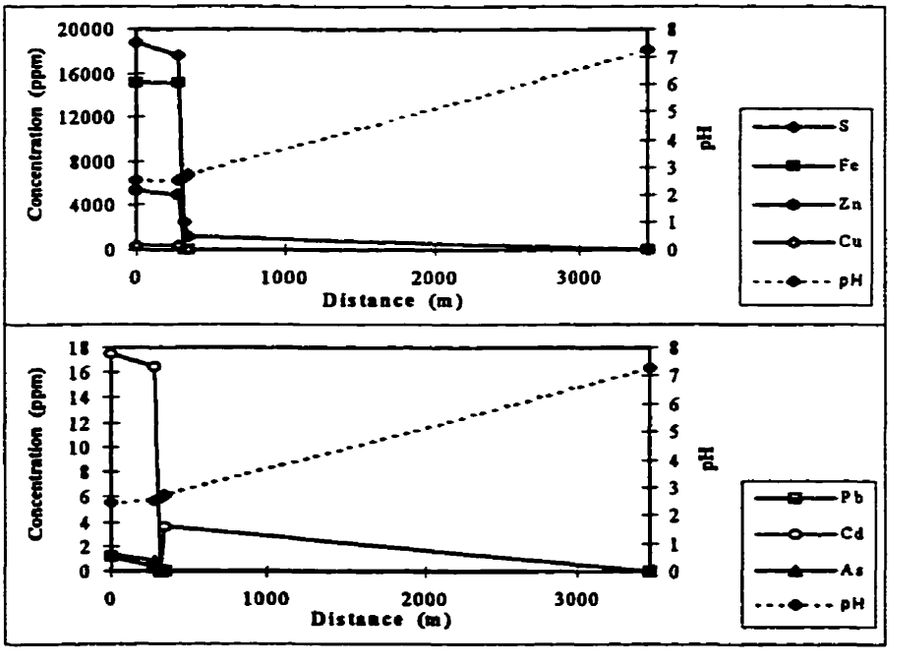

Figure 5.17: Dissolved-metal concentration and pH in the stream waters as a function of distance downstream from CMT; error bars are smaller than the data points.

downstream, water from an ephemeral spring (pH = 7.17; sample CMW04) mixed with the acidic drainage of the mill-valley tributary. The spring water had a neutral pH and had formed a small travertine deposit on the west slope just above the acidic stream. The pH of the

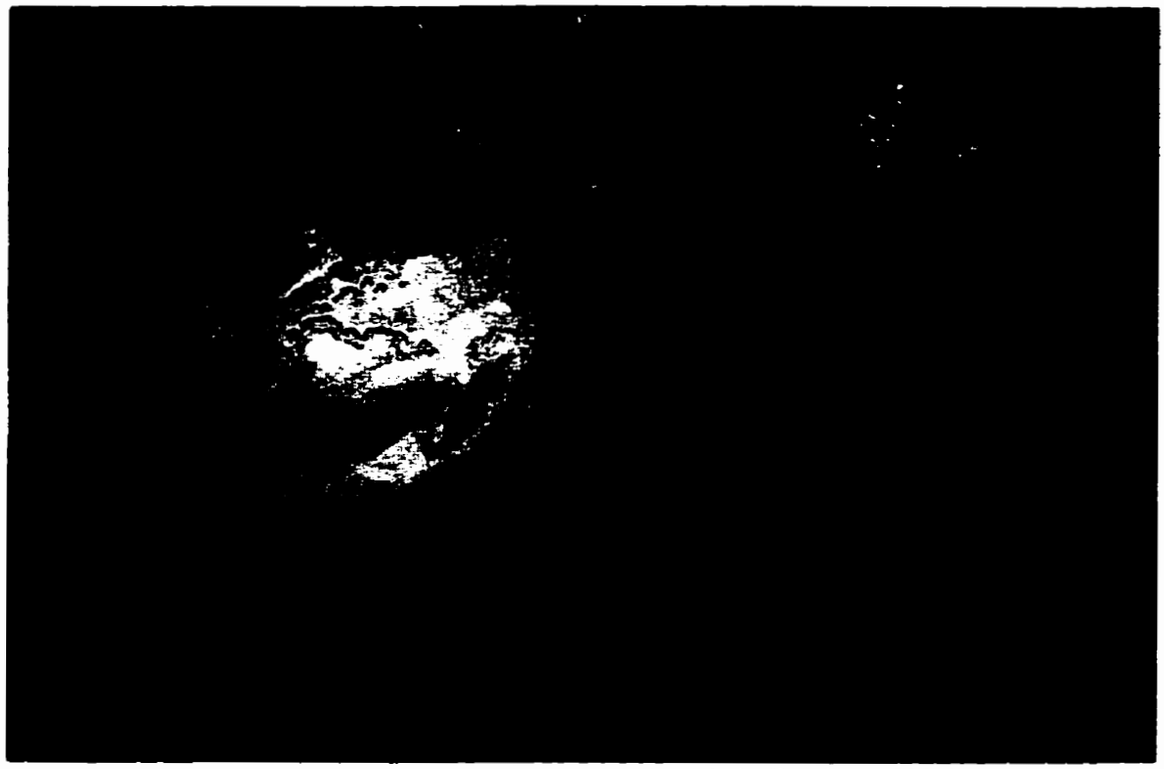

Figure 5.18: AMD water pools; dark-brown colour is indicative of high concentrations of dissolved metals and acidic conditions.

Figure 5.19: Dissolution of carbonate bedrock is caused by the AMD; rusty colour of the stream bed is due to the precipitation of Fe-oxyhydroxides and sulphates.

stream increased slightly up to 2.5 immediately below its confluence with the spring. Precipitation of Fe-oxyhydroxides/sulphates (as seen by the rusty colouration of the stream bed; Fig. 5.19) resulted in a decrease in the dissolved-metal concentrations. At a distance of 3.5 km downstream, pH increased to 7.27 and dissolved-metal concentrations fell below detection limits.

5.4 Bacterial-Growth Observations

The inoculation of CMT012 gave negative results. During the entire six-week period, the medium remained clear, indicating that no bacteria had grown. The reinoculation of a PAT001 into CMT012 also gave negative results. No precipitate or cloudiness was observed during the entire experiment (Fig. 5.20), and the pH remained acidic.

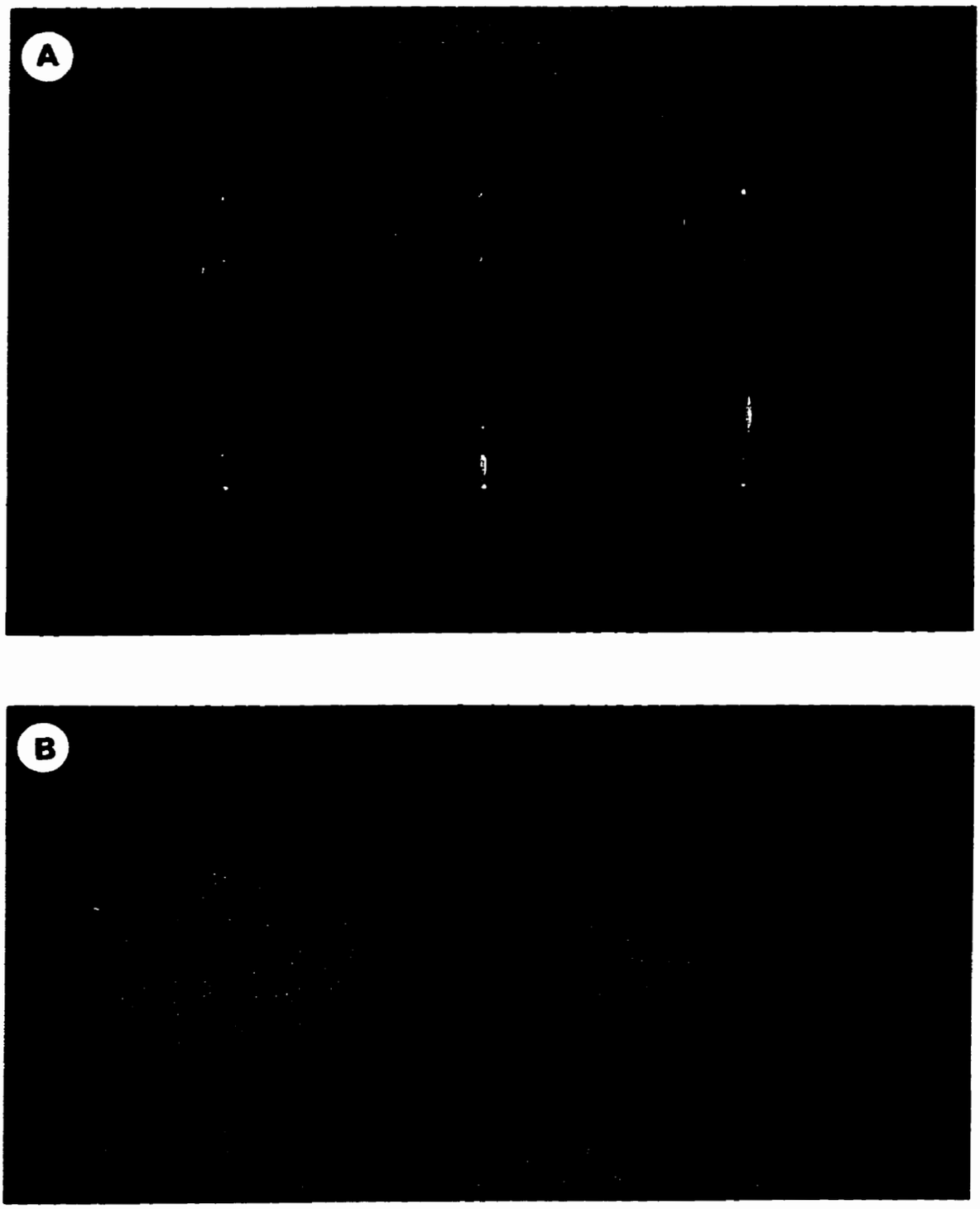

Figure 5.20: (A) CMT bacterial-growth flask experiment; (B) clear liquid and no change in the tailings colour indicate no bacterial growth.

CHAPTER 6

DISCUSSION AND CONCLUSIONS

6.1 Discussion

There is little evidence of alteration of the CPAT, and thus trends in variations diagrams (Fig. 4.4) reflect primary geochemical coherences. For example, Cd shows a positive linear correlation (r = 1.00) with Zn, indicating that Cd is hosted by sphalerite (Fig. 4.4A). Similarly, Ag correlates positively with Cu, as it is mainly hosted by or associated with chalcopyrite (Fig. 4.4B). Gold also correlates positively with Cu (Fig. 4.4C), although the trend is less well-defined than that for Ag versus Cu. The positive correlation between Sb and Pb suggests that galena is the main host of Sb, although sulfosalts (e.g., boulangerite, $Pb_5Sb_4S_{11}$) also may host Sb. Although sulfosalts have not been observed in the ore or tailings samples from either site, the positive correlations between As and Sb and between As and Cu (Fig. 4.4G and 4.4H) suggest that they are hosted by fahlore-group minerals (e.g., tetrahedrite-tennantite). The positive trend in As versus Zn (Fig. 4.4E) may be due to (1) trace As in sphalerite, or (2) substitution of Zn for Cu in fahlore group minerals (e.g., tetrahedrite-tennantite). The main host of As in the CPAT is probably arsenopyrite, as suggested by the positive correlation between As and Fe (Fig. 4.4F). Arsenopyrite was not observed in the CPA ore or tailings in this study, but it has been reported in the Cleveland deposit by other workers (McKnight and Fellows, 1978; North and McLemore, 1986).

Unlike the CPAT, there is abundant evidence of chemical weathering of the CMT. Thus, variation diagrams for the CMT must be interpreted with regard to both primary mineralogy

and secondary processes. Because of the similarity in mineralogy of the two deposits, compositional relationships in the CPAT may be used as an indication of those in the CMT prior to the onset of chemical weathering. Trends in variation diagrams for CMT reflect the superposition of secondary assemblages on primary assemblages (Fig. 6.1). The plot of Cd versus Zn shows a single linear relationship for CPAT and two linear relations for CMT, one of which converges with the CPAT assemblage (Fig. 6.1A). Trend 'P' reflects a primary signature in the CPAT, with Zn and Cd both occupying sphalerite. 'P'' is interpreted as a primary trend for the CMT. The slightly lower slope than that shown by trend P likely is due to lower Cd content of sphalerite in the Cleveland deposit than that of sphalerite in the Cyprus-Piños Altos deposit. Trend 'S' may represent a secondary relationship developing under conditions where following oxidation of sphalerite, Zn was less mobile but Cd was strongly leached from the tailings. However, the CMTE tailings samples all correspond to the secondary ("S") trend, whereas most of the CMTW samples correspond to the "P'" trend. Therefore, these results may also represent primary-ore differences, where the CMTE sphalerite is more deficient in Cd, but more enriched in Fe, relative to sphalerite in the west tailings. This "secondary" signature may be a function of the primary zonation within the skarn deposit. The secondary trend also suggests that the east tailings are more weathered than the west tailings, thus showing a stronger secondary signature for the east samples. This is consistent with lower CO_2 contents in CMTE.

The positive trends for the CPAT assemblage in Ag versus Cu and Au versus Cu (Fig. 6.1B and C, respectively) indicate the presence of Au and Au in chalcopyrite. In contrast, the CMT assemblage in Figure 6.1B and C has negative trends and poor correlations. This is a

result of the decoupling of Ag and Au from Cu during weathering of chalcopyrite. In contrast to weathering effects on chalcopyrite and its impurities, Figure 6.1D shows positive trends and moderate correlations for *both* CPAT and CMT. These indicate the limited effects of weathering on Pb in galena and its impurities (e.g., Sb), because the mobility of Pb is very low, even in the strongly oxidizing environment of the CMT.

Positive correlations in the CPAT of As versus Fe (Fig. 6.1F) and As versus Cu (Fig. 6.1H) suggest that As is present in arsenopyrite as well as tetrahedrite-tennantite ($(Cu,Fe)_{12}Sb_4S_{13}$ - $(Cu,Fe)_{12}As_4S_{13}$). The positive correlation between As and Sb in the CPAT (Fig. 6.1G) also suggests that As may be hosted by tetrahedrite-tennantite. As Zn can substitute for Cu in fahlore-group minerals, the positive correlation between As and Zn in the CPAT (Fig. 6.1E) also may reflect the presence of tetrahedrite-tennantite, or trace amounts of As in sphalerite. The negative trends and poor correlations between As and Zn, Fe, and Sb in the CMT suggest that tetrahedrite-tennantite has broken down and different relative mobilities have separated these elements during chemical weathering. The positive correlation between As and Cu in the CMT suggests that As may be present in secondary (supergene) Cu sulphides such as covellite, rather than fahlore group minerals. The scattering of the CMT data suggests that the secondary mobility of As is complex. A bulk-ore sample from the Cleveland mine (containing sphalerite, chalcopyrite and pyrite but no observable arsenopyrite) contained 98 ppm As. EMP analysis of sphalerite, pyrite and chalcopyrite revealed that concentrations of As are at or below detection limits.

The variation diagrams in Figure 6.2 show the control that the sulphides have on the distribution of metals in the primary minerals in CPAT, and how oxidation has affected these

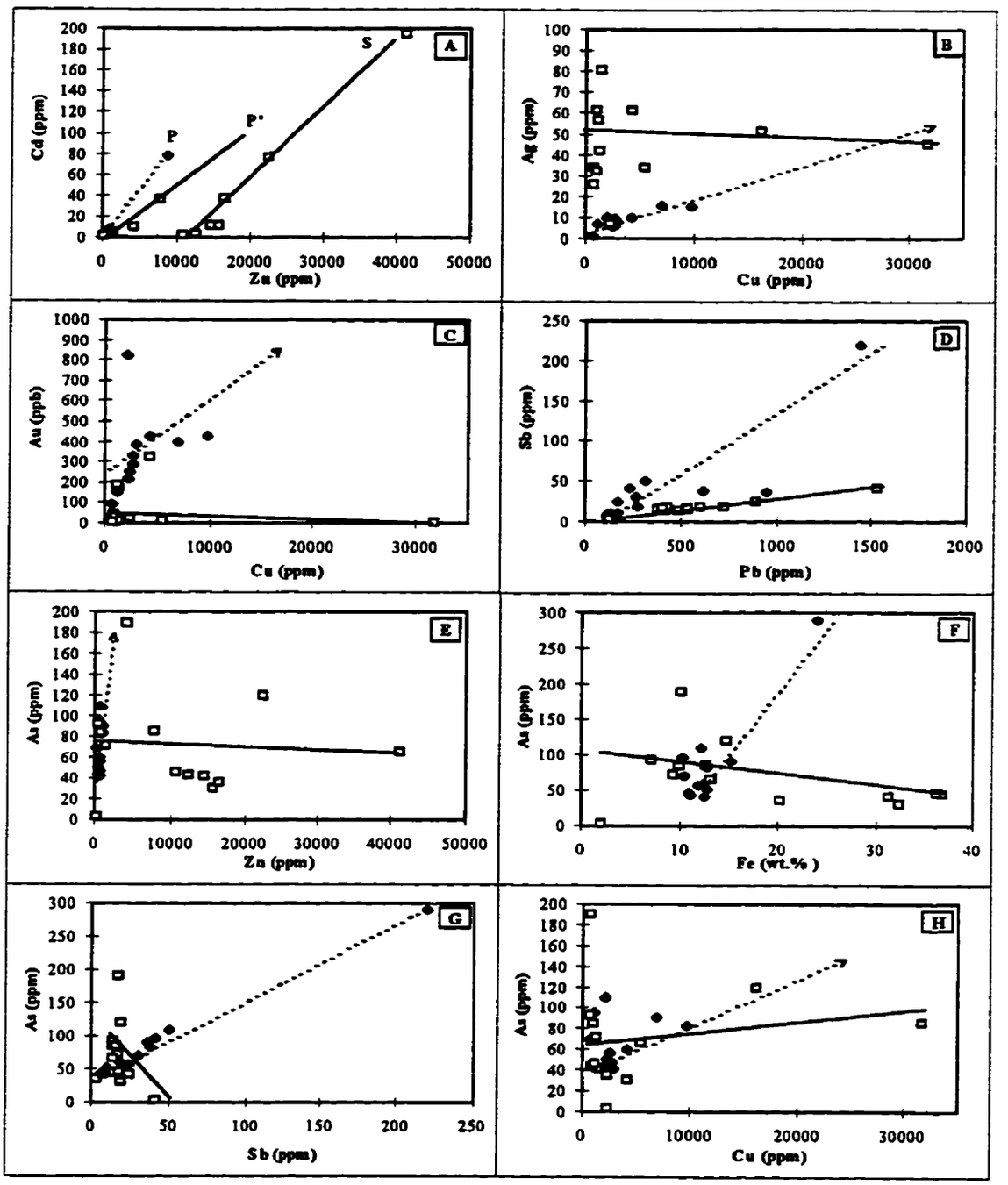

Figure 6.1: Variation diagrams comparing CMT and CPAT geochemical results. Solid line and □indicate CMT samples; dashed lines and ●indicate CPAT samples. P and P' indicate primary trends for CPAT and CMT, respectively, S indicates a secondary trend for CMT. Arrows point to the value for ore concentrate from the Cyprus-Piños Altos mine.

sulphides in the CMT. For samples that fall directly *on* the mixing lines, e.g., pyrite line (Fig. 6.2A), their bulk sulphide mineralogy is dominated by an Fe-sulphide, such as pyrite. For samples that fall *above* the mixing line, Fe contents are influenced in addition by non-sulphide Fe-minerals such as magnetite, resulting in high Fe content relative to S. For samples that fall *below* the mixing lines, other sulphides such as sphalerite, chalcopyrite, galena and arsenopyrite contribute to higher S values relative to Fe (Fig. 6.2B, C, D and E). Meanwhile, all the CPAT and CMT assemblages fall below the mixing lines in Figure 6.2B, C, D and E, indicating a high sulphide S background and low sphalerite, chalcopyrite, covellite, galena, arsenopyrite and tennantite contents relative to pyrite. All the CPAT samples have positive linear correlations. The correlations all represent primary assemblages, but the divergence of the CPAT assemblage trends from the mixing lines is a function of the proportions of different sulphide species present in a bulk sample, giving the effects of background S concentrations. However, the dominant Fe-bearing sulphide is most likely pyrite, as the CPAT samples all plot above the pyrite line, but *below* the sphalerite, chalcopyrite, covellite, galena, arsenopyrite and tennantite lines (Fig. 6.2B to E). In Figure 6.2E, the CPAT samples fall in two distinctly different trends that converge; this pattern is identical to the relation between the arsenopyrite and tennantite lines, suggesting that these two As-bearing minerals are the dominant As control in the primary assemblage[1]. The data points in Figure 6.2A plot near the pyrite line, suggesting that the sulphide mineralogy of the CMT is dominated by

---

1 In Figure 6.2 D and E, Figure 6.3C and D, and Figure 6.4B, C and D, the mixing lines are plotted against the secondary y-axis, therefore has a different y-scale than the primary y-axis which represents the data points.

pyrite; the CM ore plots directly on the pyrite line, further supporting pyrite as the dominant Fe-bearing sulphide. The positive correlation between Fe and S for both the east-pile samples and the ore (Figure 6.2A), suggests that the composition of the ore samples is closer to that of the CMTE pile than the CMTW pile. Due to the zonation common in most skarn deposits, this sort of differentiation is not unusual. The CMTW line has a positive trend and plots close to the pyrite line suggesting the presence of primary pyrite in the CMTW; the CMTE line is negative and plots further away from the pyrite line, suggesting a lack of primary pyrite. This differentiation between the east and west piles suggests that the east pile is more weathered than the west pile. The difference in the degree of weathering may be a function of the sun-facing direction of the piles. The west pile gets more sun than the east pile, and therefore dries out faster; whereas, the east pile stays wetter, thus allowing the oxidation to proceed more rapidly and extensively.

In Figure 6.2B and C, a positive correlation occurs between Zn and S, and Cu and S in both the ore and tailings of CM (with the exception of a few samples); the oxidized nature of the tailings likely is responsible for the scattered results. The trends for Zn versus S and Cu versus S in CMTW indicate an abundance of Zn and Cu relative to the CMTE; this may be a result of two factors: (1) primary zonation within the skarn deposit, and/or (2) more extensive weathering of CMTE relative to CMTW, the CMTW trend (less oxidized) following the sphalerite trend. The CMT mixing lines both have more positive slopes than the CPAT mixing line in Figure 6.2B, but the opposite occurs in Figure 6.2C. This is a reflection of the different skarn types: CPA is a Cu-skarn, resulting in a higher slope of the plot of Cu versus S relative to that for CM; CM is a Zn skarn, resulting in a higher slope of

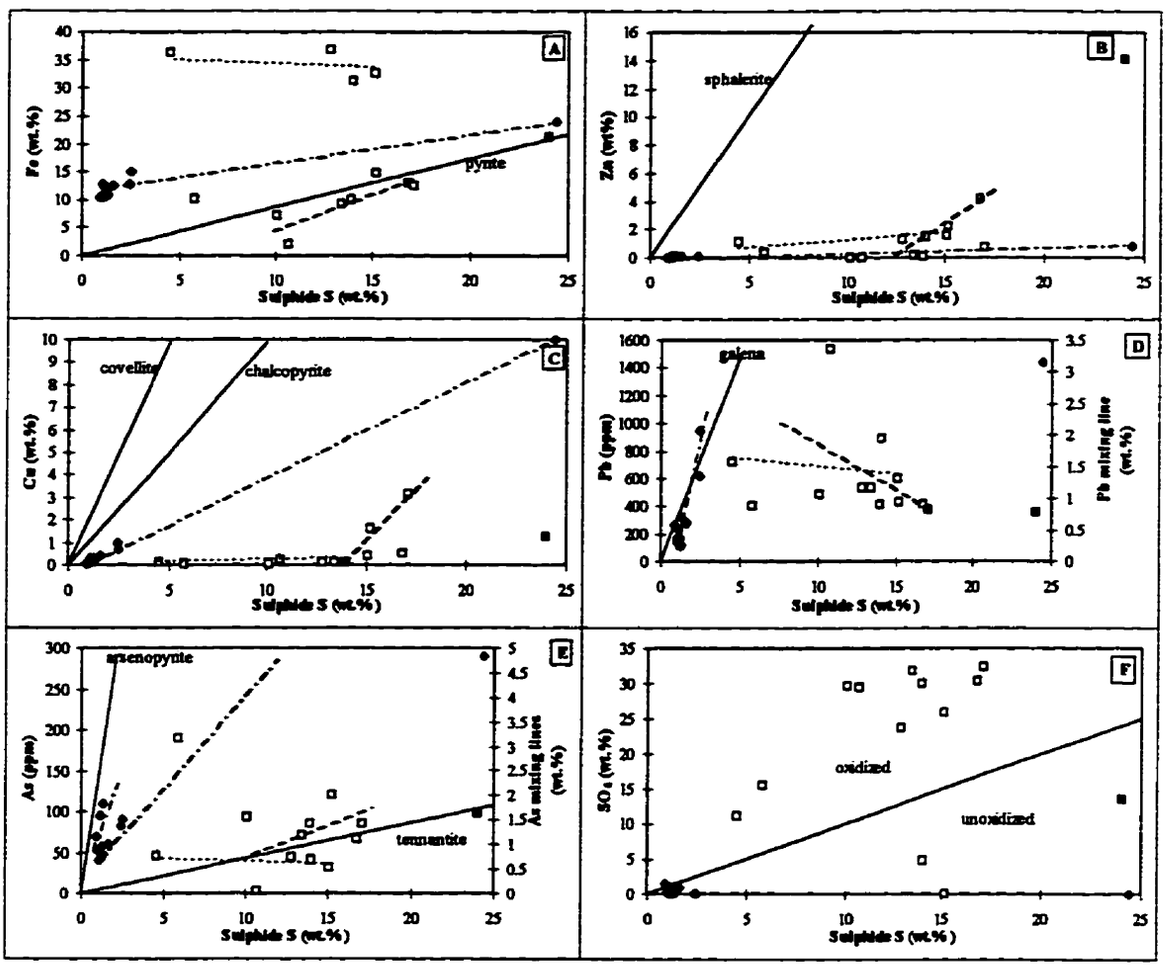

Figure 6.2: Variation diagram comparing element concentrations in the CPAT and CMT as a function of sulphide S. Solid lines are mixing lines; dashed lines and □ indicate CMT samples (short dash is CMTE and long dash is CMTW); dash-dot lines and ● indicate CPAT samples. The mixing lines in D and E are plotted on the secondary y-axis.

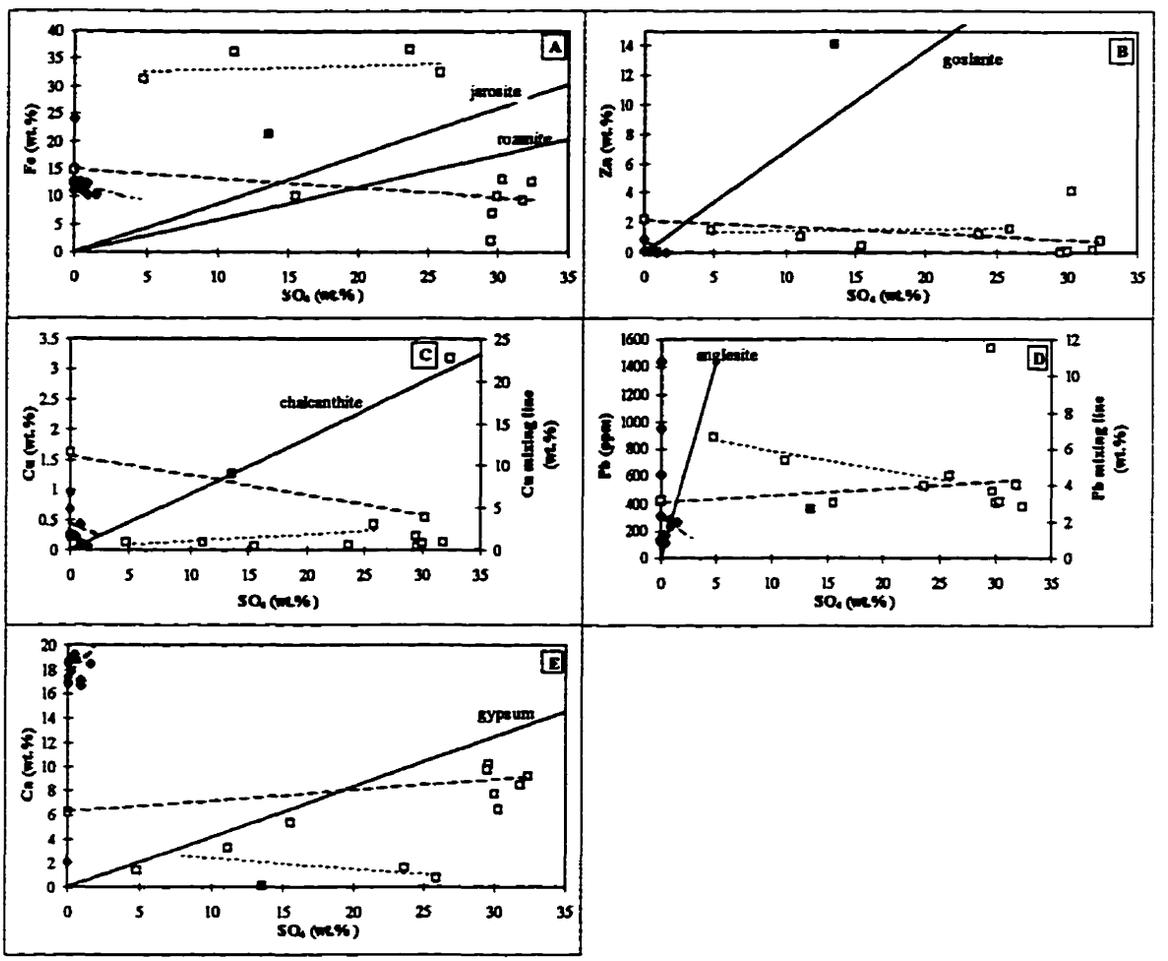

Figure 6.3: Variation diagram comparing CPAT and CMT element concentrations as a function of SO_4. Solid lines are mixing lines; dashed lines and □ indicate CMT samples (short dash is CMTE and long dash is CMTW); ■ represents CM ore; dash-dot lines and ● indicate CPAT samples. The mixing lines in C and D are plotted on the secondary y-axis.

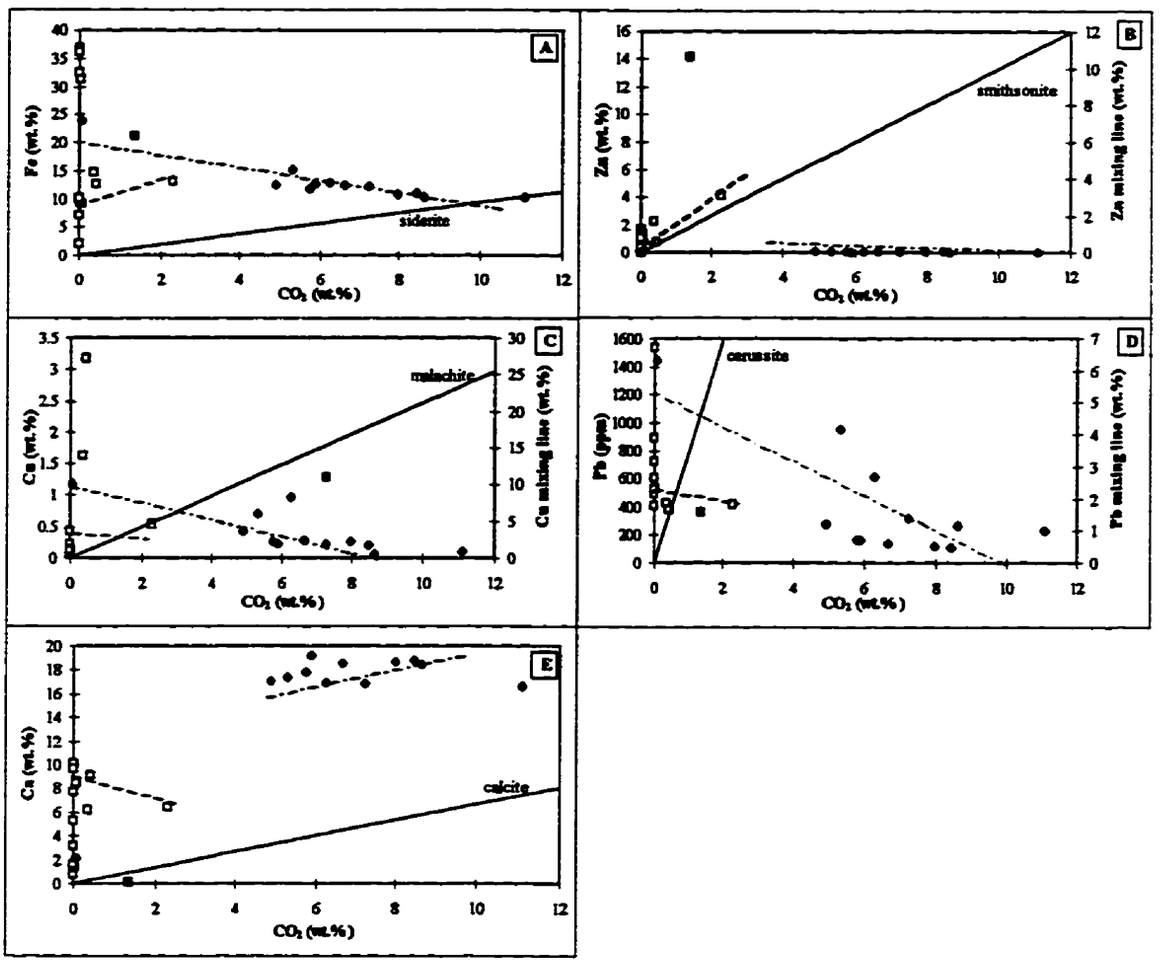

Figure 6.4: Variation diagram comparing CPAT and CMT element concentrations as a function of CO_2 (carbonate). Solid lines are mixing lines; dashed lines and □ indicate CMT samples (long dash is CMTW, no lines plotted for CMTE); ■ represents CM ore; dash-dot lines and ●indicate CPAT samples. The mixing lines in B, C and D are plotted on the secondary y-axis.

the plot of Zn versus S relative to that for CPAT.

Data for Pb and As (Fig. 6.2D and E) in the CMT are extremely scattered, suggesting complex oxidation and mobility histories. Galena is probably the main host of Pb in CPAT, as indicated by the positive trend of the CPAT assemblage; however, Pb-bearing sulfosalts would also give positive correlation with a different slope than galena.

Variation diagrams of metals versus SO_4^{2-} and CO_2 (Fig. 6.3 and 6.4) show the unoxidized nature of the CPAT, with its low SO_4^{2-} content and high CO_2 content. In contrast, the highly oxidized CMT have high and scattered SO_4^{2-} contents and low more restricted CO_2 contents. The poor correlation of the data points with the sulphate and carbonate mixing lines reflects the complex mineralogical and geochemical controls on these metals. For example, not all Zn is tied up in secondary goslarite (Fig. 6.3B), Cu in chalcanthite (Fig. 6.3C), or Pb in anglesite (Fig. 6.3 D). Metals are tied up in *many* different minerals as major and trace elements and as crystallographic impurities.

In Figure 6.3A, only one sample plots within the jarosite-rozenite "envelope"; that sample is the stream sediment sample (CMT012). This sample plots between the east and west samples with respect to SO_4^{2-}, as it is composed of tailings particles from both piles. The location of this sample within the mixing "envelope" suggests that, at this location in the stream, the dominant secondary minerals precipitated from the AMD are Fe-oxyhydrosulphate minerals, along with some Fe-oxyhydroxides (e.g., goethite).

The CPAT plot far from the gypsum line, whereas the CMT plot near the gypsum line (Figure 6.3E). Although the CPAT contains tertiary gypsum, calcite is abundant in the tailings (Fig. 6.4E), exercising the dominant control on the Ca content. Figure 6.4E indicates

the presence of calcite in the CPAT by the positive parallel correlation with the calcite line. The CPAT plots above the calcite line, indicative of the presence of other Ca-bearing phases, such as grossular, diopside and wollastonite. In contrast, gypsum is likely the dominant Ca-bearing mineral in the CMT (Fig. 6.3E), as suggested by the close association of the CMT assemblage and the gypsum line, as most of the primary calcite has been dissolved (Fig. 6.4E).

As the CPAT show little evidence of alteration, the geochemical depth-profiles directly reflect the primary mineralogy of the tailings samples (Fig. 4.3). The elevated S, Ag, Cd, Cu, As, Pb, Sb and Zn in the upper 15 cm of the vertical section reflect the relative sulphide enrichment in this upper interval. Variations in element concentrations may be a function of: (1) the grade of ore zone being mined during a given period, (2) efficiency of extraction processes, and (3) mineral partitioning during deposition (resulting from grain-size sorting). Sieve analyses were done on all the samples from the section (Appendix F). Samples showed little grain-size variation with depth, suggesting that mineral partitioning during deposition is not the cause for the variations. Unlike the elements above, concentrations of Ca, Al and CO_2 (carbonate) are low at the surface and increase with depth. This relationship may be directly related to the reactivity of the sulphide and gangue minerals at the surface of the tailings, or to the relative dilution of gangue minerals by sulfides, as the sulphide content is high at the surface. The former is most likely the case.

The Cyprus-Piños Altos tailings have undergone very little, if any, mineralogical and geochemical changes since their deposition. The addition of lime to the tailings has maintained a neutral pH, preventing sulphide oxidation and dissolution of gangue minerals such as calcite. However, the precipitation of tertiary gypsum from pore water indicates that

the tailings have not been completely unreactive. The relative reactivity of sulfides in a tailings environment is pyrrhotite > sphalerite-galena > pyrite-arsenopyrite > chalcopyrite > magnetite (Jambor, 1994). Pyrrhotite is absent in the CPAT; thus, sphalerite and galena are the most reactive sulphide minerals in the impoundment. Electron-microprobe analysis of the sphalerite in the CPAT revealed Fe concentrations as high as 10.76 wt. %. Such elevated Fe contents in sphalerite result in tetrahedral distortions of the crystal structure (Shadlum and Turpeko, 1970), thus increasing its surface reactivity with the pore water. The low sulphate/sulphide ratio (Fig. 6.5) in the bulk tailings suggests that, although most of the total sulphur is in the sulphide state, a small fraction has been oxidized to sulphate. Figure 4.5F indicates that although most of the tailings appear fresh, they do plot near the oxidation line and one sample plots in the oxidized zone. Although the dissolved concentrations of Zn and S in the pond water are relatively low (0.07 ppm and 51 ppm, respectively), the concentrations of other metals are even lower. This suggests that sphalerite is the most likely source of SO_4^{2-}, and

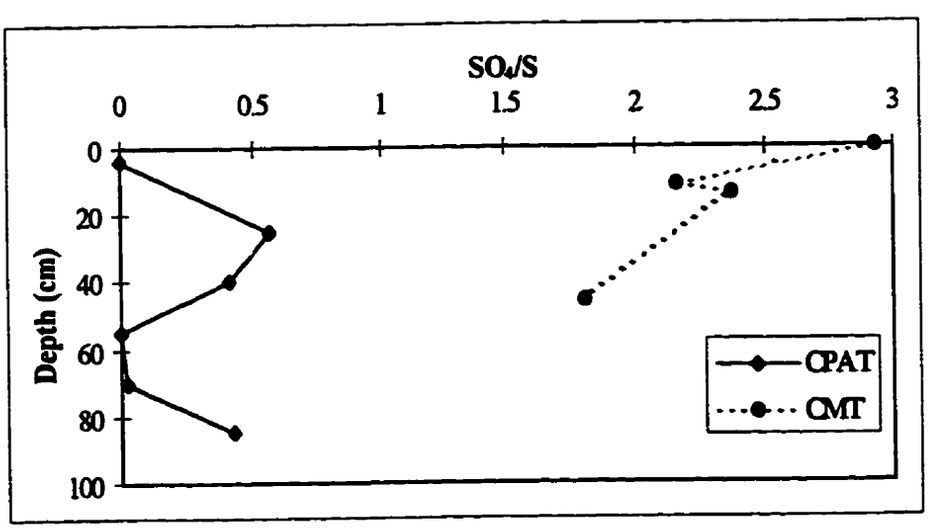

Figure 6.5: Depth-profile of SO_4^{2-}/sulphide S ratio in CPAT and CMT.

lime added during processing is the source of Ca^{2+}. During drying of the tailings in the lab, concentrations of Ca^{2+} and SO_4^{2-} in the porewaters increase (as the volume of water decreases) until gypsum saturation occurs and gypsum precipitates.

Geochemical depth-profiles of the vertical section of the CMT reflect a relationship between chemistry and environmental conditions. The hardpan, located at a depth of 46 cm, is the lower-most zone of a 50 cm-thick section sampled, and represents the local zone of acid neutralization and chemical precipitation (Blowes, 1990; McGregor, 1994). This zone is highly cemented and has elevated concentrations of metals in the solid phase. The three zones above this hardpan represent the sulphide-oxidation and acid-generation zones. These upper three levels contain completely- to partly-oxidized sulfides and are composed mainly of secondary minerals; McGregor (1994) found such zones to have high acid generation and high dissolved-metal concentrations in porewaters. Figure 5.4 shows a section through the east tailings (from 1996 site visit) that exposes the relationship between the oxidized and unoxidized tailings. The upper oxidized zone is the sulphide-oxidation and acid-generation zone (McGregor, 1994), and the lower unoxidized portion consists of primary tailings minerals that have not been altered. The unoxidized zone represents the zone of metal attenuation that has low dissolved-metal concentrations in porewaters and neutral pH. The boundary between the unoxidized and oxidized tailings is cemented, and represents the hardpan. In tailings environments, downward-moving water in the tailings becomes acidic until it reaches a zone where the acid is neutralized, and where a high proportion of gangue minerals and minimally altered sulfides remain (hardpan and unoxidized zones)

The CMT are extensively oxidized; Figure 6.2F shows that CMT plot mostly in the

oxidized zone, compared to the unoxidized CPAT. The SO_4/S ratio for CMT (Fig. 6.5) shows a decrease in sulphate with depth, corresponding to an increase in sulphide S, as expected by the transition from oxidizing to reducing zones. Acid neutralization caused by carbonate dissolution decreases the solubility of dissolved elements, thereby causing these elements to precipitate (usually as secondary carbonates, oxides and oxyhydroxides). Such a trend is clearly visible in the geochemical depth-profiles for many elements in the CMT, including Cd, Cu, Fe and Zn, as well as CO_2 (Fig. 5.12). These metals require acidic conditions to be transported from their source; increasing pH causes precipitation in the hardpan layer. The hardpan layer at CMT contains abundant unaltered sulphide and gangue minerals. The presence of sulfides in the hardpan is reflected in the increased amount of sulphide S in this zone (Fig. 5.12). The high metal concentrations in the hardpan are the result of both preservation of primary sulfides and precipitation of secondary oxides and carbonates; no secondary sulfides have been observed.

Elements such as Ag, Au, Pb and Sb tend to concentrate in the layer above the hardpan. These elements are reactive metals that form highly insoluble complexes with sulphate. As the percolating waters approached the hardpan in the west pile, the pH increased slightly. This increase was enough to cause these highly insoluble metal-sulphate complexes to precipitate. This sulphate precipitation is also apparent from the slight increase in concentration above the hardpan in the sulphate depth-profile (Fig. 5.12). The same trend occurs in the profile for structurally-bound water, suggesting that hydrated secondary minerals are most abundant above the hardpan. The concentration of Na also increases above the hardpan (Fig. 4.20); XRD results indicate that this is a zone of mass precipitation of

natrojarosite ($NaFe_3(SO_4)_2(OH)_6$).

In contrast to geochemical profiles for base and precious metals, profiles for As, Ca and K exhibit a gradual decrease in metal concentrations with depth. At the hardpan layer, jarosite, the primary K-bearing secondary mineral, becomes slightly undersaturated in the pore water, causing it to partly dissolve. This same trend has been observed at the Copper Cliff tailings site in Sudbury, Ontario (McGregor, 1994). Due to the high mobility of Ca under most conditions (Plant and Raiswell, 1983), the decrease in concentration with depth is unusual. This trend may be due to the mobility restrictions of a Ca-bearing complex, evaporation of Ca-rich pore waters near the surface, evaporative pumping, or primary-mineral distribution. In contrast, As has moderate mobility under most conditions, but is immobile under reducing conditions (Plant and Raiswell, 1983); thus, a depth-profile trend opposite of that observed would be expected. The distribution of As throughout the tailings may therefore be a function of the restricted mobility of an As-bearing complex, preferential uptake into a secondary phase, or primary-mineral distribution.

In the CMT, oxidation of sulfides resulted in the generation of acidic solutions and subsequent dissolution of gangue minerals, particularly calcite. The alteration rims on sulfides represent the effects of diffusion-limited alteration mechanisms (the small-scale shrinking-core model of Davis and Ritchie, 1986) which operated during the oxidation cycle described above. There is evidence for two distinct diffusion processes in the CMT: (1) outward diffusion of Fe, leaving a S-rich core or rim; and (2) outward diffusion of S, leaving an Fe-rich core or rim. The first process occurs most commonly in sphalerite, where native S rims cover the remaining sphalerite core (Fig. 5.6). The second process occurs most commonly in pyrite,

where a reactive Fe-rich rim is left behind; this rim reacts with the air and pore-water to produce specular hematite (Fig. 5.7). All sulfides have multi-layer rims surrounding an unaltered core. Generally, the innermost layer is the diffusion-limited rim.

Although gypsum is the most common tertiary mineral in tailings, it is also present as a minor secondary mineral in the CMT. Evidence supporting a secondary origin is the occurrence of gypsum beneath layers of secondary Fe-oxyhydroxides and oxyhydrosulphates. Secondary gypsum often contains small amounts of Fe, Zn or Cu impurities, and has a massive crystal habit. Tertiary gypsum lacks impurities and forms stubby subhedral to euhedral crystals in the matrix, or radiating clusters on mineral surfaces. The Fe oxyhydroxides and oxyhydrosulphates and secondary gypsum are formed by wet/dry cycles which resulted in desiccation cracks in precipitates on grain surfaces. Wet/dry cycles also affect the surface of the tailings pile. During a trip to the CMT in November 1996, white precipitates (mainly gypsum) were observed covering the surface of the tailings (Fig. 5.1); the visit followed an extended period of dry weather. When samples were collected in February 1995, the surface of the tailings was relatively free of efflorescent sulphates (Fig. 1.3) because there had been abundant flushing of the tailings during early snow melt. Thus, gypsum layers coating individual grains are associated with periods of drying, when porewaters become saturated with respect to gypsum through water loss. In contrast, layers of Fe-oxyhydroxides and oxyhydrosulphates are associated with wet periods when oxidative dissolution of sulfides increases the amount of dissolved Fe in porewaters.

The accuracy of the geochemical results are strongly dependent on sample homogeneity. At the CPAT site, representative sampling of the impoundment is difficult due to grain-size

sorting and hydraulic-density differentiation that occurs as a result of deposition. The CPAT physical hydrology is analogous to sedimentary environments such as a delta, where coarser grains and high-density grains occur nearest the source of deposition (i.e., spout), and the finer and lower-density grains are transported and deposited further away from the source. At the CMT site, it is also difficult to get a truly representative sample of the tailings as a whole due to the effects of physical hydrology (Robertson, 1994), and variability in mineralogy, cementation and degree of oxidation throughout the tailings, superimposed on the effects of primary skarn zonation, as seen between the CMTE and CMTW piles.

6.1.1 Stream-Water Chemistry

Metal concentrations in stream water decrease with distance downstream from the CMT (Fig. 5.17). At the location where the acidic drainage mixed with the neutral spring water, the metal concentrations decreased significantly. This decrease was due in part to dilution, but also to co-precipitation and sorption of metals by secondary phases in the stream bed, mainly Fe-oxyhydrosulphates and oxyhydroxides. The extensive precipitation of Fe-minerals resulted in rusty coloration of the stream bed below the tailings pile. The slight increase in pH and addition of dissolved carbonate at this location changed the water chemistry enough so it could no longer support the load of dissolved metals. Further downstream, the dissolved metal concentrations decreased until they were below detection limits. Low concentrations of Pb throughout the stream result from the precipitation of plumbojarosite ($Pb\ Fe_3\ (OH)_6\ (SO_4)_2$), and highly insoluble anglesite ($PbSO_4$) in the tailings. Average Pb concentrations in the tailings are as much as 12 times *higher* than average Cd concentrations, but average

dissolved Pb concentrations in the stream were up to 12 times *lower* than dissolved Cd concentrations. This relationship indicates that while Pb is immobile, Cd is easily mobilized out of the tailings in solution; Zn also is highly mobile due to relatively high solubility of $ZnSO_4$. Knowledge of these relative mobilities is therefore important when predicting the composition of acidic drainage and potential groundwater contamination.

6.1.2 Bacterial Growth

The CPAT sample used for bacterial growth gave positive results and showed that there was more than one type of active bacteria present. This positive result indicates that bacteria are active in the tailings and may be a cause for future concern, depending on the species of bacteria present. Sulfur and Fe-oxidizing bacteria prefer low-pH conditions and are known to create an ambient micro-environment to satisfy those conditions; this evidently leads to problems of AMD. However, the bacteria culture grew at a neutral pH, and managed to increase the pH to alkaline conditions. This indicates that the bacteria currently active prefer alkaline conditions and are capable of creating such conditions for themselves. Such bacteria are not a known threat for the creation of AMD.

Although the positive results indicate the presence of bacteria in the tailings impoundment, the types of bacteria that are present are uncertain. Laboratory growth of these bacteria simply indicates their presence, not their species, relative abundance, or effect on the tailings. As laboratory growth enhances the conditions for certain bacteria, the favoured bacteria grew, whereas others that require different optimum growth conditions did not grow.

The CMT sample used for bacterial incubation gave negative results. The growth medium

used in this experiment did not provide the best conditions for bacteria present to multiply. Therefore, this is not necessarily a true negative result, simply an indication that a different medium may be needed for growth. However, this negative result does indicate that *T. ferrooxidans* is not present in the AMD. Mineralogical analysis of the stream sediment showed that there were no sulphides, consistent with the absence of *T. ferrooxidans*. Similar results were found by Gould et al. (1997) on oxidized tailings that no longer contain sulphides.

6.2 Remedial Measures

6.2.1 CPAT: Current Conditions

The CPAT impoundment is in a five-year old polyethylene-lined bermed impoundment. During the 1995 site visit, the impoundment lining was in good condition; a year and a half later, the lining was severely torn in many places (Fig. 3.3). Due to the alkalinity of the tailings and arid climate, the possibility of AMD in the near future is minimal, despite the lining defects.

Remedial measures planned for the CPAT impoundment include drying the tailings, followed by a clay and vegetative cover. A large sprinkler system was emplaced to accelerate the evaporation of the tailings pond water (Fig. 3.1). Meanwhile, the exposed tailings were dry and extremely susceptible to being windblown. Strong southwesterly winds were blowing the dry tailings outside of the impoundment, allowing tailings to collect around vegetation (Fig. 3.2) in the desert downwind.

6.2.2 CPAT: Remedial Suggestions

Although the CPAT have had lime added to prevent acid-generating reactions from starting in the impoundment, with the removal of these tailings from the "closed" system imposed by the impoundment lining, their acid-generating potential increases significantly. Therefore, the windblown tailings outside the impoundment are susceptible to oxidation. The buffering capacity of the tailings themselves and the alluvial sediments in the desert will determine whether AMD will occur from the windblown tailings. To prevent further tailings from being blown out of the impoundment, I recommend that the portion of the impoundment that has dry exposed tailings be temporarily covered with a large tarp or fine mesh until the final phase of clay-cover and vegetation is completed.

6.2.3 CMT: Current Conditions

The declaration of the CMT as an U.S. EPA Superfund site has resulted in an in-depth study of possible remedial measures for this site, complete with feasibility studies and total cost. Appendix G shows a summary of the suggested measures. The preferred remedial measure of those proposed was "Alternative 5: Off-Site Treatment Through Recycling". A feasibility study has shown that reprocessing (i.e., recycling) the tailings would not be beneficial. During the 1995 site visit, no remedial measures had been employed. However, prior to the 1996 site visit, two sediment traps had been placed along the mill tributary, and there were two limestone dams (Fig. 6.6) along Little Walnut Creek downstream from the confluence of the mill-valley tributary and Little Walnut Creek. The sediment traps were to prevent further downstream transport of the tailings; both traps were full and thus no longer

Figure 6.6: Limestone dam on Little Walnut Creek, just past the confluence of the mill-valley tributary and Little Walnut Creek.

effective in their purpose. The purpose of the limestone dams was to neutralize the acidic drainage; however, judging by the brown colour of the stream water immediately downstream of the first limestone dam, the water was still acidic and contained dissolved metals.

6.2.4 CMT: Remedial Suggestions

The CMT was declared a Superfund site in 1989 due to the occurrence of high concentrations of As, Pb, Cd, and Zn. The study of the mobility of these elements within and around the tailings environment has shown that mobilization of As occurs mainly by mechanical transport. Pb is not transported easily by mechanical mechanisms due to its occurrence in cemented layers and hardpans, and is not a problem by chemical (dissolved)

transport due to the extremely low solubility of $PbSO_4$. Cd is subject to chemical transport in the form of dissolved cations; Zn is subject to both mechanical and chemical transport, but its solubility drops rapidly due to the precipitation of insoluble Zn-bearing secondary minerals. Due to the different transport mechanisms affecting each of these metals, a tailored plan is needed to remediate this site effectively and efficiently. I have proposed a plan of action for this site, using the chosen Alternative 5 as a basis.

The first phase would be to prevent further downstream transport of the tailings, followed by AMD neutralization. The current sediment traps and limestone dams can act as a sediment trap, as well as a neutralizing agent for the surficial stream waters. Immediately downstream from the first limestone dam, I would recommend a subsurface permeable reactive barrier-wall to neutralize acidic groundwater. This reactive barrier-wall may be similar to that described by Gould et al. (1997), which consists of an excavation perpendicular to the groundwater flow, filled with a mixture of organic carbon, pea gravel, and agricultural limestone.

The second phase would be to stabilize the surface of the tailings to reduce the amount of air-borne contamination during the removal of the tailings and rock piles. One method of surface stabilization would be to sprinkle the surface of the tailings with water so that the tailings particles are held down by water tension, preventing fine particles from becoming airborne. Although this method is more environmentally sound than stabilizing with organic substances or gels, it would increase surface run-off. However, the limestone dam in phase one would prevent downstream transport of the tailings and sediments.

The third phase is the transport and disposal of the tailings and rock piles off-site. Transport of the tailings would require tarps over the trucks to prevent airborne particles, and

reduced speeds on roads and highways leading to the new disposal site. The best disposal site would be in an arid to semi-arid climate desert region with a low watertable, such as that at the CPAT impoundment. The site should be excavated and lined with a clay or reactive barrier, then lined with a high-quality long-lasting polyethylene liner. All oxidized tailings (Fig. 5.4) would be mixed with an acid-neutralizing agent such as crushed limestone or a mixture of organic and limestone gravels. The unoxidized tailings (Fig. 5.4) may be recycled for metal recovery, then mixed with a neutralizing agent and added to the oxidized tailings. Once all the contaminated rock piles have been removed from the site (including sediments accumulated in the sediment traps) and disposed of in the new impoundment, the impoundment may be sealed with a layer of crushed limestone overlain by a layer of clay, then gravel; vegetation can then be induced or be left to occur naturally.

The final phase would be regular site monitoring, including surface and groundwater monitoring, at the old and new site for a period of five years, then intermittently for another 5 years. The old CMT site could then be left to be reclaimed by the forest naturally.

6.3 Conclusions

The Cyprus-Piños Altos and the Cleveland deposits had similar primary mineralogical assemblages and geochemical signatures. Because of differences in style of deposition and time since deposition of the tailings, present metal-residence sites differ substantially. However, the CPAT may be viewed as an analogue for the CMT early in its weathering history.

The CMT show chemical precipitation of metals in the hardpan layers, thus trapping many

potentially toxic metals from further mobilization into the local environment. Metals that are not concentrated in the hardpans tend to be distributed throughout the tailings and subject to mechanical and chemical transport. Metal distribution is a function of either primary mineralogical distribution, restricted mobility of a complex, or preferential uptake into a secondary phase. Preferential uptake is the dominant factor in the CMT, due to its advanced state of weathering; primary-mineral distribution is the dominant factor controlling metal distribution in the CPAT. Mine-tailings mineralogy is complex and multi-phase making it difficult to pinpoint *all* the residence sites of a given metal.

These results indicate that mechanical transport of sediment downstream is an important mechanism in mobilizing As from the tailings; however, chemical transport of As seems minimal. Zn and Cd concentrations are moderately high in the stream waters, indicating that they are mobilized both within and outside the tailings environment by chemical transport mechanisms. Zn and Cd are therefore of great concern when evaluating the toxicity of tailings and its effect on local drainage. Low mobility of Pb within the tailings and low concentrations of Pb in acidic drainage indicate that this element may pose less of a threat to the environment than other more mobile toxic trace elements (e.g., Cd) that are present in lower concentrations in tailings. An understanding of the relative mobilities of such toxic metals in different environments is therefore necessary when predicting or evaluating the impact of tailings on water quality.

6.4 Future Work

Further analysis by proton-induced X-ray emission (PIXE), which has lower detection

limits than EMP, will be conducted to verify the siting of As and other toxic elements (e.g., Cd, Sb) in primary minerals, and to confirm the residence sites of trace metals predicted in the variation diagrams. Secondary-ion mass spectrometry (SIMS) may also be used to track the location of Au in the primary minerals, particularly chalcopyrite.

REFERENCES

Al, T.A., Blowes, D.W., and Jambor, J.L., 1994, A geochemical study of the main tailings impoundment at the Falconbridge Limited, Kidd Creek division metallurgical site, Timmins, Ontario, pp. 333-364; *In*: Jambor, J.L., and Blowes, D.W., (eds.), *Environmental Geochemistry of Sulfide Mine-Wastes*, Mineralogical Association of Canada Short Course Handbook; 438 pages.

Alpers, C.N., Blowes, D.W., Norstrom, D.K., and Jambor, J.L., 1994, Secondary minerals and acid mine-water chemistry, pp. 247-270; *In*: Jambor, J.L., and Blowes, D.W., (eds.), *Environmental Geochemistry of Sulfide Mine-Wastes*, Mineralogical Association of Canada Short Course Handbook; 438 pages.

Anderson, E.C., 1957, The metal resources of New Mexico and their economic features through 1954; State Bureau of Mines and Mineral Resources Bulletin 39, 183 pages.

Barbour, L., Wilson, W., O'Kane, M., and Newman, G., 1996, Review of soil cover technologies; unpublished MEND workshop summary notes, Winnipeg, Manitoba.

Baker, T.G., 1993, Mobility of heavy metals in soils and tailings at the Hanover and Bullfrog tailings sites, Silver City, New Mexico; unpubhished M.Sc. Thesis, New Mexico Institute of Mining and Techonology, Socorro, New Mexico; 118 pages.

Bell, F.G., and Bullock, S.E.T., 1996, The problem of acid mine drainage, with an illustrative case history; *Environmental and Engineering Geoscience*, vol. 2, no. 3, pp. 369-392.

Blowes, D.W., 1990, The geochemistry, hydrology and mineralogy of decommissioned sulfide tailings: a comparative study; unpublished Ph.D. Thesis, University of Waterloo, Waterloo, Ontario.

Blowes, D.W., and Ptacek, C.J., 1994, Acid-neutralization mechamisms in inacitive mine tailings, pp.271-292; *In*: Jambor, J.L., and Blowes, D.W., (eds.), *Environmental Geochemistry of Sulfide Mine-Wastes*, Mineralogical Association of Canada Short Course Handbook; 438 pages.

Boulet, M.P., 1995, Characterization of surface textures in sphalerite produced by microbiological leaching; unpublished B.Sc. Thesis, University of Manitoba, 64 pages.

Brown, D.A., Sheriff, B.L., and Sawicki, J.A., 1997, Microbial transformation of magnetite to hematite; accepted for publication in *Geochimica et Cosmochimica Acta*.

Bush, F.V., 1915, Mining in the Piños Altos District of New Mexico; *Mining World and Engineering*, 4: 32: pp. 165-168.

Davis, G.B., and Ritchie, A.I.M., 1986, A model of oxidation in pyritic mine wastes. II. Comparision of numerical and approximate solutions; *Applied Mathematical Modelling*, vol. 10, ppm 323-329.

Ecology and Environment Inc., 1993a, Froth floatation treatability study report; unpublished report prepared for New Mexico Environment Department, Santa Fe, New Mexico, 15 pages.

Ecology and Environment Inc., 1993b, Stabilization/solidification bench-scale treatability study work plan for the Cleveland Mill Superfund Site; unpublished report prepared for New Mexico Environment Department, Santa Fe, New Mexico, 3 pages.

Ecology and Environment Inc., 1993c, Cleveland mill remedial investigation report, Silver City, New Mexico; unpublished report prepared for New Mexico Environment Department, Santa Fe, New Mexico, Document Control No. EN3017.0.0: pp. 1-90.

Frind, E.O., and Molson, J.W., 1994, Modelling of mill-tailings impoudments, pp. 19-58; *In*: Jambor, J.L., and Blowes, D.W., (eds.), *Environmental Geochemistry of Sulfide Mine-Wastes*, Mineralogical Association of Canada Short Course Handbook; 438 pages.

Gould, W.D., Béchard, G., and Lortie, L., 1994, The nature and role of microorganisms in the tailings environment, pp. 185-200; *In*: Jambor, J.L., and Blowes, D.W., (eds.), *Environmental Geochemistry of Sulfide Mine-Wastes*, Mineralogical Association of Canada Short Course Handbook; 438 pages.

Gould, W.D., Francis, M., Blowes, D.W., and Krouse, H.R., 1997, Biomineralization: microbiological formation of sulphide minerals; *in*: McIntosh, J.M., and Groat, L.A., (eds.), *Biological-Mineralogical Interactions*, MAC short course, vol. 25, pp. 169-186.

Greenway, K., 1996, Galena as food, it depends on your perspective: a study of the interaction between *Thiobacillus ferrooxidans* and *Thiobacillus thiooxidans*, and galena and the surface textures produced by microbiological leaching ; unpublished B.Sc Thesis, University of Manitoba; 78 pages.

Jambor, J.L., 1986, Detailed mineralogical examination of alteration products in core WA-20 from Waite Amulet tailings; Division report MSL 86-137 (IR); CANMET, Energy, Mines and Resources Canada.

Jambor, J.L., 1987, Character and depth of oxidation of the reactive acid tailings at the Waite Amulet mine site, Noranda, Québec; Division report MSL 87-97 (IR); CANMET, Energy, Mines and Resources Canada; 54 pages.

Jambor, J.L., and Blowes, D.W.,1989, Mineralogical examination of tailings from the Heath Steele mill, Newcastle area, New Brunswick; Division report MSL 80-137 (IR); CANMET, Energy, Mines and Resources Canada; 23 pages.

Jambor, J.L., Owens, D.R., and Blowes, D.W., 1992, Examination of possible mineral dissolution in the low-pH zone of the Heath Steele old tailings impoundment, Bathhurst-Newcastle area, New Brunswick; Division report MSL 92-83 (IR); CANMET, Energy, Mines and Resources Canada; 40 pages.

Jambor, J.L., and Owens, D.R., 1993, Mineralogy of the tailings impoundment at the former Cu-Ni deposit of Nickel Rim Mines Ltd., eastern edge of Sudbury Structure, Ontario; CANMET Division Report MSL 93-4(CF); Dept. Energy Mines Resources Canada.

Jambor, J.L.,1994, Mineralogy of sulfide-rich tailings and their oxidation products, pp. 59-012; *In*: Jambor, J.L., and Blowes, D.W., (eds.), *Environmental Geochemistry of Sulfide Mine-Wastes*, Mineralogical Association of Canada Short Course Handbook; 438 pages.

Kalin, M., van Everdingen, R.O., and McCready, R.G.L., 1992, Ecological engineering: interpretation of hydrogeochemical observations in a sulphide tailings deposit; *CIM Bulletin*, vol. 85, no. 965, pp. 64-67.

Kuenen, J.G., Roberson, L.A., and Tuoninen, O.H., 1992, The genus Thiobacillus, Thiomicrospira, and Thiospharea; *in*: Balows, A., Truper, H.G., Dworkin, M., Harder, W., and Schleifer, K.H., (eds.), *The Prokaryotes*, Sedond Edition, Vol. 3, pp. 2637-2657.

Lasky, and Wootton, T.P., 1933, Metal resources of New Mexico. New Mexico Bureau of Mines and Mineral Resources Bulletin 7; pp. 58-59.

Lesaca, R.M., 1975, Monitoring of heavy metals in Philippine rivers, bay waters and lakes, pp. 285-307; *In*: International conference on heavy metals in the environment,

Symposium proceedings; vol. 2, part 1, 461 pages.

Lindgren, W., Graton, L.C., and Gordon, C.H., 1910, *The ore deposits of New Mexico*; USGS Professional Paper 68, pp. 297-301.

McGregor, R.G., 1994, The solid phase controls on the mobility of metals at the Copper Cliff tailings area, near Subdury, Ontario; unpublished M.Sc. Thesis, University of Waterloo, Waterloo, Ontario.

McIntosh, J.M., Silver, M., and Groat, L.A., 1997, Bacteria and the breakdown of sulfide minerals; *in*: McIntosh, J.M., and Groat, L.A., (eds.), *Biological-Mineralogical Interactions*, MAC Short Course, vol. 25, pp. 63-92.

McKnight, J.F., and Fellows, M.L., 1978, Silicate mineral assemblages and their relationship to sulfide mineralization, Piños Altos mineral deposit, New Mexico; *Arizona Geological Society Digest*, 11: pp. 1-8.

North, R.M., and McLemore, V.T., 1986, Silver and gold occurrences in New Mexico; New Mexico Bureau of Mines and Mineral Resources, Resources Map 15: pp. 1-32.

Orava, D.A., and Swider, R.C., 1996, Inhibiting acid mine drainage throughout the mine life cycle; *CIM Bulletin*, vol. 89, no. 999, pp. 52-56.

Paige, S., 1910, The ore deposits near Piños Altos, New Mexico; *Contributions to Economic Geology*, USGS Bulletin 470: pp. 109-125.

Petruk, W., and Pinard, R.G., 1986, Mineralogical and image analysis study of samples from core WA20 of the Waite Amulet tailings; Division report MSL 86087 (IR); CANMET, Energy, Mines and Resources Canada; 19 pages.

Plant, J.A., and Raiswell, R., 1983, Principles of Environmental Geochemistry; *in*: Thornton, I., (ed.), *Applied Environmental Geochemistry*; London Academic Press Geology Series, pp. 1-39.

Ptacek, C.J., and Blowes, D.W., 1994, Influence of Siderite on the Pore-Water Chemistry of Inactive Mine-Tailings Impoundments: *In* Alpers, C.N., and Blowes, D.W., (eds.), *Environmental Geochemistry of Sulfide Oxidation*, American Chemcial Society Symposium Series 550, American Chemical Society; pp. 172-189.

Robertson, W.D., 1994, The physical hydrology of mill-tailings impoundments, pp.

1018; *In*: Jambor, J.L., and Blowes, D.W., (eds.), *Environmental Geochemistry of Sulfide Mine-Wastes*, Mineralogical Association of Canada Short Course Handbook; 438 pages.

Rollinson, H.R., 1993, Using geochemical data: evaluation, presentation, interpretation: Longman Group Limited, UK, 352 pages.

Scharer, J.M., Nicholson, R.V., Halbert, B., and Snodgrass, W.J., 1994, A computer program to assess acid generation in pyritic tailings; *In*: Alpers, C.N., and Blowes, D.W., (eds.), *Environmental Geochemistry of Sulfide Oxidation*, Americal Chemical Society Symposium Series 550, Washington, 681 pages.

Shadlum, T.N., and Turpetko, S.A., 1970, Relationship between microhardness and isomorphous iron content in synthetic sphalerite: *Dokl. Acad. Sci*, USSR, Earth Sciences, 194: pp. 141-143.

Soulé, J.H., 1948, West Piños Altos Zn-Pb Deposits; U.S. Department of Interior, R.I. 4237: 5

Spence, B., 1994, Bacterial leaching of a complex sulphide ore: surface corrosion textures and heavy element release; unpublished B.Sc. Thesis, University of Manitoba, ??? pages.

Suzuki, I., Takeuchi, T.L., Yuthasastrakosol, T.D., and Oh, J.K., 1990, Ferrous iron and sulfur oxidation and ferric iron reduction activities of *Thiobacillus ferrooxidans* are affectd by growth on ferrous rion sulfur, or sulfide ore; *Applied and Environmental Microbiology*, vol. 56, no. 6, pp. 1620-1626.

Suzuki, I., Chan, C.W., and Takeuchi, T.L., 1994, Oxidation of inorganic sulfur compounds by *Thiobacillus*, pp. 60-67; *In*: Alpers, C.N., and Blowes, D.W., (eds.), *Environmental Geochemistry of Sulfide Oxidation*, Americal Chemical Society Symposium Series 550, Washington, 681 pages.

Taylor, B.E., and Wheeler, M.C., 1994, Sulfur- and oxygen-isotope geochemistry of acid mine drainage in the western United States, pp. 481-514; *In*: Alpers, C.N., and Blowes, D.W., (eds.), *Environmental Geochemistry of Sulfide Oxidation*, Americal Chemical Society Symposium Series 550, Washington, 681 pages.

Thompson, J.A.J., 1975, Copper in marine waters: effects of mining wastes, pp. 273-284; *In*: *International Conference on Heavy Metals in the Environment*, Symposium proceedings, vol. 2, part 1, 461 pages.

Trauger, F.D., 1972, Water resources and general geology of Grant County, New Mexico; New Mexico Bureau or Mines and Mineral Resources, Hydrologic Report 2, 211 pages.

U.S. EPA, 1993, Cleveland Mill Proposed Plan of Action; April 8 issue, 19 pages.

U.S. EPA, 1994, Cleveland Mill Superfund Site Update; March 31 issue, 15 pages.

Walder, I.F., 1993a, Hanover mill tailings: Chemical and mineralogical characterization and heavy metal mobility of a mill tailings (from Zn-Pb skarn deposits) and surrounding areas at Hanover, Grant County, New Mexico; Unpubl. report, Mining Remedial Recovery Company, Tucson, Arizona, 142 pages.

Walder, I.F., 1993b, Bullfrog mill tailings: Chemical and mineralogical characterization and heavy metal mobility of a mill tailings (from Zn-Pb skarn deposits) and surrounding areas at Vanadium, Grant County, New Mexico; Unpubl. report, Mining Remedial Recovery Company, Tucson, Arizona, 146 pages.

Walder, I.F., Chavez, W.X., and Greame, R.W., 1994, Element mobility in Pb-Zn skarn mill tailings, Grant County, New Mexico; *Society for Mining, Metallurgy and Exploration Inc.*, Pre-print 94-185, 5 pages.

Wootton, T.P., 1940, Gold mining and gold deposits in New Mexico, New Mexico Bureau of Mines Circular No. 5; 24 pages.

APPENDIX A ICP Analysis of Water Samples

Sample #	Location[1] m	pH	Ag ppm	As ppm	Cd ppm	Cu ppm	Fe ppm	Hg ppm	Pb ppm	Total S ppm	Se ppm	Zn ppm
CMW 01	N/A[2]	5.50	B.D.	B.D.	B.D.	B.D.	0.4	B.D.	B.D.	47.0	B.D.	0.2
CMW 02	B.D.	2.50	0.100	1.40	17.50	454	15145.0	B.D.	1.16	18800.0	B.D.	5305.0
CMW 03	280	2.53	0.100	0.80	16.50	431	15170.0	0.01	0.40	17700.0	B.D.	4929.0
CMW 04	300	7.17	B.D.	B.D.	0.03	B.D.	B.D.	B.D.	B.D.	731.6	B.D.	3.4
CMW 05	320	2.61	B.D.	0.01	0.01	0.80	7.4	B.D.	B.D.	2467.0	B.D.	31.0
CMW 06	340	2.72	B.D.	0.06	3.57	1.20	17.0	B.D.	0.01	1155	0.02	37.0
CMW 07	N/A[3]	7.18	B.D.	0.10	0.05	B.D.	B.D.	B.D.	B.D.	52.0	0.05	0.4
CMW 08	2000	7.27	B.D.	B.D.	0.04	B.D.	B.D.	B.D.	0.01	25.0	0.01	0.1
PATW 01	N/A[4]	7.01	B.D.	B.D.	B.D.	B.D.	B.D.	B.D.	0.02	25.0	0.01	B.D.
PATW 02	N/A[4]	8.27	B.D.	0.03	B.D.	B.D.	B.D.	B.D.	0.04	51.0	B.D.	B.D.
Detection limit	--	--	0.003	0.012	0.0015	0.002	0.0015	0.0085	0.014	0.02	0.0037	0.0009

N/A = not applicable; B.D. = below detection limit; [1] distance downstream from CMT, as shown in Figure 2.2; [2] collected from the upstream reservoir; [3] collected in pool in mine; [4] collected from impoundment.

APPENDIX B Analyses of Bulk Tailings Samples

Elements	Al	Ag	Au	As	Ba	Be	Bi	Br	Ca	Cd	Co	Cr
Units	wt. %	ppm	ppb	ppm	ppm	ppm	ppm	ppm	wt. %	ppm	ppm	ppm
PAT001	2.29	8.30	215	110.0	230	< 2	65	< 0.5	16.800	4.1	54	25
PAT002	2.34	15.40	430	83.0	50	< 2	69	< 0.5	16.985	7.9	82	29
PAT003	2.25	15.80	398	91.0	< 50	< 2	72	< 0.5	17.420	7.6	90	26
PAT004	2.61	9.90	430	60.0	150	< 2	89	< 0.5	17.105	4.0	65	28
PAT005	2.49	6.10	252	51.0	70	< 2	72	< 0.5	19.265	2.5	54	30
PAT006	2.36	8.40	388	42.0	70	< 2	87	< 0.5	18.550	3.5	51	28
PAT007	2.55	9.35.00	330	47.0	190	< 2	136	< 0.5	18.710	3.4	58	29
PAT008	2.62	9.80	828	43.0	100	< 2	117	< 0.5	18.815	2.9	66	27
PAT009	2.42	6.75	149	96.0	200	< 2	60	< 0.5	16.650	2.2	65	33
PAT010	2.29	1.25	90	70.0	100	< 2	36	< 0.5	18.510	1.9	35	29
PAT011	2.57	6.30	287	57.0	150	< 2	56	< 0.5	17.840	3.9	51	26
PAT012	0.34	161.05	2280	290.0	< 50	< 2	379	< 0.5	2.190	78.7	460	< 5
CMT001	0.49	34.05	18	93.0	< 50	< 2	197	< 0.5	10.120	2.2	19	12
CMT002	0.52	32.30	8	85.0	< 50	< 2	198	< 0.5	7.710	3.8	36	12
CMT003	0.50	41.90	170	72.0	< 50	< 2	246	< 0.5	8.430	4.9	29	8
CMT004	0.51	33.70	12	66.0	< 50	< 2	204	< 0.5	6.400	195.5	98	14
CMT005	0.59	139.70	22	3.7	< 50	< 2	1062	< 0.5	9.720	1.4	16	8
CMT006	0.59	51.60	< 2	120.0	< 50	4	442	< 0.5	6.210	76.9	83	9
CMT007	0.68	45.80	7	86.0	< 50	< 2	390	< 0.5	9.155	36.4	49	14
CMT008	0.33	61.60	327	31.0	< 50	< 2	494	< 0.5	0.750	11.7	83	13
CMT009	0.37	80.75	15	42.0	< 50	< 2	537	< 0.5	1.405	11.2	66	13
CMT010	0.22	7.10	< 2	36.0	< 50	< 2	57	< 0.5	0.155	38.0	91	9
CMT011	0.36	61.40	40	44.0	< 50	< 2	510	< 0.5	1.600	3.5	76	14
CMT012	0.84	25.45	9	190.0	< 50	< 2	146	< 0.5	5.340	11	35	14
CMT013	0.41	56.70	187	46.0	< 50	< 2	490	< 0.5	3.200	1.9	17	12
CMO-1	0.12	58.20	0	98.0	< 50	< 2	297	< 0.5	0.140	823.5	120	< 5
D.L.	0.01	3	2	0.5	50	2	1	0.5	0.5	5	1	5

Elements	Cs	Cu	Fe	Hf	Hg	Ir	K	Mg	Mn	Mo	Na	Ni	P
Units	ppm	ppm	wt. %	ppm	ppm	ppb	wt. %	wt. %	ppm	ppm	wt. %	ppm	wt. %
PAT001	3	2228	12.1	< 1	< 1	< 5	0.33	0.52	9068	84.0	0.09	14	0.054
PAT002	3	9702	12.8	< 1	< 1	< 5	0.25	0.53	8421	89.5	0.05	17	0.049
PAT003	2	6931	15.1	< 1	< 1	< 5	0.16	0.41	8201	66.5	0.04	18	0.045
PAT004	3	4245	12.5	1	< 1	< 5	0.24	0.45	8580	103.0	0.09	12	0.045
PAT005	2	2363	12.7	< 1	< 1	< 5	0.27	0.47	8264	64.0	0.08	11	0.047
PAT006	3	2871	12.4	< 1	< 1	< 5	0.29	0.50	8081	48.5	0.08	10	0.047
PAT007	2	2683	10.9	< 1	< 1	< 5	0.32	0.48	7720	64.0	0.10	13	0.051
PAT008	3	2056	11.1	< 1	< 1	< 5	0.32	0.51	7810	57.5	0.09	11	0.052
PAT009	3	1113	10.3	< 1	< 1	< 5	0.49	0.86	9430	47.5	0.11	24	0.076
PAT010	2	715	10.4	< 1	< 1	< 5	0.34	0.81	8933	24.0	0.08	13	0.062
PAT011	2	2651	11.8	< 1	< 1	< 5	0.30	0.45	8397	85.0	0.11	11	0.045
PAT012	< 1	99999	24.0	< 1	< 1	< 5	0.03	0.17	2502	759.0	0.01	96	0.002
CMT001	1	701	7.08	< 1	< 1	< 5	0.24	0.04	70	4.0	0.01	2	0.031
CMT002	< 1	979	9.95	< 1	< 1	< 5	0.22	0.05	86	4.5	0.01	9	0.03
CMT003	1	1259	9.25	< 1	< 1	< 5	0.22	0.05	135	5.5	0.02	7	0.036
CMT004	< 1	5442	13.0	< 1	< 1	< 5	0.17	0.09	1762	3.5	0.01	20	0.031
CMT005	< 1	2308	2.06	< 1	< 1	< 5	0.33	0.04	61	1.0	0.02	50	0.006
CMT006	< 1	16173	14.7	< 1	< 1	< 5	0.14	0.06	1116	7.0	< 0.01	47	0.034
CMT007	< 1	31738	12.6	< 1	< 1	< 5	0.08	0.10	293	2.0	< 0.01	11	0.035
CMT008	< 1	4231	32.5	< 1	< 1	< 5	0.04	0.06	1117	5.5	< 0.01	14	0.019
CMT009	< 1	1374	31.3	< 1	< 1	< 5	0.07	0.06	1151	8.0	0.01	10	0.016
CMT010	< 1	2315	20.1	< 1	< 1	< 5	0.01	0.06	1180	1.0	< 0.01	17	0.022
CMT011	< 1	933	36.8	< 1	< 1	< 5	0.04	0.04	1801	11.0	< 0.01	7	0.023
CMT012	< 1	741	10.1	< 1	< 1	< 5	0.32	0.13	693	6.0	0.08	6	0.032
CMT013	< 1	1202	36.2	< 1	< 1	< 5	0.10	0.04	2112	8.5	0.01	6	0.025
CMO-1	< 1	12666	21.2	< 1	< 1	< 5	0.02	0.11	3810	29	< 0.01	12	0.008
D.L.	1	2	0.01	1	1	5	2	0.01	1	1	0.01	1	0.001

Elements	Pb	Rb	Sb	Sc	Se	Sr	Ta	Th	Tl	U	V	W	Y
Units	ppm	ppm	ppm	ppm	ppm	ppm	ppm	ppm	wt. %	ppm	ppm	ppm	ppm
PAT001	314	< 5	50.0	2.2	< 3	84	< 0.5	2.0	0.06	7.4	21	340	12
PAT002	615	27	38.0	2.1	< 3	59	< 0.5	1.3	0.06	5.0	18	340	11
PAT003	948	< 5	36.0	1.9	< 3	51	< 0.5	1.2	0.05	4.6	18	520	11
PAT004	278	21	19.0	2.2	< 3	61	0.7	1.4	0.06	5.5	21	470	12
PAT005	167	20	10.0	2.2	< 3	67	0.8	1.3	0.06	5.6	19	500	12
PAT006	137	26	9.0	1.9	< 3	67	0.9	1.3	0.06	5.5	19	430	11
PAT007	124	< 5	9.9	2.4	< 3	93	0.8	1.4	0.07	4.7	21	430	12
PAT008	111	24	5.7	2.5	< 3	96	< 0.5	1.8	0.07	4.5	22	580	12
PAT009	231	28	41.0	2.7	< 3	120	< 0.5	2.2	0.06	8.9	22	330	13
PAT010	265	27	30.0	2.3	< 3	74	< 0.5	2.3	0.05	5.8	18	330	11
PAT011	167	26	24.0	1.8	< 3	75	0.7	1.5	0.05	6.8	19	430	12
PAT012	1444	< 5	220.0	0.6	60	14	< 0.5	< 0.2	0.01	3.4	2	55	2
CMT001	488	25	14.0	0.6	< 3	86	0.5	< 0.2	0.02	1.1	9	130	2
CMT002	408	18	14.0	0.7	< 3	73	< 0.5	0.7	0.01	0.9	7	110	2
CMT003	535	22	17.0	0.7	< 3	82	< 0.5	< 0.2	0.02	0.8	8	130	2
CMT004	412	< 5	14.0	0.9	< 3	65	1.1	0.6	0.01	3.9	6	150	4
CMT005	1533	< 5	41.0	1.2	< 3	74	< 0.5	0.7	0.04	1.2	9	130	2
CMT006	427	< 5	19.0	1.4	< 3	54	< 0.5	1.3	0.01	6.7	5	< 1	4
CMT007	378	< 5	16.0	2.4	< 3	58	< 0.5	1.6	0.01	8.7	4	110	4
CMT008	601	< 5	19.0	0.7	< 3	12	< 0.5	0.3	0.01	0.9	6	20	2
CMT009	888	< 5	24.0	0.9	< 3	14	< 0.5	0.7	0.01	0.9	6	< 1	2
CMT010	133	< 5	2.9	0.5	< 3	4	< 0.5	0.5	0.01	1.3	3	< 1	2
CMT011	531	< 5	15.0	0.9	< 3	17	< 0.5	0.5	0.01	0.9	6	25	2
CMT012	406	27	17.0	1.6	< 3	60	< 0.5	0.6	0.05	1.3	15	210	4
CMT013	718	< 5	18.0	1.0	< 3	25	< 0.5	< 0.2	0.01	0.8	16	< 1	2
CMO-1	360	< 5	13.0	0.6	< 3	0	0.8	< 0.2	0.01	< 0.5	3	220	2
D.L.	1	5	0.1	0.1	5	0.5	0.5	0.2	0.01	0.5	0.01	1	0.5

Elements	Zn	La	Ce	Nd	Sm	Eu	Yb	Lu	Sulphide S	SO_4	CO_2	H_2O^+	H_2O^-
Units	ppm	ppm	ppm	ppm	ppm	ppm	ppm	ppm	wt. %	wt. %	wt. %	wt. %	wt. %
PAT001	560.5	19.3	24	14	2.0	0.6	1.0	0.17	1.35	0.030	7.250	0.91	0.42
PAT002	1050.0	5.9	10	8	1.7	0.6	0.7	0.10	2.44	0	6.260	0.76	0.33
PAT003	1060.5	5.6	8	9	1.8	0.6	0.8	0.09	2.49	0	5.310	0.86	0.31
PAT004	560.0	10.5	18	9	1.9	0.6	1.0	0.14	1.60	0.897	4.900	0.77	0.36
PAT005	437.0	10.4	16	8	2.0	0.6	0.9	0.12	1.07	0.428	5.890	0.83	0.37
PAT006	547.5	10.0	16	7	1.8	0.6	0.8	0.12	1.10	0	6.660	0.77	0.27
PAT007	534.0	13.5	20	< 5	1.9	0.6	0.9	0.12	1.29	0.0329	7.980	0.88	0.34
PAT008	500.0	10.0	17	10	2.0	0.6	1.0	0.10	1.20	0.508	8.450	0.75	0.34
PAT009	437.5	22.4	29	17	2.1	0.7	1.1	0.18	1.14	0.945	11.100	1.84	0.84
PAT010	197.5	7.0	14	10	1.7	0.4	0.7	0.15	0.921	1.560	8.640	1.30	0.63
PAT011	590.0	14.0	18	10	1.9	0.7	0.8	0.14	1.26	0.179	5.750	1.13	0.40
PAT012	8712.0	6.8	13	< 5	0.2	< 0.2	< 0.2	< 0.05	24.40	0	0.060	2.56	0.86
CMT001	451.0	2.9	4	< 5	0.3	< 0.2	< 0.2	< 0.05	10.10	29.600	0.011	9.56	0.34
CMT002	821.0	3.2	5	< 5	0.4	< 0.2	< 0.2	< 0.05	13.90	30.000	0.015	9.55	0.98
CMT003	1505.5	3.0	5	< 5	0.4	< 0.2	< 0.2	< 0.05	13.40	31.800	0.051	10.47	1.19
CMT004	41212.0	3.1	5	< 5	0.5	< 0.2	< 0.2	< 0.05	16.80	30.300	2.290	8.24	1.07
CMT005	201.5	5.2	7	7	0.7	< 0.2	< 0.2	< 0.05	10.70	29.500	0	10.43	0.37
CMT006	22356.5	3.2	4	< 5	0.5	< 0.2	< 0.2	< 0.05	15.20	0	0.359	5.69	0.359
CMT007	7777.0	2.2	3	< 5	0.6	< 0.2	< 0.2	< 0.05	17.10	32.400	0.417	10.02	1.17
CMT008	15600.0	2.0	< 3	< 5	0.2	< 0.2	< 0.2	< 0.05	15.10	25.900	0	10.46	1.01
CMT009	14475.5	3.0	< 3	< 5	0.3	< 0.2	< 0.2	< 0.05	14.00	4.780	0.018	5.82	0.018
CMT010	16473.0	1.2	< 3	< 5	0.3	< 0.2	< 0.2	0.06	NA	NA	NA	NA	NA
CMT011	12428.0	1.5	< 3	< 5	0.2	< 0.2	< 0.2	< 0.05	12.80	23.700	0.007	9.13	1.48
CMT012	4068.5	4.2	8	< 5	0.7	< 0.2	0.3	< 0.05	5.81	15.500	0.011	8.56	1.29
CMT013	10720.0	2.3	< 3	< 5	0.2	< 0.2	< 0.2	< 0.05	4.51	11.100	0.015	5.95	0.015
CMO-1	141000.0	0.6	< 3	< 5	< 0.1	< 0.2	< 0.2	< 0.05	24.00	13.500	1.350	0.40	0.17
D.L.	0.2	0.5	3	5	0.1	0.2	0.2	0.05	0.01	0.01	0.01	0.01	0.01

APPENDIX C XRD Patterns

PAT001 continuous-scan

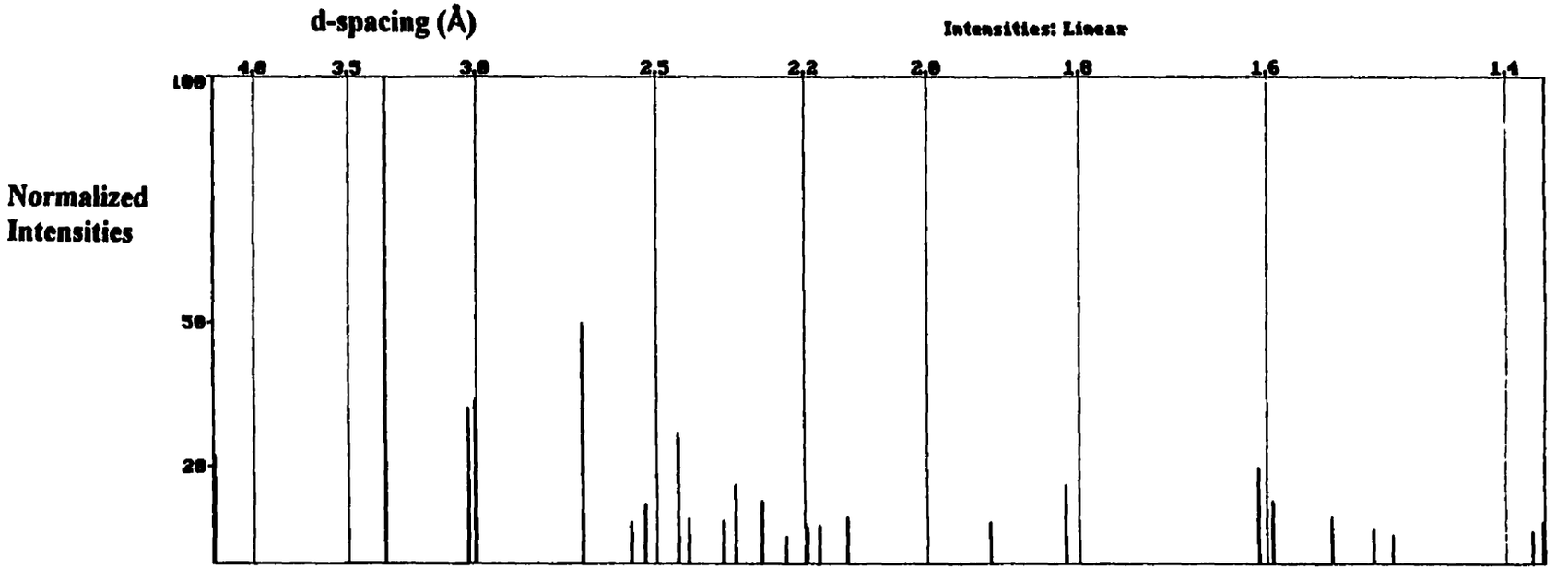

PAT002 continuous-scan

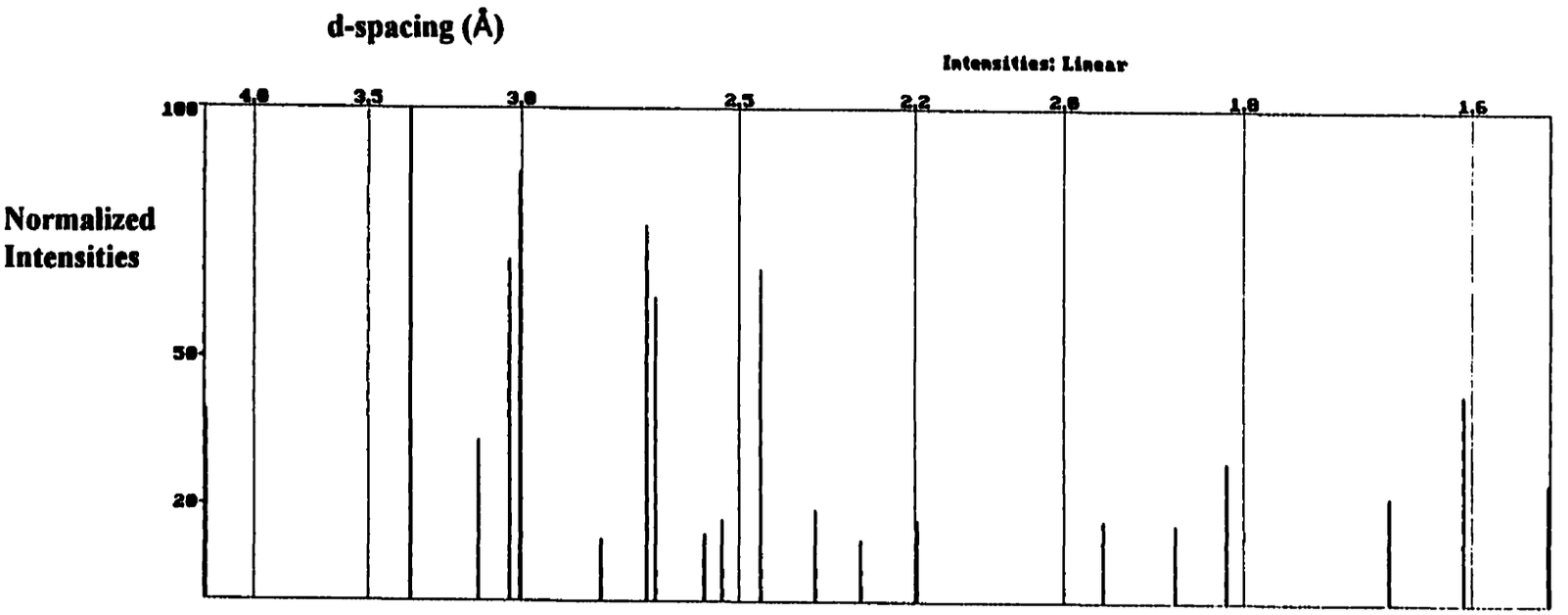

PAT003 continuous-scan

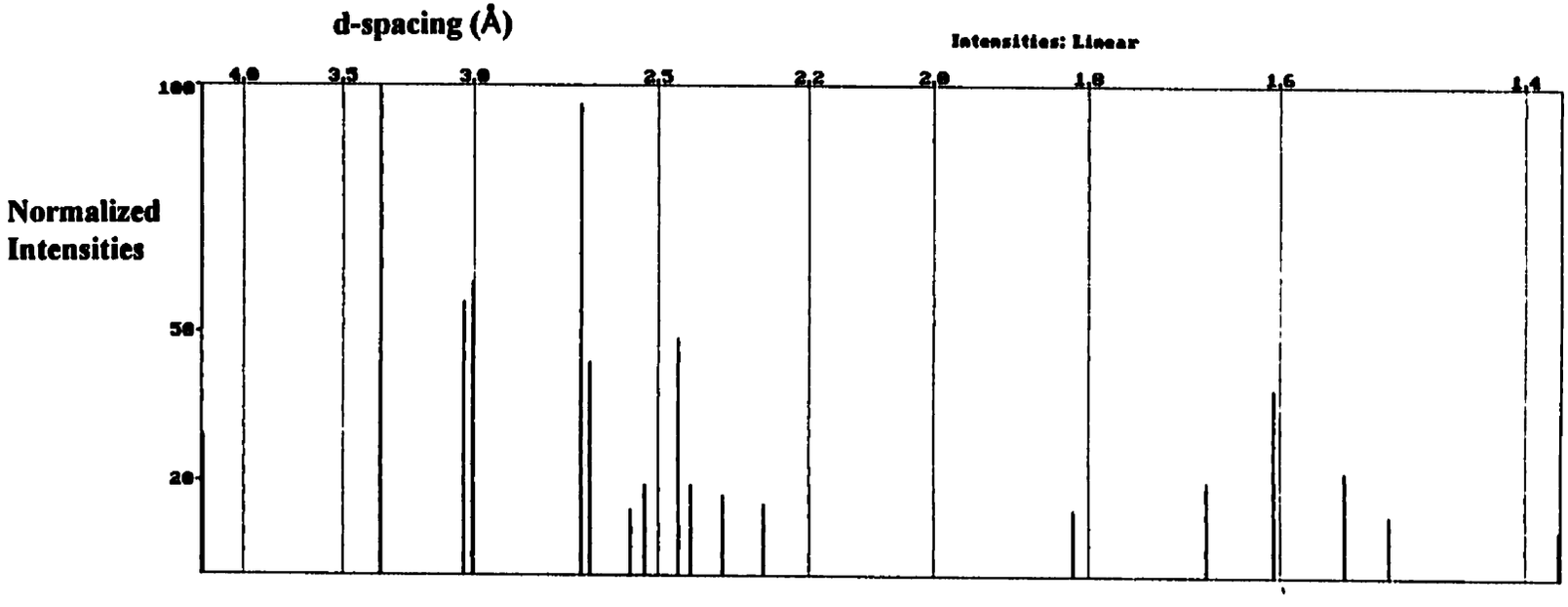

PAT004 *continuous-scan*

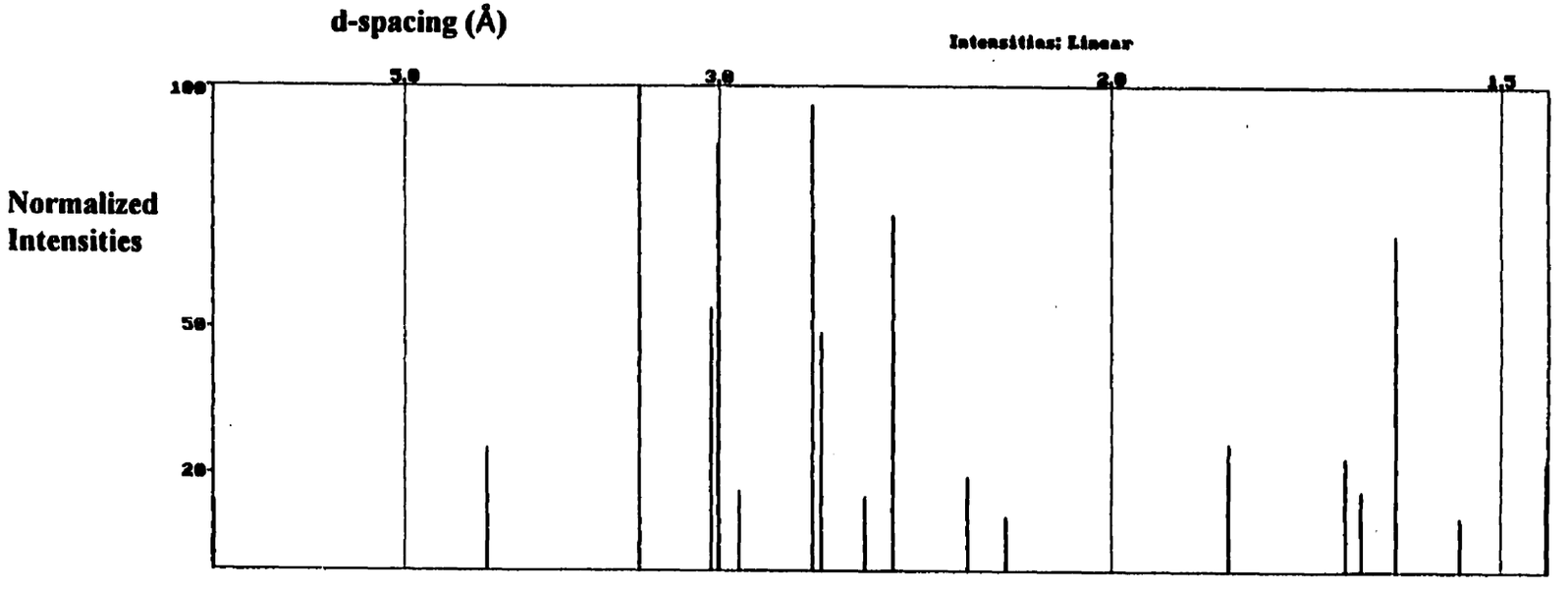

PAT005 continuous-scan

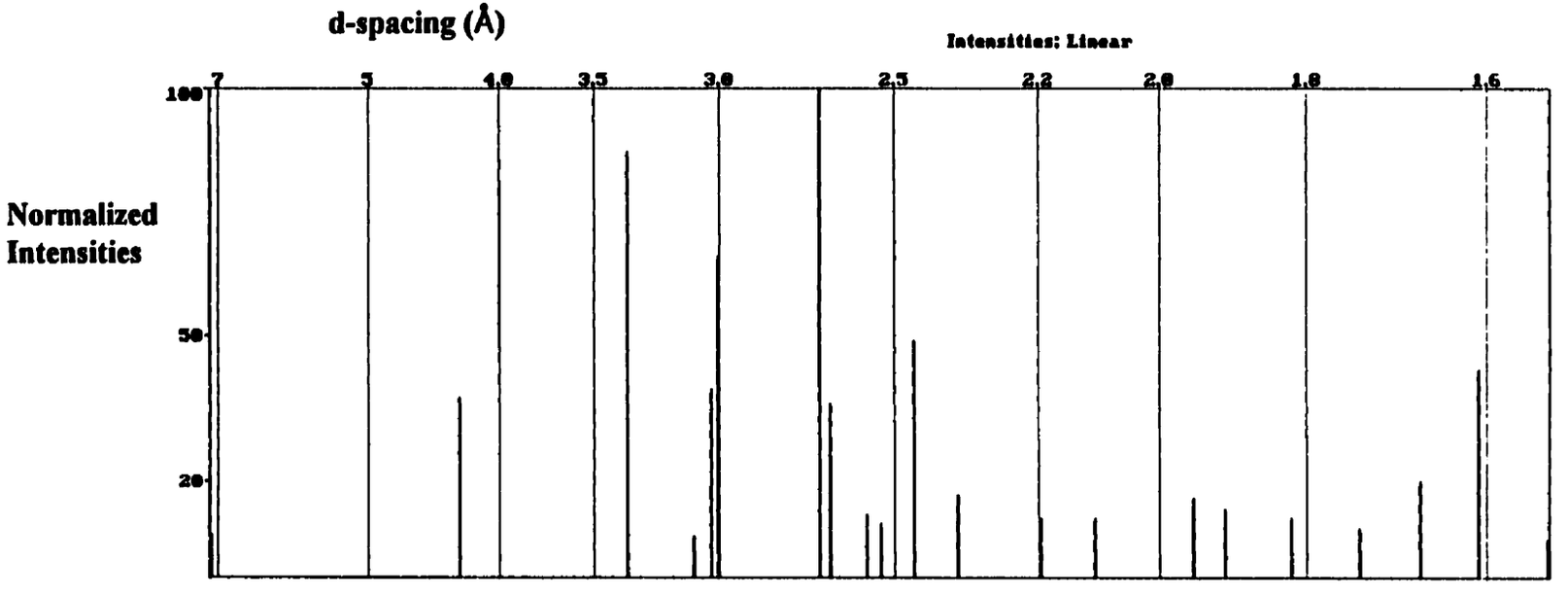

PAT006 continuous-scan

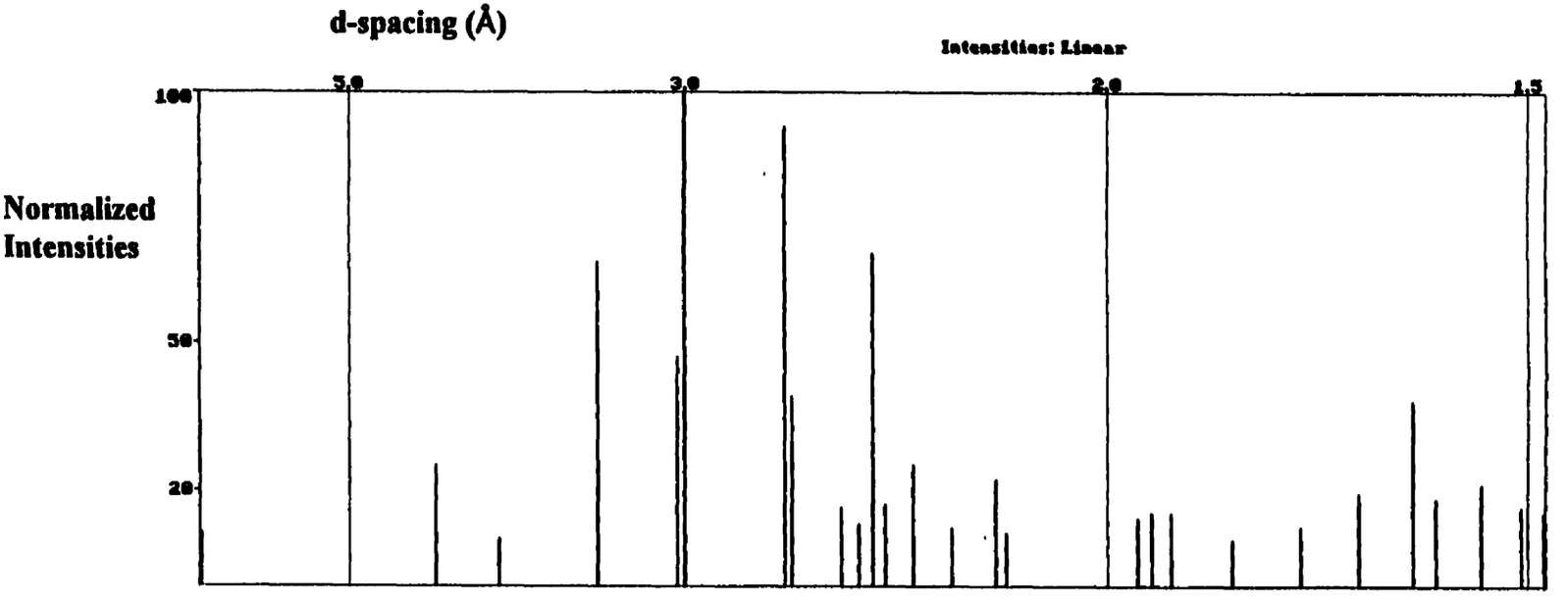

PAT007 continuous-scan

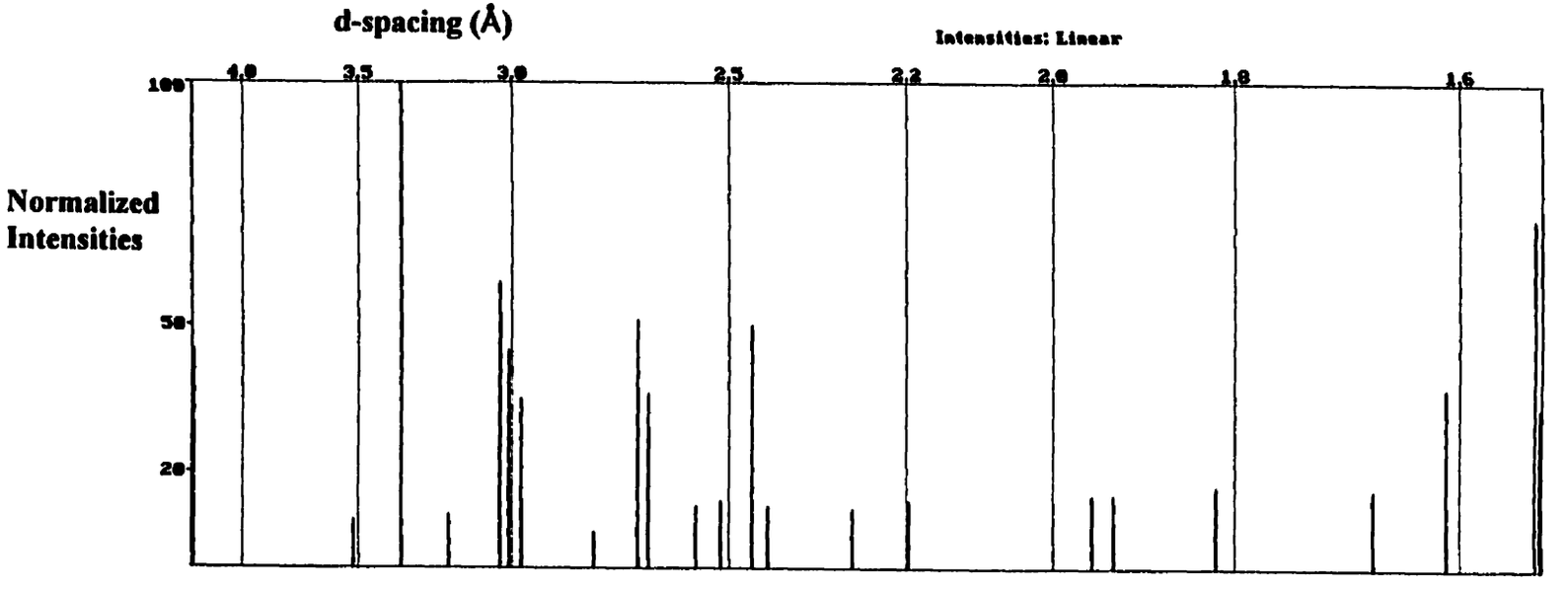

PAT008 continuous-scan

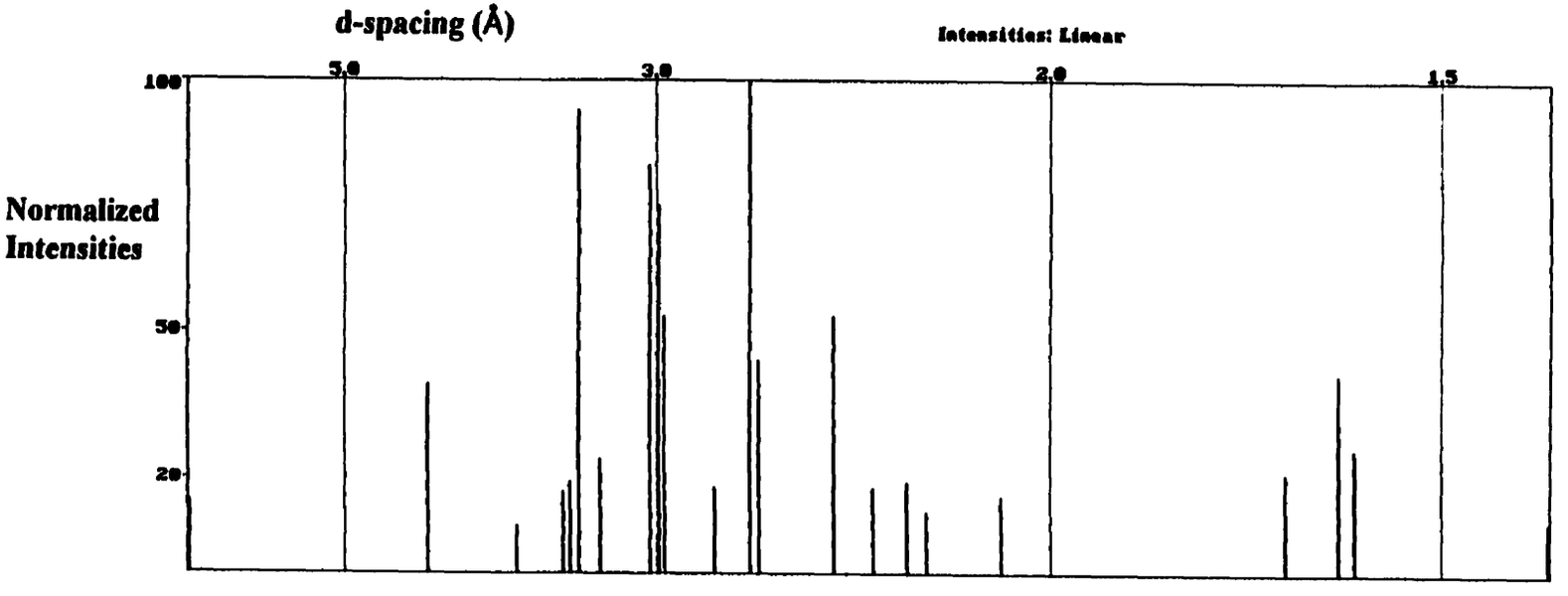

PAT009 continuous-scan

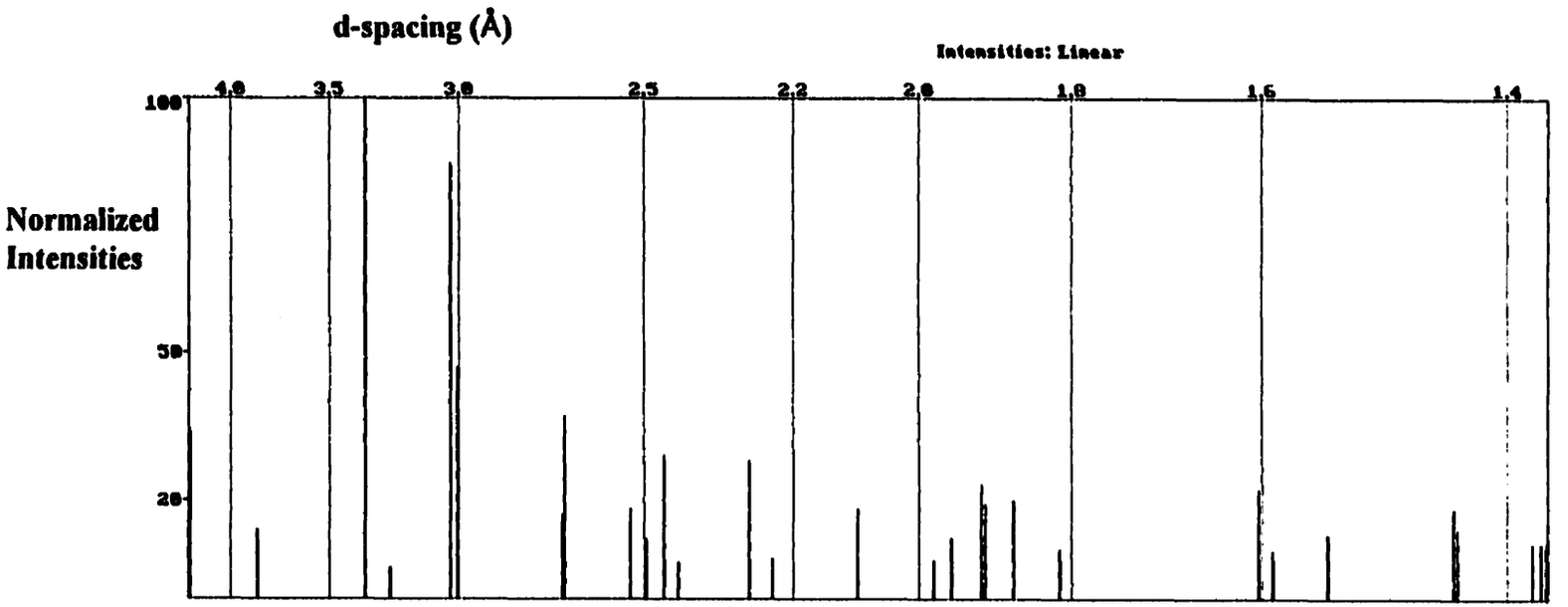

PAT010 continuous-scan

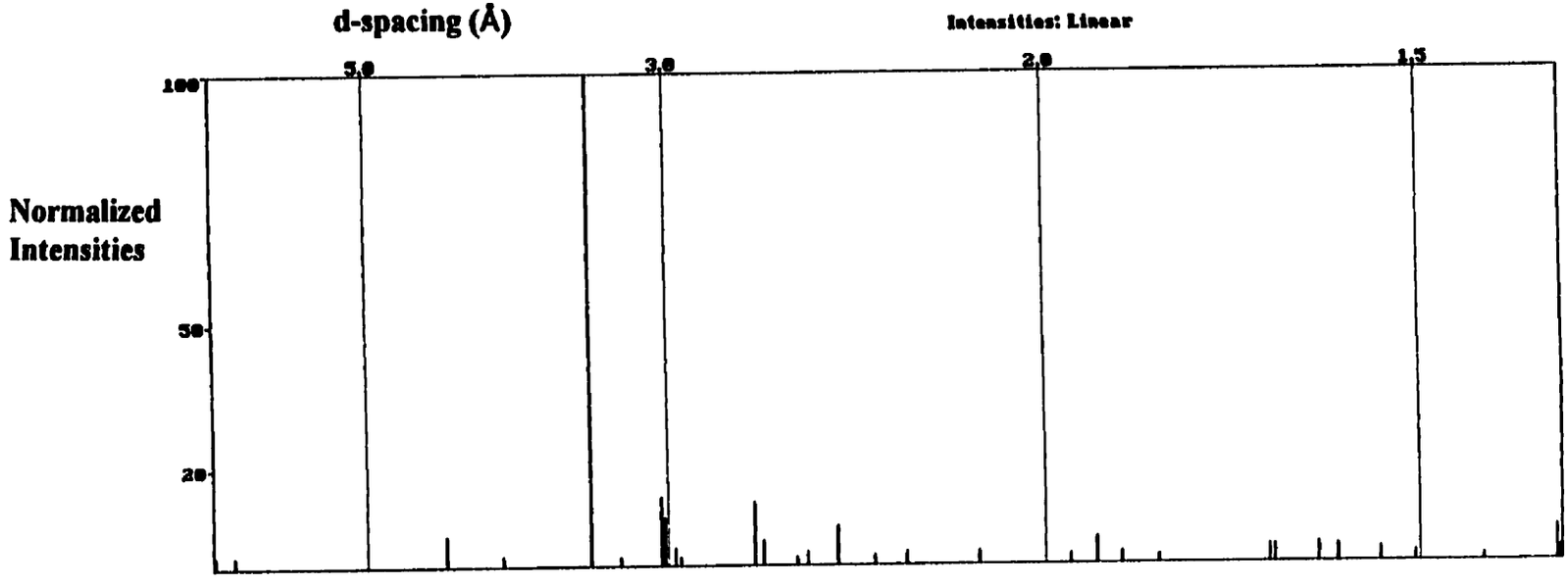

PAT011 continuous-scan

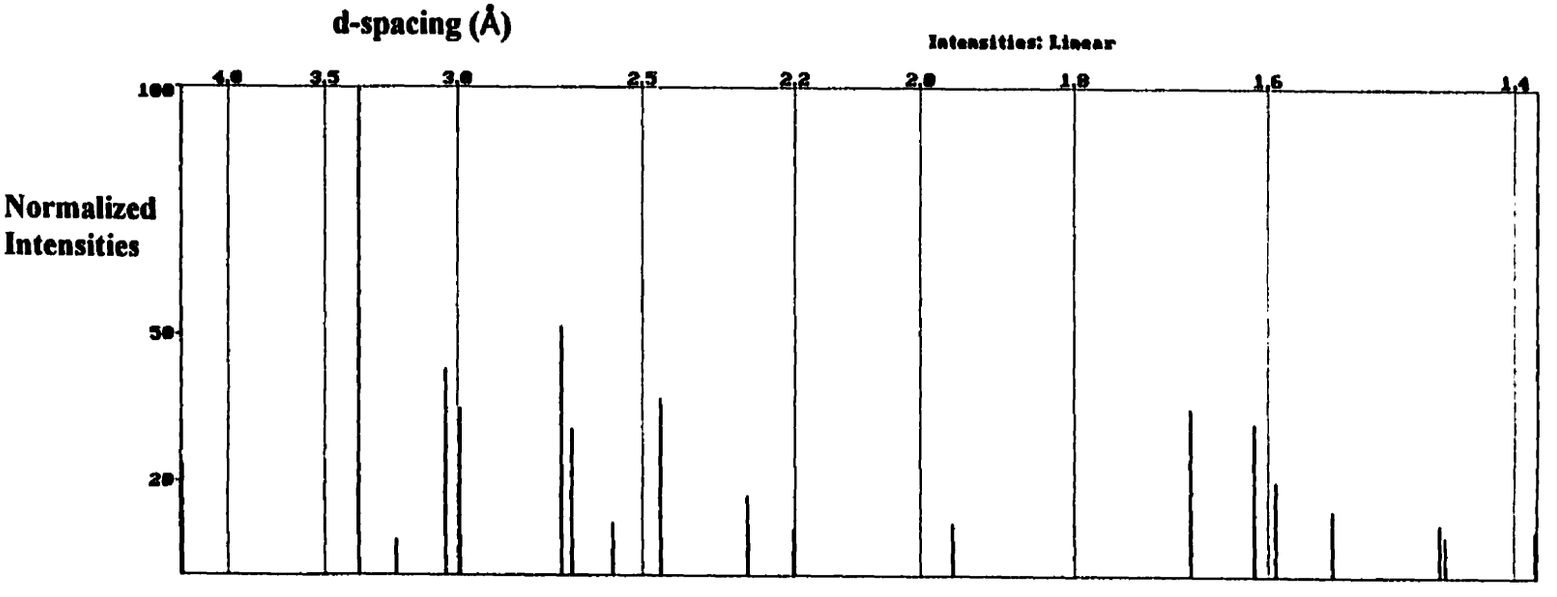

CMT001 step-scan

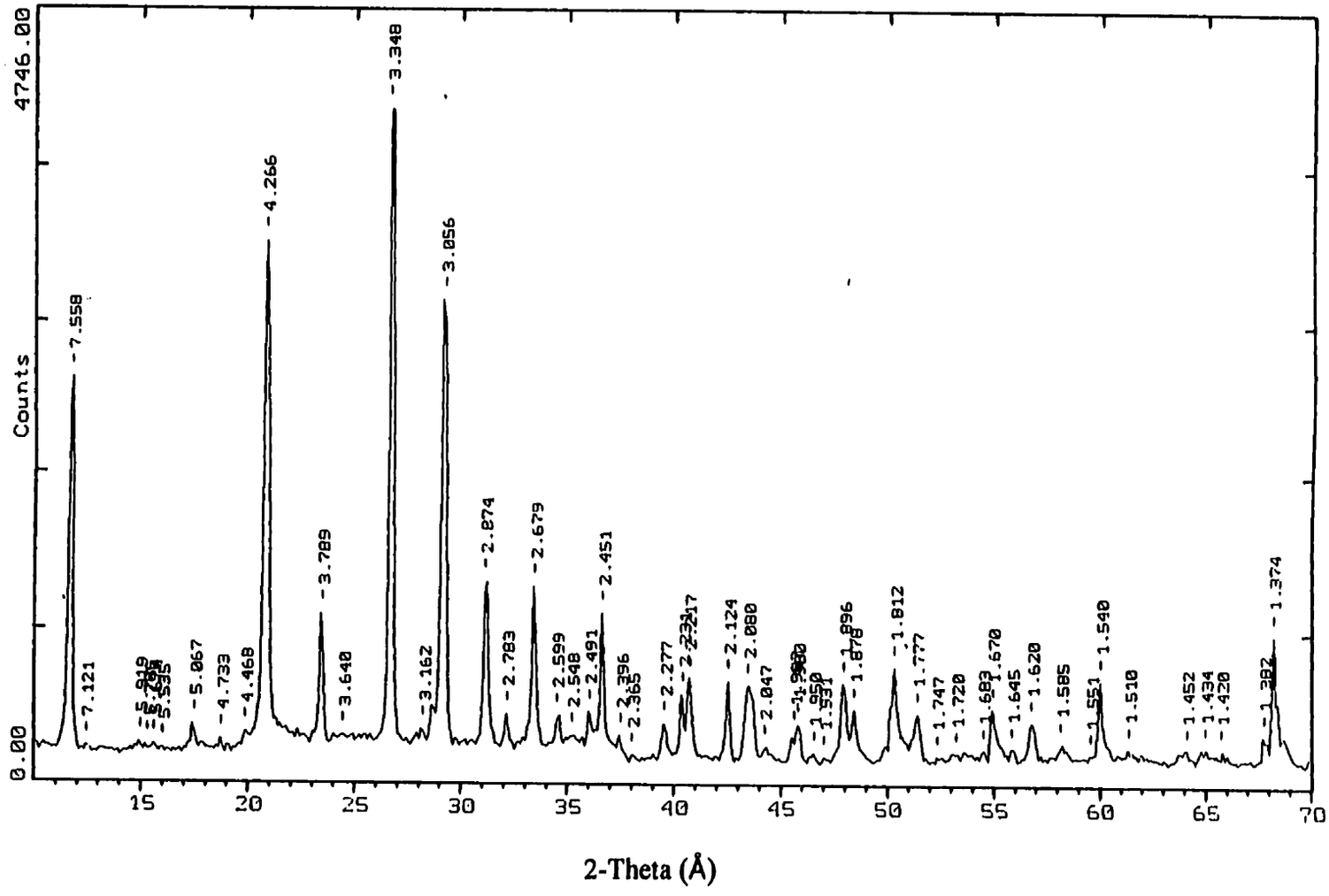

CMT002 step-scan

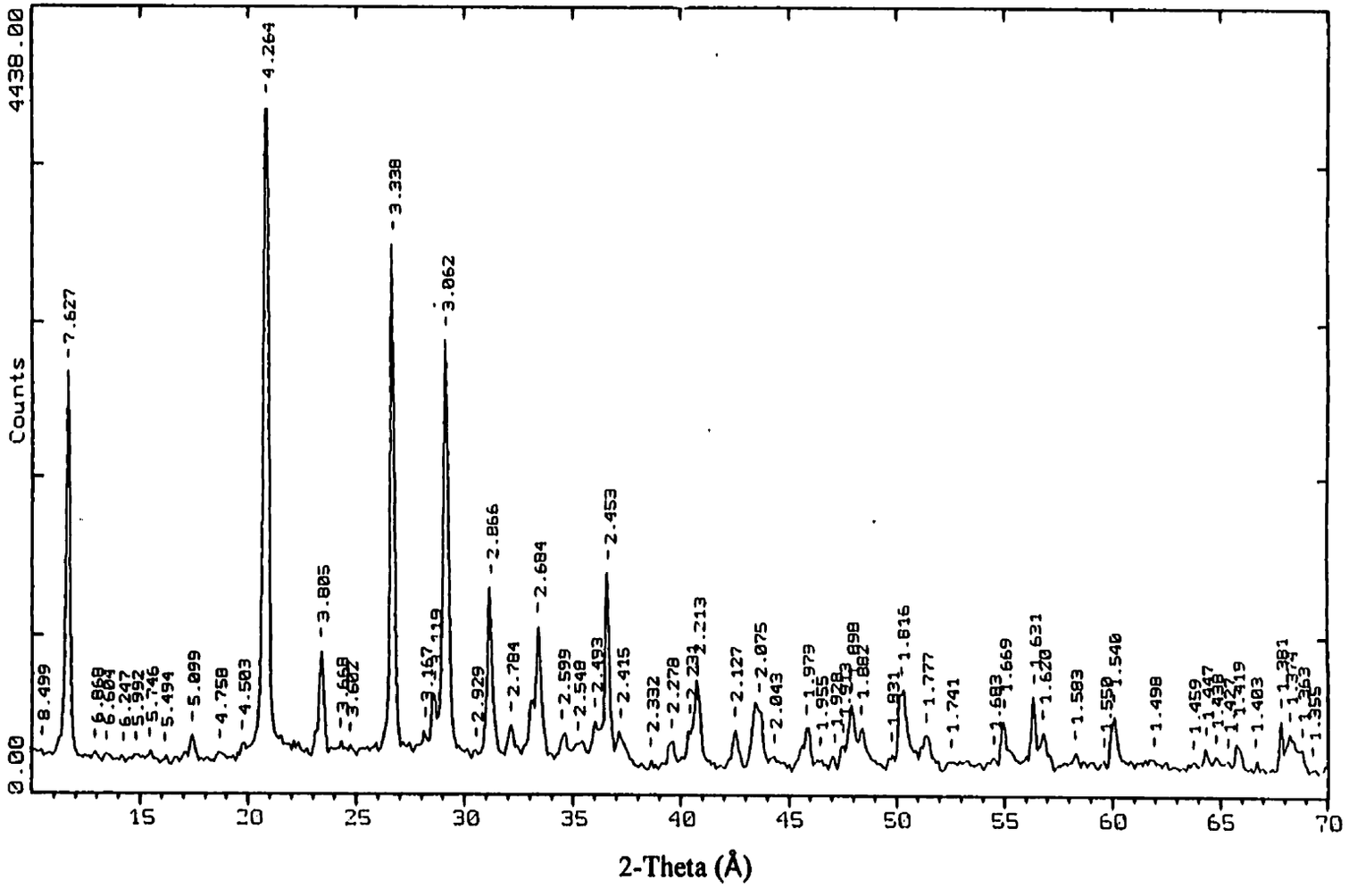

CMT003 step-scan

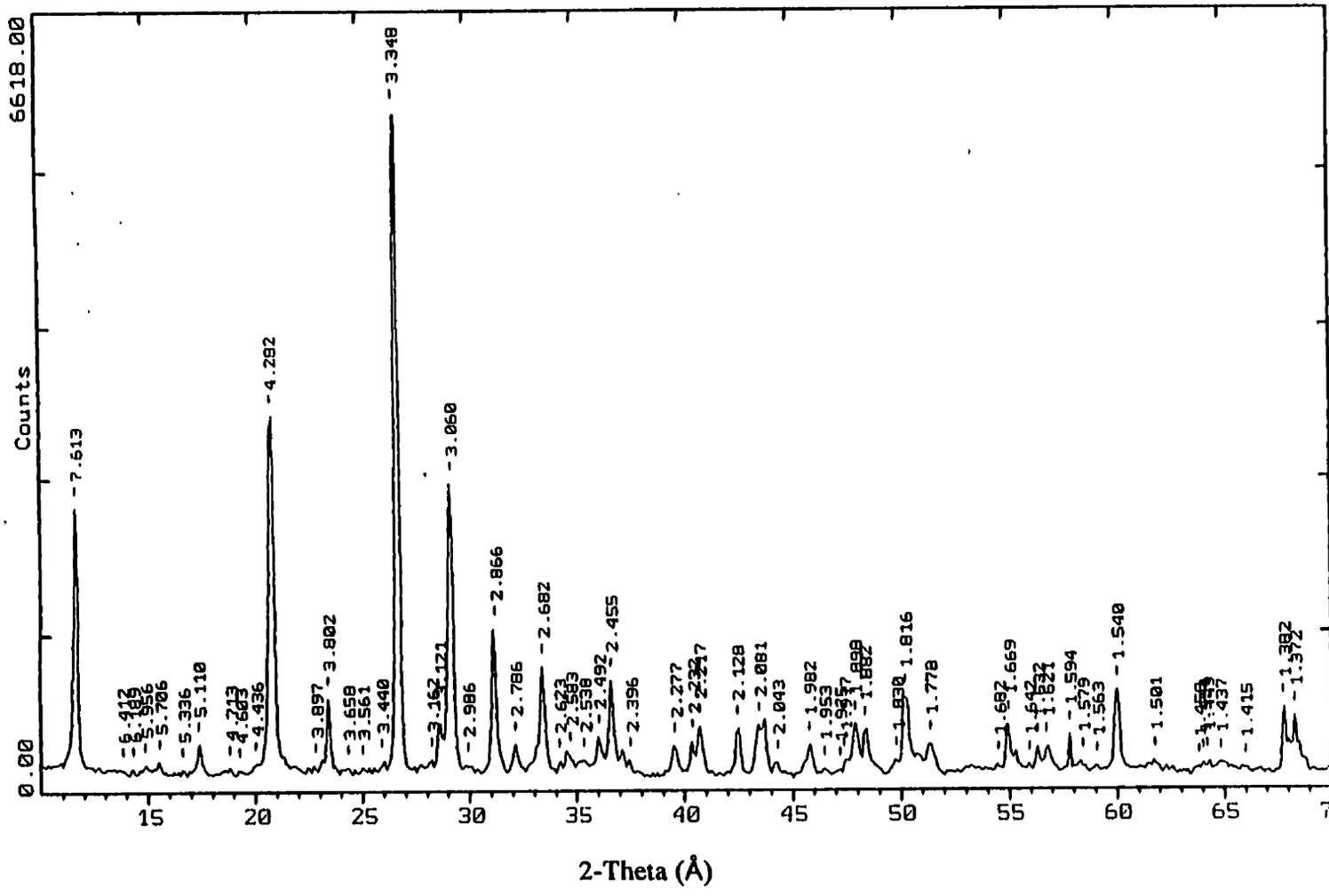

CMT004 step-scan

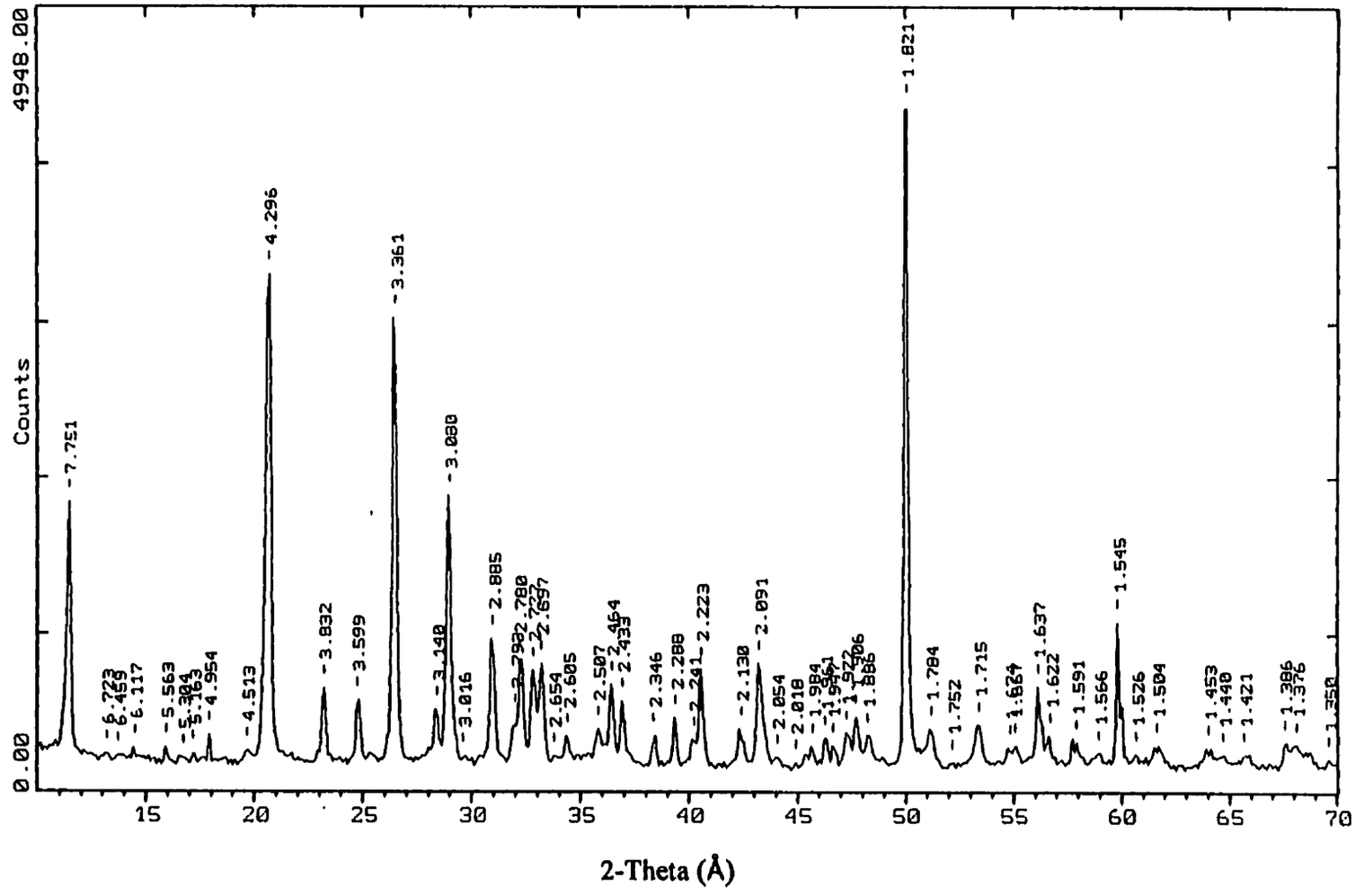

CMT005 step-scan

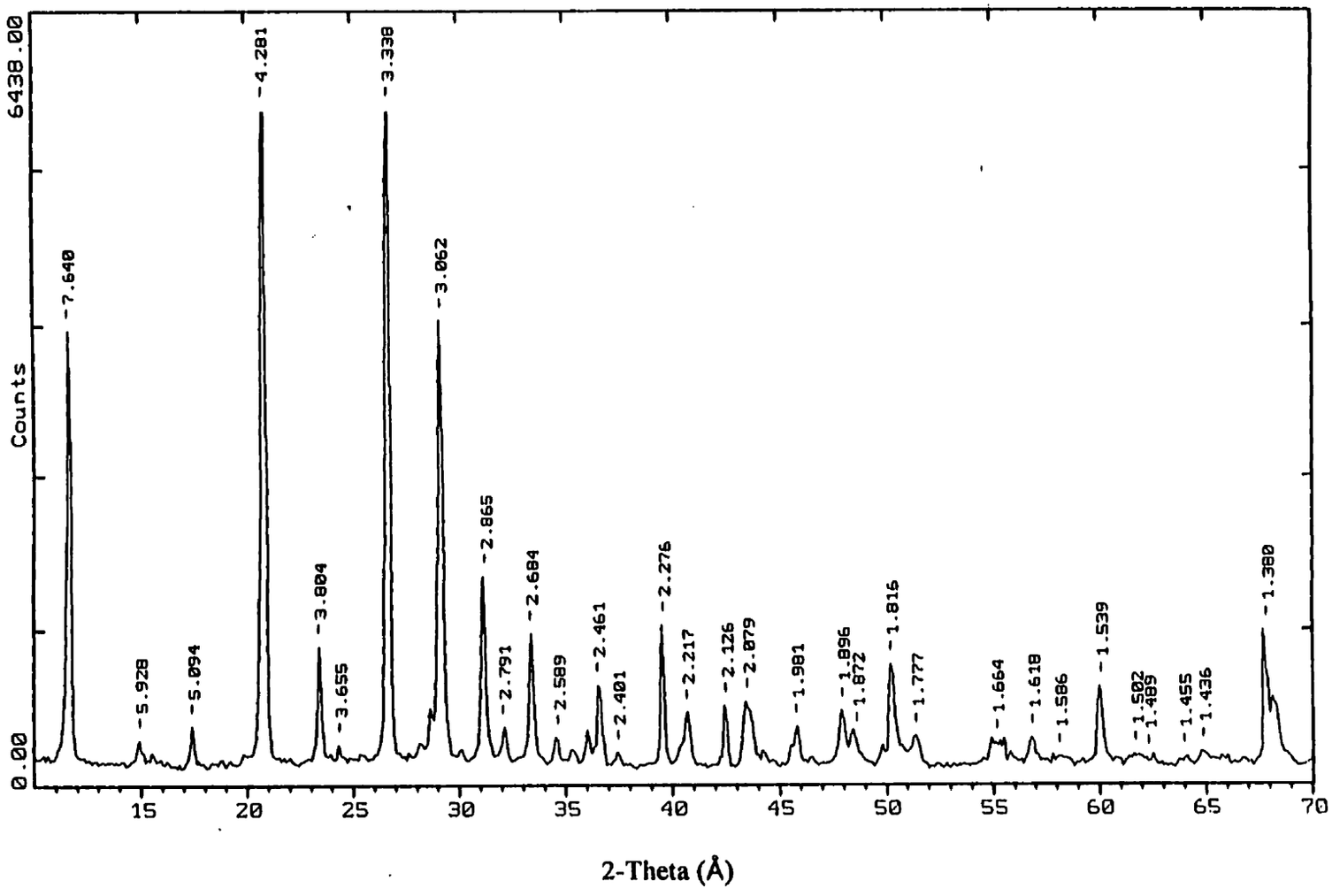

CMT006 continuous-scan

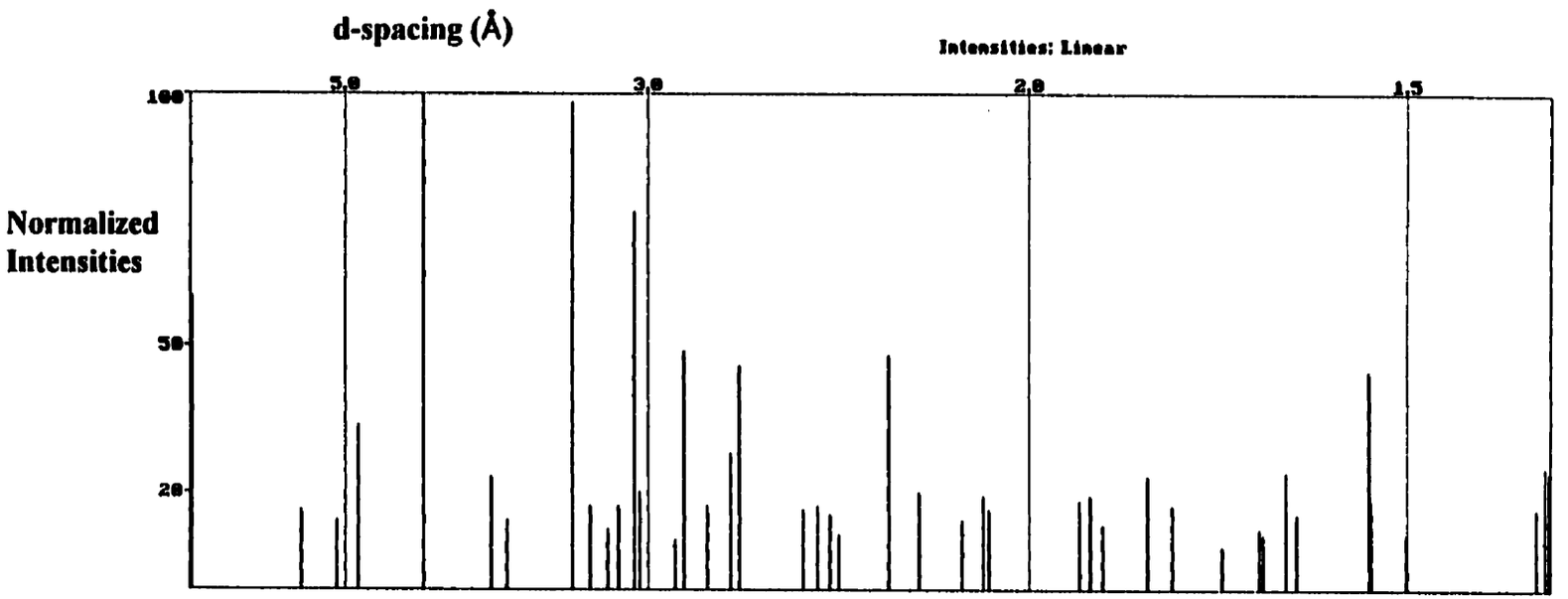

CMT008 step-scan

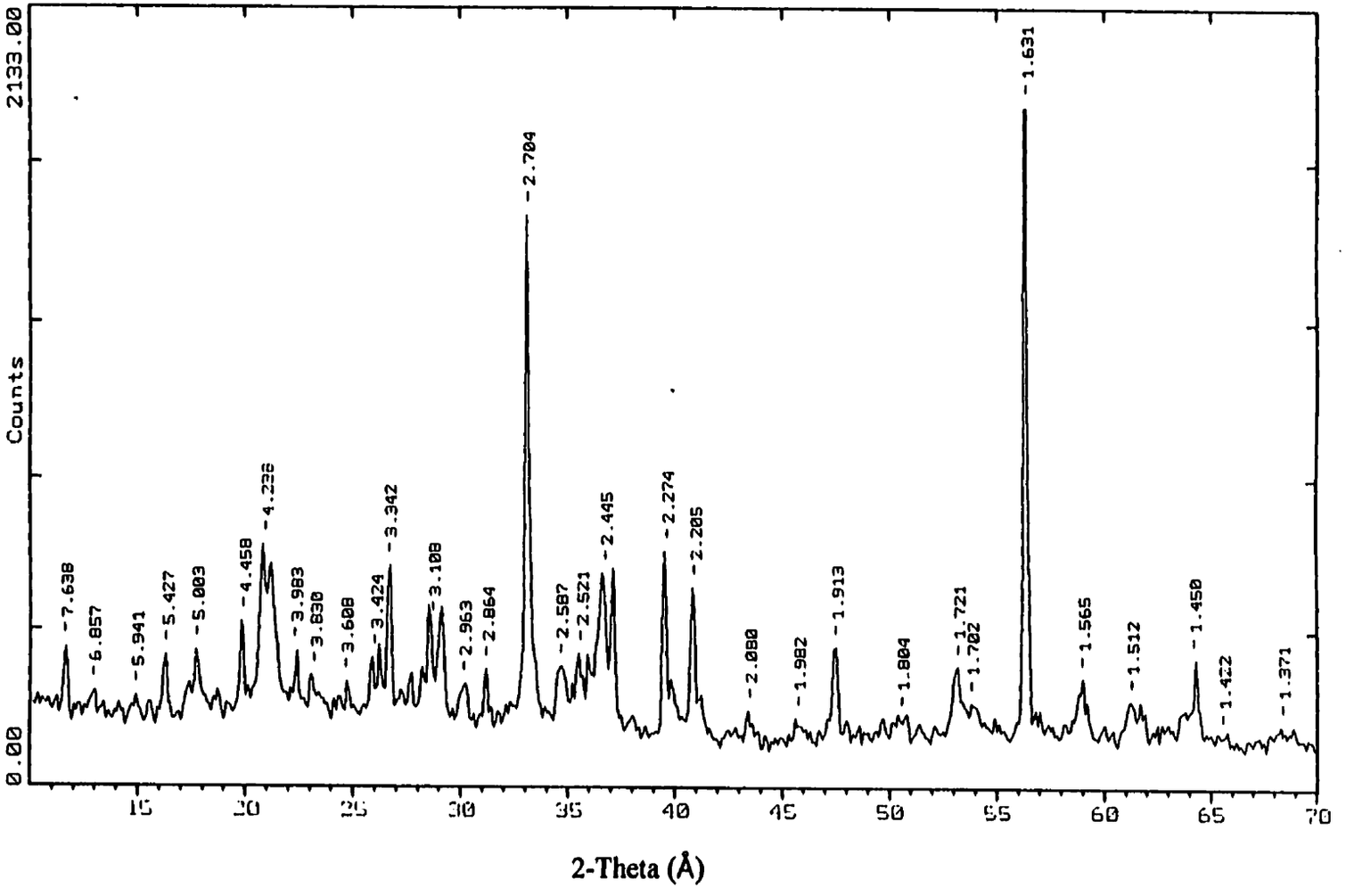

CMT009 continuous-scan

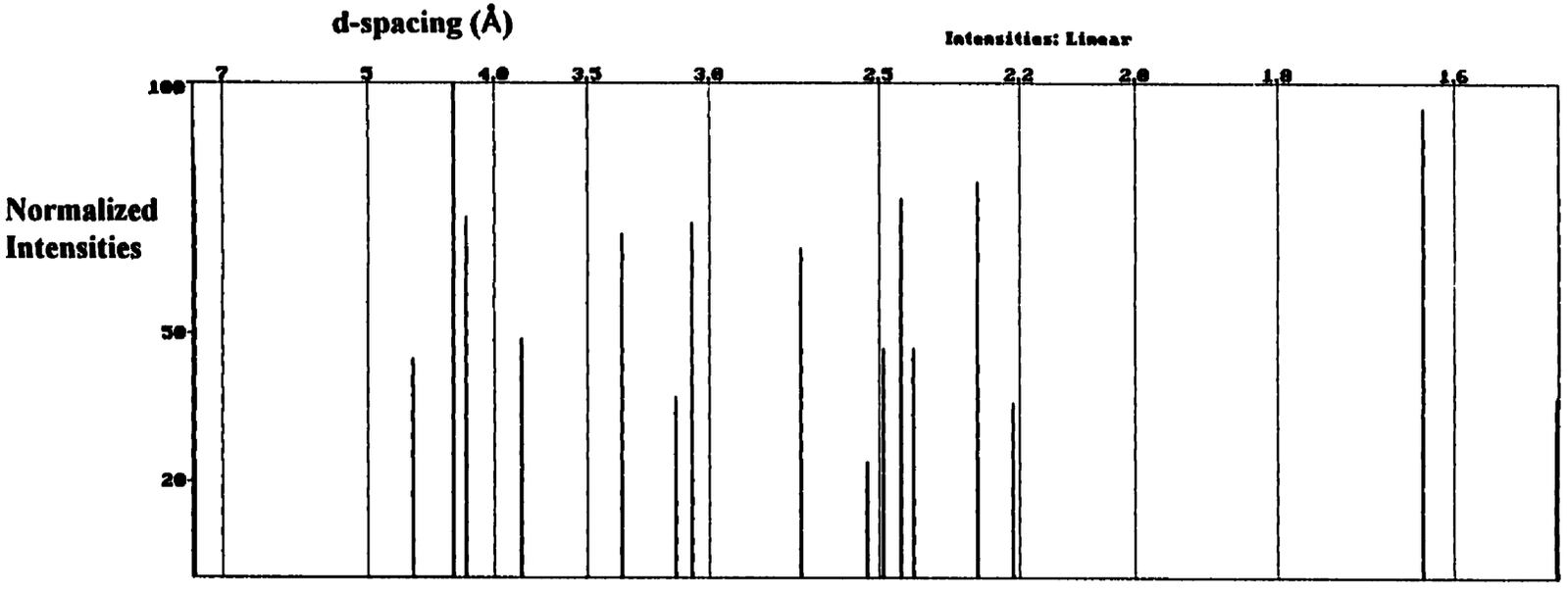

CMT010 step-scan

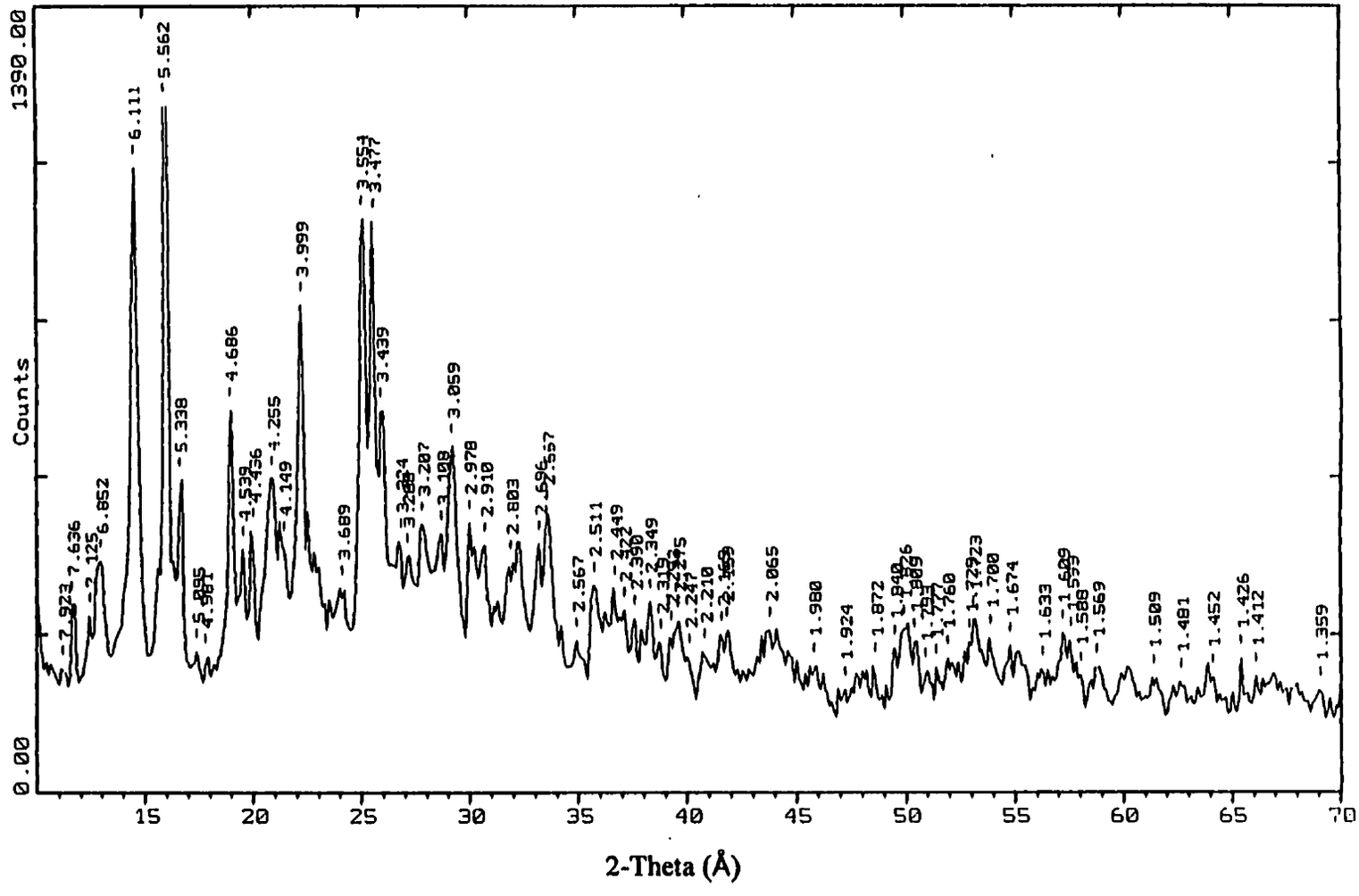

CMT011 step-scan

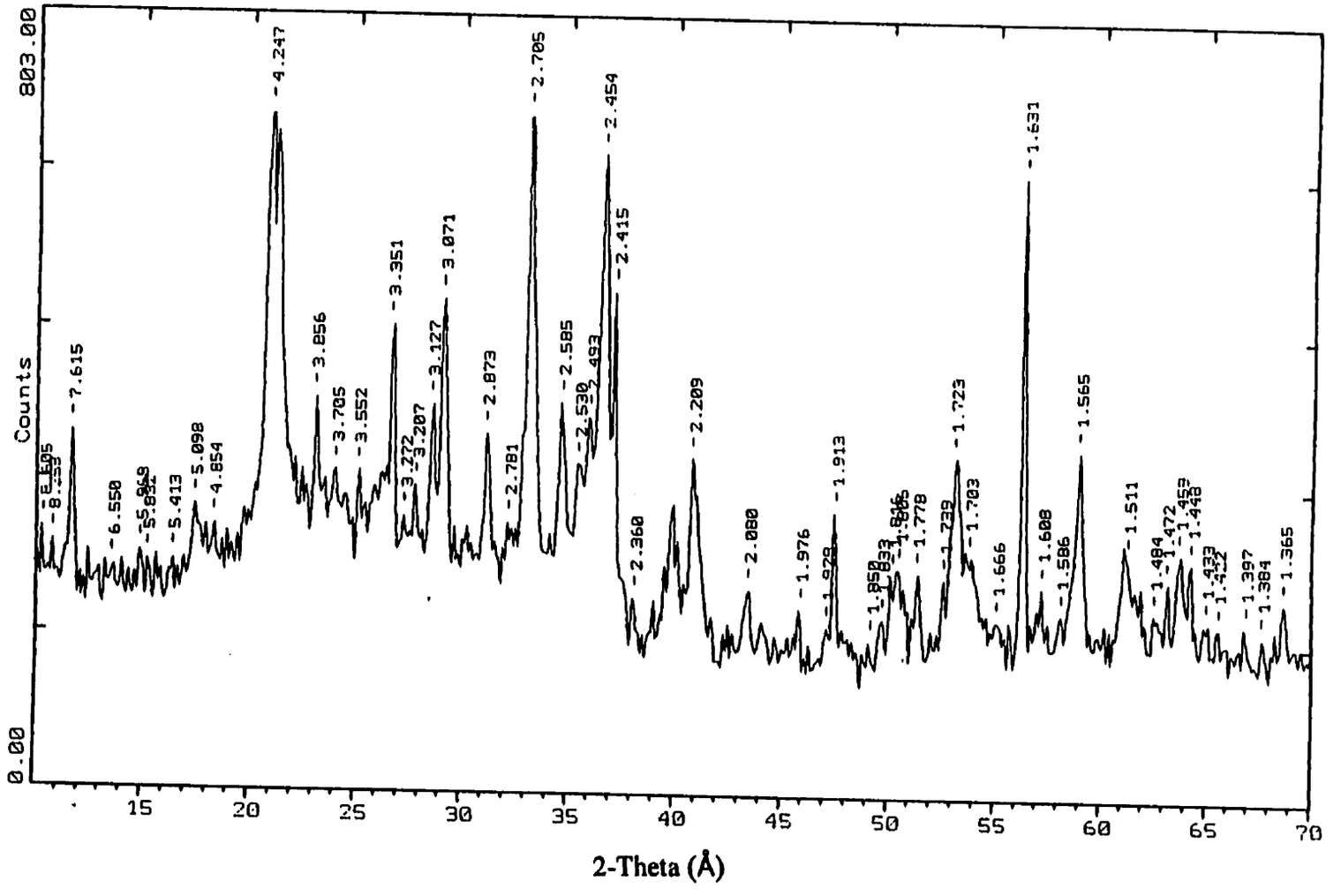

CMT012 step-scan

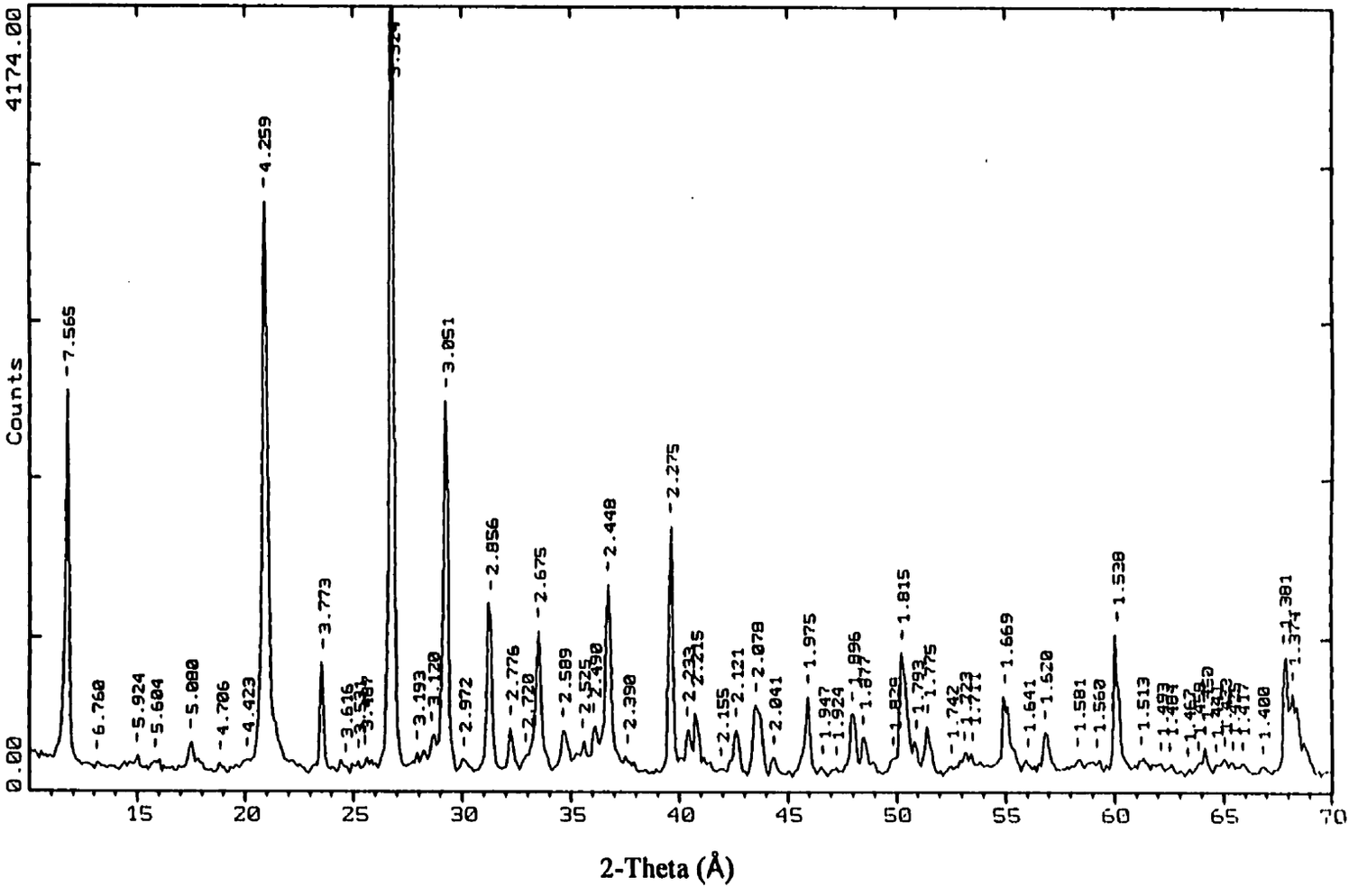

Diffractogram of goethite done by the *Gandolfi XRD method*: (a) Gandolfi diffractogram (computer generated), (b) matching goethite pattern from PEAKSEARCH software program.

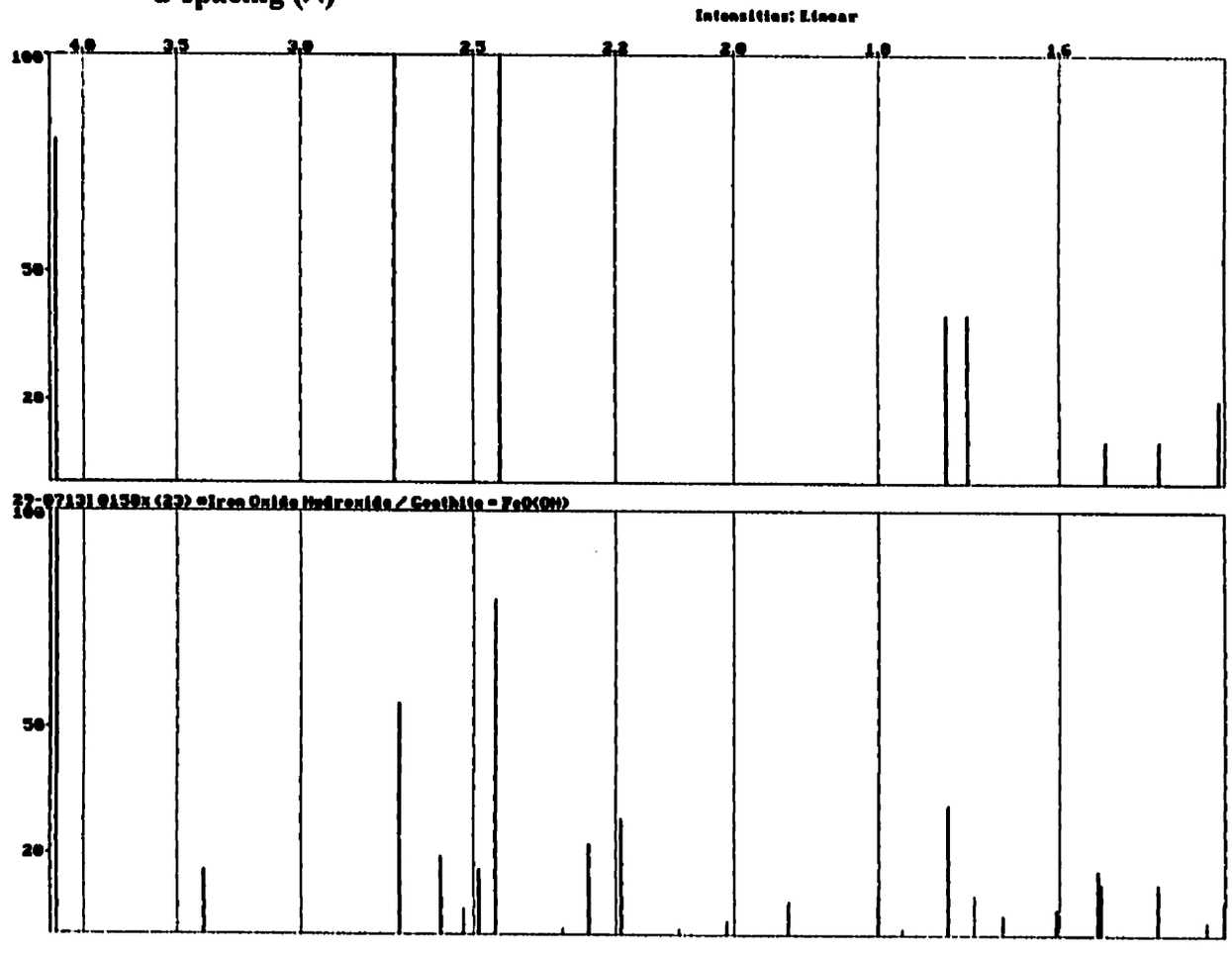

APPENDIX D Chemical compositions of sulphides.

SPHALERITE

Sample #:	PAT012	PAT012	CMO-1	CMO-1	CMT007	CMT007	CMT004	CMT004
Probe #:	PAT12SP1	PAT12SP2	CMO1SP1	CMO1SP2	CMT7SP1	CMT7SP2	CMT4SP1	CMT4SP2
Elements	**Wt. %**	**Wt. %**	**Wt. %**	**Wt. %**	**Wt. %**	**Wt. %**	**Wt. %**	**Wt. %**
As	0.00	0.01	0.02	0.00	0.01	0.00	0.00	0.01
Zn	53.73	52.73	54.08	53.55	53.34	54.21	56.06	55.73
S	33.45	33.78	33.27	33.40	33.02	33.35	33.20	33.47
Fe	10.38	10.76	10.77	11.02	9.48	9.28	9.73	9.79
Cd	0.26	0.28	0.25	0.22	0.23	0.22	0.28	0.21
Cu	0.31	0.46	0.07	0.04	0.01	0.00	0.02	0.00
Total	98.12	98.01	98.42	98.22	96.07	97.07	99.29	99.20

PYRITE

Sample #:	CMT009	CMT009	CMT009	CMT002	CMT002	PAT012	PAT012	PAT012	CMO-1	CMO-1
Probe #:	CMT9PY1	CMT9PY2	CMT9PY3	CMT2PY1	CMT2PY2	PAT12PY1	PAT12PY2	PAT12PY3	CMO1PY1	CMO1PY2
Elements	**Wt %**	**Wt %**	**Wt %**	**Wt %**	**Wt %**	**Wt %**	**Wt %**	**Wt %**	**Wt %**	**Wt %**
As	0.01	0.03	0	0.02	0	0.03	0.01	0.03	0	0.05
Fe	46.20	46.64	47.03	46.59	45.99	46.98	44.15	43.36	44.52	44.68
S	52.43	53.44	53.37	52.59	53.32	53.22	52.26	49.10	52.86	53.04
Zn	0.08	0.06	0	0	0	0.04	0	0	0.02	0.02
Cu	0.01	0.02	0	0	0.02	0.54	2.84	0.34	0.01	0
Co	0.03	0.01	0.03	0.06	0.02	0.41	0.06	0.08	0.06	0.08
Cr	0.02	0.01	0	0.03	0.02	0.01	0	0	0.01	0.01
Total	98.77	100.20	100.43	99.28	99.37	101.23	99.33	92.90	97.48	97.87

Sample #:	CMT007	CMT007	CMT004	CMT004
Probe #:	CMT7PY1	CMT7PY2	CMT4PY1	CMT4PY1
Elements	**Wt %**	**Wt %**	**Wt %**	**Wt %**
As	0	0.01	0.03	0
Fe	46.49	46.64	47.01	46.71
S	53.74	53.25	53.60	53.81
Zn	0	0.01	0.07	0.04
Cu	0.01	0.03	0	0
Co	0.04	0.05	0.01	0.05
Cr	0.01	0.02	0	0
Total	100.29	99.97	100.72	100.60

CHALCOPYRITE AND COVELLITE

Sample #:	PAT012	PAT012	PAT012	CMO-1	CMO-1	CMT007	CMT007
Probe #:	PAT12CP1	PAT12CP2	PAT12CV1*	CMO1CP1	CMO1CP2	CMT7CP1	CMT7CP2
Elements	**Wt. %**	**Wt. %**	**Wt. %**	**Wt. %**	**Wt. %**	**Wt. %**	**Wt. %**
As	0.02	0.00	0.00	0.01	0.00	0.03	0.00
Fe	30.69	30.40	1.43	29.90	30.85	29.78	30.12
S	35.09	34.24	31.93	34.69	34.59	35.65	35.23
Cu	34.64	34.66	65.67	33.15	34.49	32.88	33.11
Total	100.44	99.30	99.03	97.75	99.94	98.34	98.46

* covellite

APPENDIX E Mineral Formulae

Secondary, tertiary and quaternary minerals and their formulae.

Mineral	Formula	Mineral	Formula
anglesite	$Pb(SO_4)$	jarosite	$KFe_3(SO_4)_2(OH)_6$
argentojarosite	$AgFe_6(SO_4)_2(OH)_{12}$	lepidocrocite	γ-FeO(OHO)
bianchite	$(Zn, Fe)SO_4 \cdot 6H_2O$	maghemite	γ-Fe_2O_3
boyleite	$ZnSO_4 \cdot 6H_2O$	malachite	$Cu_2(CO_3)(OH)_2$
chalcanthite	$CuSO_4 \cdot 5H_2O$	melanterite	$FeSO_4 \cdot 7H_2O$
chalcocite	Cu_2S	native sulfur	S
epsomite	$MgSO_4 \cdot 7H_2O$	natrojarosite	$NaFe_3(SO_4)_2(OH)_6$
ferrihydrite	$5Fe_2O_3 \cdot 9H_2O$	plumbojarosite	$PbFe_6(SO_4)_2(OH)_{12}$
goethite	α-FeOOH	rosasite	$(Cu, Zn)_2CO_3(OH)_2$
gypsum	$CaSO_4 \cdot 2H_2O$	rozenite	$FeSO_4 \cdot 4H_2O$
hematite	Fe_2O_3	shwertmannite	$Fe_8O_8(OH)_6SO_4$
hydrated lead carbonate	$PbCO_3 \cdot 2H_2O$	silver sulphate	$AgSO_4$
hydronium jarosite	$(H_3O)Fe_3(SO_4)_2(OH)_6$	szomolnokite	$FeSO_4 \cdot H_2O$

APPENDIX F CPAT Sieve Analysis Results

Weight of sieved sample remaining on each sieve screen.

Sample #	Initial Wt. (g)	Final Wt. (g)	No. 18 (g)	No. 35 (g)	No. 60 (g)	No. 120 (g)	No. 230 (g)	Pan (g)
PAT 001	50.03	49.61	0.41	0.23	1.99	17.86	19.70	9.42
PAT 002	50.06	49.93	0.19	5.65	25.30	15.92	2.31	0.56
PAT 003	40.00	39.73	0.06	1.56	10.72	18.30	6.54	2.55
PAT 004	40.03	39.50	0.09	1.71	11.08	18.25	5.81	2.56
PAT 005	40.01	39.79	0.01	0.94	8.17	18.29	8.65	3.73
PAT 006	40.99	40.74	0.03	1.67	11.02	18.65	6.64	2.73
PAT 007	50.01	49.60	0.02	1.43	12.73	21.59	8.78	5.05
PAT 008	40.81	40.64	0.01	0.81	8.78	19.10	7.98	3.96

APPENDIX G Summary of U.S. EPA Feasibility Report

Summary of the U.S EPA feasibility study of alternatives for the remediation of the CMT site as proposed in U.S. EPA (1993a).

Alternative 1: No Action / Limited Action

Present worth: $249,878 US
Implementation time: 2 months

Summary: No remedial action taken; the contaminated tailings would continue to oxidize and leach.

Alternative 2: Excavation and Capping

Present worth: $3,110,035 US
Implementation time: 4 months

Summary: Excavation and consolidation of contaminated tailings, soils and stream sediments and disposed of on-site, followed by polyethylene and geo-textile cap, and subsequently covered with soil and revegetated; followed by diversion of surface water from capped area.

Alternative 3: Excavation, On-site Solidification/Stabilization, and On-Site Disposal

Present worth: $6,404,521 US
Implementation time: 4 months

Summary: Excavation of contaminated tailings, soils and stream sediments, and treating them by stabilization and solidification on-site. The contaminant would be stored on-site, capped and revegetated; surface water would be diverted from the capped area.

Alternative 4: Excavation, On-Site Solidification/Stabilization, and Off-Site Disposal

Present worth: $11,264,380 US
Implementation time: 4 months

Summary: Excavation of contaminated tailings, soils and stream sediments, and treating

them by stabilization and solidification on-site. The contaminant would be stored off-site in a landfill permitted for such material.

Alternative 5: Off-Site Treatment Through Recycling

Present worth: $7,999,370 US
Implementation time: 4 months

Summary: Excavation of contaminated tailings, soils and stream sediments, and transportation off-site; recycling the metals, and disposal of the residual material, followed by stabilization and solidification in a containment structure.

NOTE: Alternative 5 is the chosen alternative as of 1994.